Theoretical Atom Optics:

Evanescent Wave Atom Optics and Bose-Einstein Condensation

Daniel Gordon

A thesis submitted for the degree of
Doctor of Philosophy at
The Australian National University

October 1999

This thesis is an account of research undertaken in the Department of Physics and Theoretical Physics, Faculty of Science, at the Australian National University between March 1996 and February 1999.

This research was supervised by Dr Craig Savage, but unless otherwise indicated, the work presented herein is my own.

None of the work presented here has ever been submitted for any degree at this or any other institution of learning.

Daniel Gordon
5 October 1999

Acknowledgments

I am thankful to a great many people who helped me during the last three years, both with regards to my work as a physicist and in providing support, encouragement and happiness during my time as a PhD student.

Firstly, I would like to thank my supervisor, Dr. Craig Savage, who has, I believe, truly cared about my development as a physicist and who has done a lot to shape that development. Thanks for getting me this far, and I can hardly believe I'm handing the thing in.

Thanks also to my friends and colleagues at the ANU and in the wider physics community. Particular thanks go to my office mates Joseph Hope and Glenn Moy, who have both helped me through the years 'hey guys, what do you think of this problem...' and provided a lot of fun and laughter to take my mind off the serious work ('care for another game of Marathon?').

I would also like to thank everyone in the physics department. It's been a great department and a great place to work. In particular, Ian Littler, Mark Andrews, Jurgen Eschner, Hans Bachor, David McLelland, Brett Cuthbertson, John Close, Stewart Midgely, Geoff Erickson, Mike Ashley, Rado Faletic and Matt Gaston have provided me with useful discussions, information and computer help from time to time (I hope I didn't miss anyone!). Also, a big thanks to Felicity Davey, Zeta Hall and Jenny Wilcoxson.

In the wider physics community I would like to thank Ralph Deutschmann and Chris Westbrook for their help on atom diffraction, likewise Ken Baldwin from the Research School of Physical Sciences, and all of those people at conferences who provided comments and discussions.

The folks at the ANU Supercomputer Facility have been extremely helpful, so many thanks go to Judy Jenkinson, David Singleton and Ben Evans.

Lastly, of course a huge thanks goes to all those people who have made it all worthwhile by giving support, love, encouragement, nurture and happiness. Thanks to my family - I couldn't have done it without your support. Thanks to my friends. Julia, thanks.

This PhD has been supported by an Australian Postgraduate Award. The ARC provided support for the atom-diffraction work. Computations were performed at the ANU Supercomputer Facility.

Abstract

We develop a theoretical description of a multi-level atom interacting with an evanescent wave diffraction grating, and numerically model the dynamics for two experimentally relevant parameter regimes. Our results are found to be consistent with experimental data. We show that, unlike scalar or two-level atoms, multi-level atoms can exhibit high beamsplitting efficiencies at grazing incidence. The effects of various parameters, including laser polarisation and detuning, are investigated.

We calculate the density profile and excitation spectrum of a two-species Bose-Einstein condensate, and show that in certain parameter regimes the spatial symmetry of the system can be spontaneously broken. This symmetry breaking is due to repulsive intrerspecies atom-atom interactions. The excitation spectrum of the system shows that the lowest energy, antisymmetric, excitation approaches zero-frequency as the region of symmetry breaking is approached in parameter space, and then rises again following the transition of the condensate to a symmetry broken state.

We propose a scheme to create macroscopic or mesoscopic quantum superpositions ('Schrödinger cat' states) using a two-species Bose-Einstein condensate. The scheme relies on the nonlinear evolution caused by the atom-atom interactions present in the system along with Raman beams which couple the two species. We analyse this system in the two-mode approximation, and consider possible experimental problems including decoherence.

Contents

Chapter 1

Introduction

1.1 Atom optics and Bose-Einstein condensation

This thesis deals with the relatively recent field of *atom optics*. This field is primarily concerned with replicating conventional optics using atoms rather than light. Much of conventional optics relies on using the wave nature of light to manipulate it: for example, refraction and diffraction are wholly wave phenomena. In atom optics, the quantum mechanical de-Broglie wave nature of the atoms is analogous to the wave nature of light in conventional optics. The term 'atom optics' is often used somewhat loosely and can also refer to the manipulation of the motion of atoms using light fields, without regard to their wave nature. Chapter 2 of this thesis is concerned with a device which does rely on the the wave nature of atoms - a reflective diffraction grating for atoms. Interestingly, this chapter is concerned more with the differences rather than the similarities of this device to optical diffraction gratings. It is shown that the internal structure of atoms can lead to effects not seen in conventional optics; these effects can greatly increase the range of possibilities available in an experiment.

The development of the laser in the early 1960's completely transformed the field of optics by providing an intense, coherent light source - essentially the perfect wave of high school optics textbooks. Fields such as interferometry were revolutionised, since the use of coherent light allowed for far greater accuracy. Furthermore, lasers have found use in a great number of industrial applications, from manufacturing to telecommunications, compact disk players and so on. In 1995, the first observation of a dilute gas Bose-Einstein condensate (BEC) by Anderson *et al.* [1] allowed atom optics to proceed into a realm analogous to that brought about by the conventional laser. Essentially, a laser beam consists of many photons behaving collectively, or coherently, in such a way that they are described by a single classical field —the classical electromagnetic field. A dilute gas BEC consists of a large number of bosonic atoms (typically 10^5 - 10^7) which, like the photons in a conventional laser, can

be described by a single classical field. To a good approximation, we can say that a large fraction of the atoms share the same single particle wavefunction. Just as the laser revolutionised the field of optics, dilute gas Bose-Einstein condensation promises to revolutionise the field of atom optics as well as having important applications in fields such as atomic physics. Chapter 3 of this thesis describes a particular aspect of Bose-Einstein condensation: namely, the behaviour of two-species BECs.

The invention of the laser also allowed experiments which went beyond the regime of the classical electromagnetic field - experiments which dealt directly with the quantum state of the light field. Such experiments form the subject matter of the field known as quantum optics. A well known example is squeezing, in which the uncertainty in one observable is reduced, leading to a reciprocal increase in the uncertainty of the canonically conjugate observable. In optics experiments, these two observables typically consist of the quadrature amplitudes of the light field. Bose-Einstein condensates have the potential to allow analogous effects - suggesting a possible new field of study which might be termed *quantum atom optics* [2]. In Chapter 4, we investigate a scheme for manipulating the many-body quantum state of a two-species BEC in such a way that a Schrödinger cat state, or macroscopic superposition state, is produced. The demonstration of such states, or the repeated failure to produce them even if experimental problems are overcome, would be important quite independently of the field of quantum atom optics. It would allow us to verify whether the usual rules of quantum mechanics are valid beyond the microscopic regime, a proposition which is by no means universally accepted (e.g.. see Penrose [3]).

1.1.1 Interaction of an atom with light: the spontaneous and dipole forces

Conventional optics relies on transparent materials and reflective surfaces to manipulate the light field. In atom optics, on the other hand, atoms are manipulated by lasers and occasionally by magnetic fields. In Chapter 2, we shall be concerned with the former case.

The simplest way to manipulate atoms with lasers is by using what is termed the spontaneous force. If a two-level atom is illuminated by a resonant laser, it will tend to absorb a photon and thus gain a momentum kick of magnitude equal to the momentum of the photon, and in the direction of the laser beam. It will then at some later time spontaneously emit a photon in some random direction, and this cycle will be repeated many times. The net effect is for the atom to be pushed stochastically in the direction of the laser

beam, and the resulting force on the atom is termed the spontaneous force. Although it can be used to push atoms around, trap them etc., it has the drawback that it does not preserve the coherence of the atomic de-Broglie wave, due to spontaneous emission. In cases where it is important to preserve coherence, the dipole force is used:

If an atomic transition is driven with off-resonant light, then a spatial gradient in the light field will introduce a spatial potential for the atom through the interaction of the electric field with the atomic dipole. This interaction in its most basic form is described by a two-level atom interacting with a detuned light field which can be represented by the Jaynes-Cummings Hamiltonian:

$$\hat{H} = \hat{\mathbf{p}}^2/2M + \hbar\omega_A \, |e\rangle\langle e| + \hat{\mathbf{d}} \cdot \hat{E}(\hat{\mathbf{r}}, t)\,, \tag{1.1}$$

where M is the mass of the atom, $|e\rangle$ is the excited state of the atom (with ground state $|g\rangle$, ω_A is the energy difference between the excited and ground states, $\hat{\mathbf{d}}$ is the dipole operator for the transition and $\hat{E}(\hat{\mathbf{r}}, t)$ is the operator for the electric field at position $\mathbf{r}$ and time t. In what follows, we use a semiclassical approximation under which the electric field is assumed to be a classical field. Furthermore, we use the rotating wave approximation and transform into an interaction picture with $\hat{H}_0 = \hbar\omega_L \, |e\rangle\langle e|$, where ω_L is the frequency of the laser field. Under these operations the Hamiltonian becomes [4]:

$$\hat{H} = \hat{\mathbf{p}}^2/2M + \hbar\Delta \, |e\rangle\langle e| + d(|e\rangle\langle g| \, E(\hat{\mathbf{r}}) + |g\rangle\langle e| \, E^*(\hat{\mathbf{r}}))\,, \tag{1.2}$$

where $\Delta = \omega_A - \omega_L$ is the light field detuning and d is a parameter describing the strength of the atom-field coupling.

The eigenstates of the Hamiltonian (1.2) minus the kinetic energy of the atom $\hat{\mathbf{p}}^2/2M$ are known as *dressed states*. The dressed states and their energies are given by the following expressions:

$$\begin{aligned} |1\rangle &= \sin\theta \, |g\rangle + \cos\theta \, |e\rangle\,, \; E_1 = \frac{\hbar}{2}(\Delta + \mathcal{R})\,, \\ |2\rangle &= -\cos\theta \, |g\rangle + \sin\theta \, |e\rangle\,, \; E_2 = \frac{\hbar}{2}(\Delta - \mathcal{R})\,, \end{aligned} \tag{1.3}$$

where $\cos(2\theta) = \Delta/\mathcal{R}$, $\sin(2\theta) = \Omega/\mathcal{R}$ and the *Rabi frequency* Ω and generalised Rabi frequency $\mathcal{R}$ are defined by

$$\Omega = 2d|E|/\hbar\,, \tag{1.4}$$

$$\mathcal{R} = \sqrt{\Delta^2 + \Omega^2}\,. \tag{1.5}$$

We can see that for blue detuning $\Delta < 0$ the state $|1\rangle$ is adiabatically connected

to the ground state of the atom $|g\rangle$ whilst $|2\rangle$ is connected to $|e\rangle$, whereas the situation is reversed for red detuning $\Delta > 0$.

In the limit where the light field seen by the atom is changing slowly enough to lead to adiabatic motion, and for detunings large enough to lead to a relatively small excited state population, we can adiabatically eliminate the excited state: The Hamiltonian then becomes

$$\hat{H} = \hat{\mathbf{p}}^2/2M + V(\mathbf{r}), \tag{1.6}$$

with the potential

$$V(\mathbf{r}) = \frac{d^2|E(\mathbf{r})|^2}{\hbar\Delta}. \tag{1.7}$$

1.1.2 Atom trapping

We have seen that light can be used to influence the motion of atoms, through both conservative and dissipative forces. In many experiments it is useful to have the atoms held in a single region of space. A device which does this is called an atom trap. Trapped atoms can subsequently be manipulated at leisure, and hence atom traps expand the range of experiments available. They have been used in atomic diffraction experiments as described in Chapter 2 [5–7], and are essential to dilute gas Bose-Einstein condensation, which forms the subject matter of Chapters 3-6 of this thesis.

Much of the following material is based on the review by Savage [4].

Probably the simplest trap is known as optical molasses. Strictly, this is not a trap as such because the atoms are not confined to any one point, but as its name suggests, it acts like molasses to greatly slow the mean motion of the atoms. In one dimension, optical molasses consists of two red-detuned counterpropagating beams. If the atom travels toward either of the beams, the transition is Doppler shifted toward resonance for that beam and away from resonance for the other beam. Thus the net spontaneous force tends to push the atom in the direction opposite to its motion, leading to a velocity dependent (viscous) force which tends to keep the atom in one place. In three dimensions, six beams are used, one pair for each axis. Because the beams act to slow atomic motion, optical molasses is really cooling technique.

One very common trapping configuration is the magneto-optical trap, or MOT. In a MOT, the same laser configuration as for optical molasses is used, except that the counterpropagating beams are circularly polarised in opposite directions relative to one another. Placed along the axis of each pair of counter-propagating beams is a pair of anti-Helmholz coils, one producing a positive magnetic field and one producing a negative field. The circularly polarised laser beams act on particular magnetic sublevels of a given transition, and the

magnetic fields act to shift the relevant sublevels closer to resonance with the lasers as the atoms move into regions of increasing magnetic field, i.e. away from the centre of the trap. As the atom comes into resonance, the spontaneous force thus tends to push the atom back to the trap centre. The MOT also acts to cool atoms in the same manner as optical molasses.

Both optical molasses and MOTs are unsuitable for very low temperature applications. This is because the lowest temperature achievable by such methods is governed by a fundamental limit known as the *doppler limit*, and even if some other additional cooling technique were employed, the presence of spontaneous emission places a further fundamental limit, known as the recoil limit, on the minimum temperature. These limits will be discussed further in the section on cooling.

A third type of trap commonly used in the production of Bose-Einstein condensates is the magnetic trap. Basically, magnetic traps operate on the principle that magnetic fields will interact with the magnetic dipole moment of atoms, producing a force. Such traps are good for applications involving sub recoil atom cooling, since there are no light fields and hence no spontaneous emission. These traps will be discussed in detail in Section 1.1.4.

Finally, we shall mention gravito-optical traps and far off-resonance light traps. Gravito optical traps work on a simple principle: blue detuned light fields, which repel the atoms by means of the the optical dipole force, are used to create a cup or bowl shaped structure into which are placed the atoms. Gravity holds the atoms within this structure. There exist many possible configurations for such traps utilising evanescent light fields, Gaussian donut modes etc. Far off resonance light traps, or FORT traps, work on a similar principle in that they use the optical dipole force for confinement. A typical FORT trap might consist of a single linearly polarised waisted Gaussian light beam red detuned from a given atomic transition [8]. Atoms are held at the point of highest intensity in the light field. These traps again allow atoms to be held at sub-recoil temperatures.

1.1.3 Atom cooling

For many atom optical applications, it is important that the atoms are cooled to very low temperatures. As has already been mentioned, optical molasses is one way of cooling atoms. This type of cooling is known as Doppler cooling. It works by bringing atoms travelling with non-zero velocity into resonance with red-detuned lasers. Thus the cooling rate will be proportional to the doppler shift and hence to the velocity. There is also a certain heating rate associated with spontaneous emission. As the atoms are cooled, the velocity decreases and there will come a point at which the heating and the cooling rates exactly

balance each other out, and at this point no more cooling can take place. This fundamental limit to the temperature is known as the Doppler limit; it is given by

$$T_{\text{Dop}} = \frac{\hbar\gamma}{2k_B}, \tag{1.8}$$

where γ is the linewidth of the transition and k_B is Boltzman's constant.

It is possible to cool to below the Doppler limit by employing a number of other different methods. One is known as Sisyphus cooling [9], after Sisyphus, who was forced by Zeus to roll a rock uphill forever. As we have seen, the excited and ground states of a two-level atom in a detuned laser field experience a shift in energy due to the interaction with the light field. An atom moving in a standing wave made of blue detuned light will preferentially absorb a photon when the excited state component is greatest, which occurs at a potential energy maximum. After such an absorption, the atom will again find itself at the bottom of the potential energy curve for the excited state dressed state. It is then again most likely to spontaneously emit back down to the ground state when the excited state component is greatest, again at the potential energy maximum. After a cycle of absorption and emission, we find that the atom has made a net loss of energy, since it has had to move on average up the potential energy curves. Thus there is a net cooling effect. A more sophisticated version of Sysiphus cooling occurs in polarisation gradient cooling, where the full structure of the Zeeman sublevels and polarised light fields are used. Both of these methods are fundamentally limited by what is known as the recoil limit; since they rely on spontaneous emission, the atoms can at most be cooled to temperatures corresponding to the momentum of one photon. The recoil limit is

$$T_R = \frac{\hbar^2 k^2}{2mk_B}, \tag{1.9}$$

where m is the mass of the atom and k is the magnitude of the wavevector of the laser.

In order to cool to below the recoil limit, one must employ methods which do not feature spontaneous emission. One such method is known as dark state cooling, or velocity-selective coherent population trapping (VSCPT) [10]. This method works by employing a level scheme and laser configuration for which one of the dressed states does not interact with the laser. Such a state is known as a dark state. As the atoms undergo a random walk in phase space due to spontaneous emission from the excited state, some of them enter this dark state and thereafter cannot leave it because no absorption can take place. There is no fundamental limit to the temperatures achievable by VSCPT.

Finally, conceptually the simplest and to date the most effective cooling

method in terms of the temperatures achievable is evaporative cooling. To date, all BECs produced in the lab have relied on evaporative cooling in magnetic traps. This method will be discussed in the following section.

1.1.4 Bose-Einstein condensation

If a collection of identical Bosons (particles with integer spin) is cooled below a certain critical temperature, the system will develop a macroscopic occupation of a single quantum state. The theory of this phenomenon was first described by Bose [11] and Einstein [12], hence the name Bose-Einstein condensation, or BEC. It plays an important role in the superfluid properties of supercooled liquid helium and has been used to explain the properties of low-temperature superconductors. However, these systems cannot be thought of as pure condensates in the sense that their behaviour is just as much to do with the strong interactions between the particles (helium atoms or electrons) as it is to do with BEC. They are instead best thought of as superfluids rather than condensates —the distinction being that pure condensates describe systems in which almost all particles are in a particular single particle quantum state. For this reason, it has long been considered desirable to produce a dilute gas Bose-Einstein condensate in which the particles interact with each other only weakly. Such a system would exhibit properties purely due to the quantum macroscopic nature of the condensate.

In order to produce a Bose-Einstein condensate, it is necessary to cool to temperatures at which the de-Broglie wavelengths of the individual atoms overlap. If the wavepackets do not overlap, then the individual atoms are distinguishable by their position and hence effects due to Bose-enhancement do not play a great role in the behaviour of the gas. However, when the wavepackets begin to overlap, they become completely indistinguishable and it is at this point that quantum statistical effects, such as Bose-Einstein condensation, come into play. The de-Broglie wavelength of an atom is proportional to its velocity, which is in turn proportional to the temperature of the sample. In three dimensions, the de-Broglie wavelengths will overlap when there is more than one atom per cubic de-Broglie wavelength, and hence we can derive for an ideal gas the condition that

$$nT^{-\frac{3}{2}} > 2.612 \left(\frac{mk_B}{2\pi\hbar^2} \right)^{3/2}, \tag{1.10}$$

where n is the density of atoms, m is the atomic mass and k_B is Boltzman's constant. This means that achieving BEC requires low temperatures and/or high densities. Thus achieving BEC in dilute gases requires much lower tem-

peratures than, say, the critical temperature for superfluid helium. These temperatures eluded experimental physicists until 1995 when Anderson *et al.* [1] reported dilute gas Bose-Einstein condensation in ^{87}Rb. Since then, the rate of experimental progress has been impressive. At the time of writing, there are many groups regularly producing BECs in rubidium [1], sodium [13,14], lithium [15] and hydrogen [16].

To date, all BECs have been produced in magnetic traps, although the storage of a BEC in a FORT trap has been demonstrated [17]. A configuration of anti-Helmholz coils will produce a quadrupole magnetic field with a zero-minimum. This creates a problem: only some magnetic sublevels within a given hyperfine level will be attracted toward the centre of the trap, and the rest will be repelled or not affected by the field at all. In regions with zero magnetic field, the hyperfine sublevels become degenerate and hence spin flip transitions can occur in which the state of the atom is changed from a trapped to an untrapped sublevel. This problem was overcome in the first observation of dilute gas BEC [1] by applying RF fields which cause the centre of the trap to orbit around a central point. If this orbit moves fast enough, then the atom effectively sees a potential which is averaged over the whole orbit and hence the time averaged field acquires a non-zero quadratic minimum at the centre of the orbit. Such a configuration is known as a TOP, or Time-averaged Orbiting Potential, trap.

There are several other ways of getting around the problem of a zero minimum of the magnetic field. The minimum in the field can be 'plugged' with a blue detuned laser field [13], although this technique is not frequently used. A static field with a non-zero minimum can also be made. One way of doing this uses permanent magnets [15]. Another successful technique employs a more complicated configuration of coils than the anti-Helmholz pair used in the TOP trap. Such a configuration is known as a cloverleaf trap [14], and is a variation of the Ioffe-Pritchard type trap [18,19].

Since 1995, a large number of impressive experiments have been performed with Bose-Einstein condensates, and the volume of theoretical papers shows that theory has certainly not lagged behind. The excitation spectrum of BECs has been measured by perturbing the trapping potential [20–22] and has been found to agree well with theoretical predictions [23,24]. BECs have been produced with attractive interatomic interactions [15,25]. They have been coherently output coupled from a trap in an experiment claimed to be a demonstration of a pulsed atom laser [26]. Output fringes from two Bose-condensed clouds expanding toward one another have been observed [27]. BECs containing two types of atoms have been made [28–31] and have been used to construct a simple kind of interferometer which demonstrates the phase co-

herence between the two components [31]. BECs have been confined in an optical trap [32]. A BEC has been used to slow the speed of light to 17 ms^{-1} [33]. The fact that more and more groups around the world are producing BECs will no doubt mean that the already rapid rate of experimental progress will continue to grow.

1.2 Summary of original work

The major results of this thesis are as follows:

1. It is shown that efficient grazing incidence beamsplitting in an evanescent wave diffraction grating will only occur if the multi-level nature of the atomic transition is employed. The beamsplitting process is modelled by numerically solving the time dependent Schrödinger equation for the cases of metastable Ne and Cs. The results obtained are consistent with experiment. This work is published in Optics Commun. [34] and the original work carried out as part of this thesis can be found in Sections 2.7-2.10, although the work in Section 2.7.1 was carried out as the candidate's honours project. The code used to calculate the numerical results of this chapter is a significant expansion and modification of a code written for the candidate's honours thesis, which in turn is based on a code written by C.M. Savage to model the dynamics of a two-level atom in an evanescent field.

2. It is shown that in certain parameter regimes, the mutual repulsion of the two species in a two-species Bose-Einstein condensate can lead to a spontaneous breaking of spatial symmetry. The excitation spectrum for this system is obtained, and the effects of this symmetry breaking are clearly seen as an excitation frequency which goes to zero as particle number is increased and then rises again following the system's collapse to a new symmetry broken stable state. This work is published in Physical Review A [35], and the original work forms the content of Chapter 4 of this thesis except where it is explicitly noted otherwise.

3. A scheme for creating Schrödinger cat states using two-species Bose-Einstein condensates is proposed. Such states consist of a superposition of two macroscopically distinguishable states, one with an excess number of atoms belonging to one species and one with an excess number of atoms belonging to the other species. This work has been published in Physical Review A [36] and forms the content of Chapter 5 of this thesis, except where it is explicitly noted otherwise.

1.3 Notation

I have tried to be consistent in notation throughout the text. A boldface quantity indicates a three-dimensional vector quantity (e.g. $\mathbf{r}$). A hat (e.g. $\hat{a}$) is used to indicate an operator. The abbreviation 'H.c.' stands for 'Hermitian conjugate'.

Chapter 2

Atomic diffraction from an evanescent wave

This chapter reviews the work so far carried out, both in theory and experiment, on evanescent wave diffraction gratings. Part of the original work presented here appears in the paper [34]. The basis of the theory of multi-level diffraction was developed as part of the candidate's 1995 Honours thesis [37], however, the calculations presented in Section 2.11 (published in [34]) and Section 2.12, the theory presented in Sections 2.7.2,2.8 and much of the analysis were performed as part of the degree for which this thesis is submitted.

A review of atomic diffraction can be found in [38].

2.1 Introduction

This chapter is concerned with a particular atom-optical component —the evanescent wave diffraction grating. The fact that this component can diffract an atomic beam into two or more coherent beams means that it could possibly be used in the future as a beam-splitter in an atomic interferometer. Such an interferometer would be particularly useful for measuring the gravitational field of the earth or its gradient, with applications in basic research as well as in oil/minerals exploration.

2.2 The basic model

The evanescent wave mirror was first proposed by Cook and Hill [39]. It consists of a prism into which is shone a laser beam that is totally internally reflected off one of the faces (see Fig. (2.1)), creating an evanescent light field external to this face. If the laser is blue detuned relative to a given atomic transition, then the evanescent light field will provide a reflective potential for the atom.

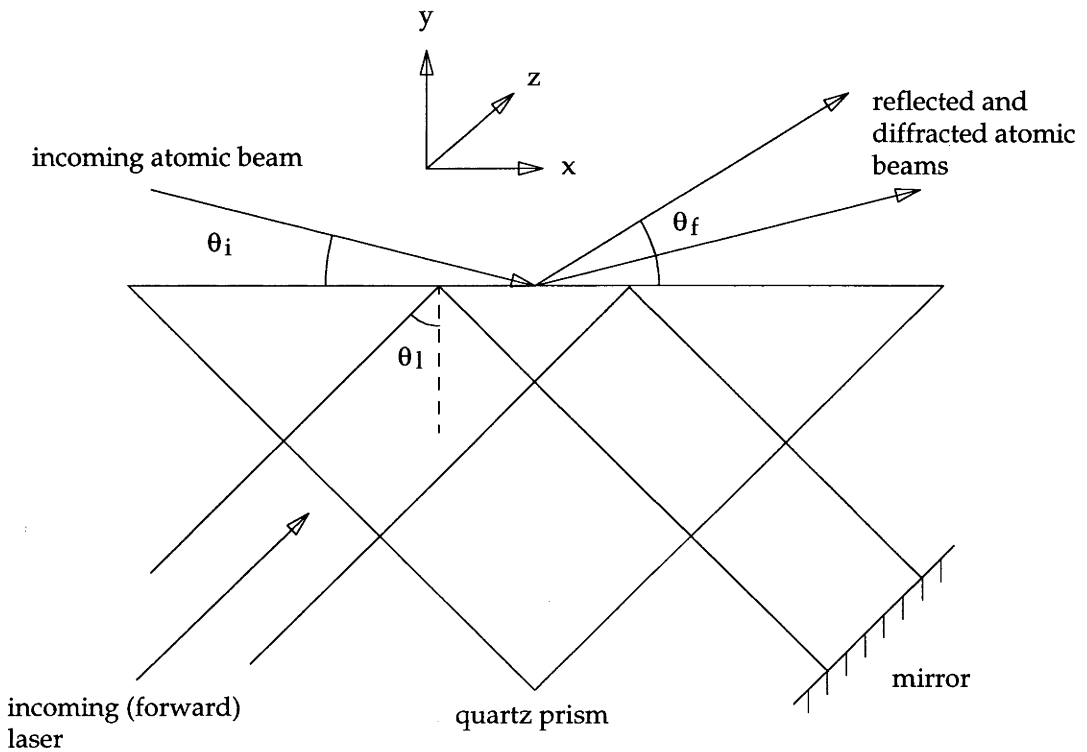

Figure 2.1: The geometry of the lasers and atomic beam in the evanescent field diffraction experiment. Removing the mirror creates a purely reflective grating.

If we imagine retro-reflecting the laser beam so that it retraces its path, then the evanescent light field will contain a standing wave component. The light induced potential is then spatially periodic, and hence we should have the possibility of observing diffraction [40]. One might naively hope that, in analogy with the optical case, one should be able to see diffraction if the component of the atomic de-Broglie wave vector in the x-direction (parallel to the glass surface) is comparable to the wave-vector of the evanescent wave along the surface. As we shall see, this condition does not in fact guarantee diffraction. The difference comes about because, unlike light reflecting from an optical mirror, the process of reflection for an evanescent wave grating takes place over a distance comparable to the atomic de-Broglie wavelength and thus the evanescent reflective potential can be considered to be 'soft' or 'spongy'. We shall see that this difference leads to far more restrictive conditions on obtaining scalar diffraction than in the optical case. However, as shall also be seen, the multi-level structure of the atom can be used to overcome this problem. In particular, this chapter will show that the full hyperfine structure of atomic transitions can work to give a large diffraction efficiency.

In order to explore these issues, we shall discuss three different models of

diffraction: the scalar model, the two-level model and the multi-level model. It is in the latter case that the original results of this chapter are presented. The multi-level model is the most general in that it includes the other two models as special cases.

2.3 The experiments

At the time of writing, evanescent wave diffraction has been definitely demonstrated by three groups. In addition, an experiment currently underway at ANU has shown evidence of diffraction.

The first demonstration of evanescent wave diffraction was reported in 1994 by Christ *et al.* [41] at Bonn university. Using a slowed beam of metastable Ne atoms, they were able to observe a diffraction efficiency of some 3%. The results of this experiment are modelled in Section 2.11.

Following this result, Brouri *et. al.* [42] at Paris-Nord university reported high efficiency diffraction at grazing incidence using a different transition in Ne. This experiment used a dielectric coating to generate a surface plasmon excitation and hence enhance the evanescent wave. A unique feature of this experiment was that the plane of incidence of the atoms was tilted with respect to the laser plane of incidence so as to decrease the Doppler shift for the thermal atomic beam.

In 1997 Landragin *et. al.* [5] at the Orsay Institut d'Optique observed normal incidence diffraction in metastable Cs, using a cloud of atoms dropped from a MOT. As shall be seen, such normal incidence diffraction is different in nature to grazing incidence diffraction, and in fact bears more resemblance to diffraction from an optical grating than the latter. Recently, the same group has simulated grazing incidence diffraction by using a counterpropagating laser which is detuned relative to the copropagating laser, thus producing a running wave. They have reported efficient diffraction using this setup [6].

An experiment is currently underway at the Australian National University which uses Cs atoms launched upwards from a MOT towards a tilted evanescent wave grating. This setup is quite versatile, as it allows the incident velocity to be varied by adjusting the launch velocity of the atoms. At the time of writing, the experiment shows a good reflection signal and evidence of diffraction [7], although the experiment is still in progress.

2.4 Physical processes

At its most basic level, atomic diffraction from an evanescent wave grating can be viewed in terms of the conservation of energy and momentum. We consider the setup shown in Fig. (2.1). The light field is blue detuned with respect to some atomic transition $|g\rangle$ to $|e\rangle$, where $|g\rangle$ and $|e\rangle$ are the atomic ground and excited states of the transition in question. The magnitude of the wavevector of the light field in the x direction is Q. The atom enters the light field at some angle θ_i and experiences a repulsive potential due to the dipole force (see Chapter 1), eventually leaving in one or more possible reflection/diffraction channels with angle θ_f and in either the state $|g\rangle$ or $|e\rangle$. We shall limit ourselves to considering only the former case, since excited state atoms which leave the light field will very quickly spontaneously emit back down to the ground state, destroying their coherence properties and giving them a random momentum kick into the bargain.

In modelling diffraction, it is possible to ignore one of the spatial directions (the z-direction in Fig. (2.1)). This assumes that the laser field does not vary in this direction, which requires that the spot size of the evanescent field is bigger than the portion of the atomic beam being considered. In such a case, there can be no momentum transfer in this direction, because the k-vector of the laser field is perpendicular to it, and no mechanical effects, because the potential is constant.

Considering for the moment the case of a grating with no retro-reflected laser beam and hence no standing wave component of the evanescent field, we see that a ground state atom which has left the field can have had no momentum transferred to it in the x-direction by the field, since it must have undergone an even number of absorptions and emissions from the field. Furthermore, conservation of energy demands that the atom must leave the field at the same speed at which it entered, and these two facts come together to ensure that $\theta_f = \theta_i$ i.e. the atom experiences only specular reflection.

Now we move on to consider the case where the laser field contains a retro-reflected component. The evanescent field now consists of two-components: a forward beam which carries photons with momentum in the positive x direction an a backward beam which carries photons with momentum in the negative x direction. A ground state atom leaving the evanescent field must have experienced an even number of stimulated absorptions/emissions, but now the presence of two laser fields means that momentum can be transferred from the light field to the atom. As an example, the atom can absorb a photon from the forward beam, putting it into the excited state $|e\rangle$ and giving it a kick of $\hbar Q$ in the positive x-direction, and then emit into the backward beam, putting it into back into the ground state and giving it another $\hbar Q$ kick in the positive

x direction, resulting in a total momentum kick of $2\hbar Q$. In this case, we shall say that the atom has left the light field in the $n = 2$ diffraction order, where n stands for the number of quanta of momentum absorbed in the x-direction. However, the atom has absorbed no energy from the light field since it leaves in the ground state, and hence must slow down in the y-direction to satisfy conservation of energy. This can be represented graphically by the diagram Fig. (2.2).

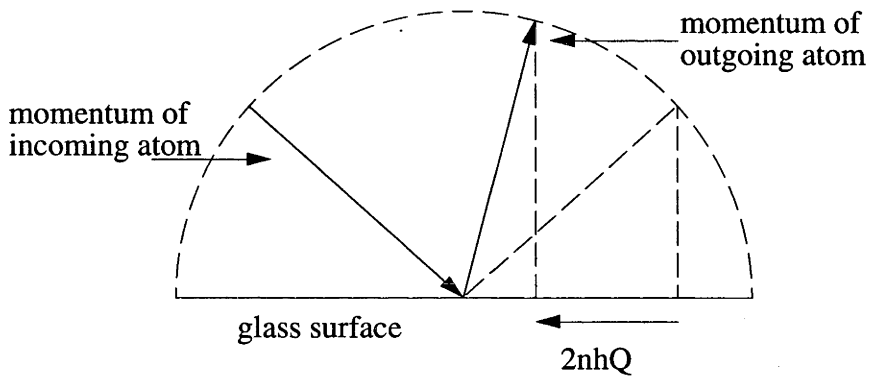

Figure 2.2: A graphical representation of how the conservation of energy and momentum leads to large angle diffraction. Conservation of energy constrains the momentum of the incoming and outgoing atom to lie on the same circle. Absorption and emission of photons leads to a change of $2n\hbar Q$ in the x-component of momentum of the outgoing atom, thus leading to a corresponding change in the y-component in order to satisfy energy conservation. For grazing incidence, large angle diffraction can result.

We can calculate the angle of diffraction θ_f for the nth diffraction order (n even):

$$\begin{aligned} \text{K.E.}_{\text{init}} &= \text{K.E.}_{\text{final}} \\ p_{i,x}^2/2m + p_{i,y}^2/2m &= (p_{i,x} + n\hbar Q)^2/2m + p_{f,y}^2/2m\,, \end{aligned} \tag{2.1}$$

where m is the mass of the atom, $v_{i,x}$ and $v_{i,y}$ are the initial velocity components in the x and y directions, $v_{f,y}$ is the final velocity component in the y-direction, and the final velocity in the x-direction is $v_{i,x} + n\hbar Q/m$ for the nth diffraction order. The angle of diffraction for the nth order is now calculated as:

$$\tan\theta_f = \frac{\sqrt{v_{i,y}^2 - 2v_{i,x}n(\hbar/m)Q - n^2(\hbar/m)^2Q^2}}{v_{i,x} + n(\hbar/m)Q}\,, \tag{2.2}$$

where $v_{i,x} = v_i\cos\theta_i$, $v_{i,y} = v_i\sin\theta_i$ with v_i being the speed of the incoming

atom prior to interaction with the evanescent field. If the argument of the square root in Eq. (2.2) is negative, then the conditions of conservation of energy and momentum can not be satisfied for the diffraction order in question and hence there will be no diffraction into that order.

It is in the angle of diffraction that the evanescent wave grating differs from other diffraction devices. If the atom approaches the glass surface at grazing incidence (θ_i small), then, in order to satisfy the conservation of momentum and energy, the motion in the y-direction (perpendicular to the glass) must change by a relatively much larger amount than would be the case if the atom had approached the glass at near normal incidence. Thus the grating produces a large separation in the angles of diffraction for different orders. The ability to produce large angle diffraction means that resolution of the atoms by a detector is not such a problem. Also, the subsequent manipulation of the atoms, perhaps for the purpose of interferometry, would be made much easier.

Finally, we mention some commonly used terminology. In Eq. (2.1), the x-component of the final kinetic energy is often expressed as:

$$\frac{p_{f,x}^2}{2m} = \frac{p_{i,x}^2}{(2m)} + n\hbar\Delta_D + n^2\hbar\Delta_R\,, \tag{2.3}$$

where $\Delta_D = p_{i,x}Q/m$ is termed the doppler shift and $\Delta_R = \hbar Q^2/(2m)$ is the recoil shift. $\hbar\Delta_R$ is equal to the energy gained in the x-direction via recoils from the absorption and emission of photons, while Δ_D is equal to the frequency difference of the doppler shifted forward and backward laser beams in the atom's frame of reference. In this frame, diffraction can be interpreted as being due to an energy transfer due to absorption from a light field at one frequency and emission into another field at a different frequency, with the total energy shift of such an absorption/emission cycle being twice the doppler shift Δ_D.

2.5 The scalar model of atomic diffraction

As its name suggests, the scalar model of diffraction treats the atoms as scalar particles i.e. it ignores the internal structure of the atoms. Thus the atoms can be described by a wavefunction $\psi(\mathbf{r})$, which depends on the position only, evolving under the Schrödinger equation. The interaction of the atoms with the evanescent light field is described by a simple spatially dependent potential. This model is most similar in spirit to the optical model of diffraction from a grating, since it is best viewed in terms of the interaction of a simple wave with a spatially periodic structure. The theory reviewed here was developed by the group at the Institut d'Optique in Orsay [38].

Suppose that we first consider a purely running wave grating with no retroreflected laser beam. The classical Lagrangian describing the motion of the atom is

$$L_0 = \frac{1}{2}m\dot{\mathbf{r}}^2 - V_0 e^{-2qy}\,, \tag{2.4}$$

where V_0 is the strength of the potential induced by the light-dipole interaction and q is the decay length of the evanescent field. Now, if we retro-reflect a small amount of the incident light, we have

$$L = L_0 - \varepsilon V(\mathbf{r})\,, \tag{2.5}$$

where

$$\varepsilon V(\mathbf{r}) = \varepsilon V_0 e^{-2qy}\cos(2Qx) \tag{2.6}$$

is the standing wave component of the scalar potential and ϵ is small. Thus the total perturbed optical potential is

$$V_{TOT}(\mathbf{r}) = V_0 e^{-2qy}(1 + \varepsilon\cos(2Qy))\,. \tag{2.7}$$

ε is termed the contrast since it is a measure of the relative amplitude of the standing wave compared to the total field amplitude.

Our aim is to calculate the atomic population in the various diffraction orders. This can be done by employing a semiclassical path-integral calculation in which the presence of a standing wave component in the field is treated as a perturbation to the running wave case. One uses the WKB approximation for the path integral expansion for the wavefunction at some time t_f after the atom has left the evanescent field:

$$\psi(\mathbf{r}_f, t_f) = \exp\left[\frac{i}{\hbar}S(\mathbf{r}_f, t_f|\mathbf{p}_i, t_i)\right]\,, \tag{2.8}$$

where

$$S(\mathbf{r}_f, t_f|\mathbf{p}_i, t_i) = \mathbf{p}_i\cdot\mathbf{r}_{t_i} + \int_{t_i}^{t_f} dt\, L\,[\mathbf{r}(t), \dot{\mathbf{r}}(t)] \tag{2.9}$$

is the action from a plane wave with momentum $\mathbf{p}_i$ at time t_i to position $\mathbf{r}_f$ at time t_f. $\mathbf{r}(t)$ is the classical trajectory of the atom, with the boundary conditions that $\mathbf{p}(t_i) = \mathbf{p}_i$ and $\mathbf{r}(t_f) = \mathbf{r}_f$. $\mathbf{r}_i$ of course depends on p_i and r_f, since it must lie on the classical trajectory. Note that ψ in Eq. (2.8) is not normalised, since we are dealing with nearly plane waves.

Since it is often the case that the perturbed trajectory $\mathbf{r}(t)$ is not analytically known whilst the unperturbed trajectory $\mathbf{r}_0$ describing the atomic motion under the Lagrangian L_0 is, it is useful to employ a perturbation calculation

which expands quantities in the small parameter ϵ:

$$\mathbf{r}(t) = \mathbf{r}_0(t) + \epsilon \mathbf{r}_1(t) + \epsilon^2 \mathbf{r}_2(t) + \cdots , \tag{2.10}$$

where $\mathbf{r}_0(t)$ is the classical trajectory for the unperturbed lagrangian L_0 which has its endpoint at $\mathbf{r}_f$. One also expands the action:

$$S = S_0 + \epsilon S_1 + \epsilon^2 S_2 + \cdots , \tag{2.11}$$

where it can be shown [38] that:

$$\begin{aligned} S_0 &= \mathbf{p}_i \cdot \mathbf{r}(t_i) + \int_{t_i}^{t_f} dt\, L_0[\mathbf{r}_0(t), \dot{\mathbf{r}}_0(t)] , \\ S_1 &= -\int_{t_i}^{t_f} dt\, V[\mathbf{r}_0(t)] , \\ S_2 &= -\frac{1}{2}\int_{t_i}^{t_f} dt\, \mathbf{r}_1(t) \cdot \nabla V[\mathbf{r}_0(t)] \ldots \end{aligned} \tag{2.12}$$

The point of these expansions is that the classical trajectory $\mathbf{r}_0(t)$ which describes the motion of the atom in a purely reflective running wave potential can be calculated analytically, and is in fact given by

$$\begin{aligned} x_0(t) &= x_i + p_{i,x} t/m , \\ y_0(t) &= -\frac{1}{2q} \ln \left[\frac{p_{i,y}^2}{2mV_0} \mathrm{sech}^2(q p_{i,y} t/m) \right] . \end{aligned} \tag{2.13}$$

The expansion (2.12) is now truncated after the first two terms. The second term describes the phase-shift accumulated along the *unperturbed* trajectory due to the presence of the standing wave part of the potential $\epsilon V(\mathbf{r})$. Provided that the *actual* trajectory $\mathbf{r}(t)$ is similar enough to the unperturbed trajectory $\mathbf{r}_0(t)$, this expansion will account for the diffracted populations. Under the perturbation calculation discussed here, this is done by simply taking the fourier transform of the final wavefunction calculated under Eq. (2.8)

For the evanescent wave potential of Eq. (2.4), the expression for the populations in the various orders n is given by a Bessel function [38].

2.5.1 The thin phase-grating interpretation

An insight into the physics of scalar atomic diffraction can be gained by approximating the potential as a hard wall describing a level curve on the evanescent wave potential. The height of the potential along this curve is equal to the initial kinetic energy in the y-direction (perpendicular to the glass). Thus the curve indicates points from which the atom is classically reflected.

This curve, in the x-y plane, is approximately described by

$$y(x) \approx \frac{\varepsilon}{2q} \cos 2Qx \,. \tag{2.14}$$

Thus, using the hard wall model, the incoming atom will acquire an x-dependent phase shift upon reflection from this barrier of $\delta\phi = 2k_{i,y}y(x)$. It can be shown [38, 43] that the condition for low order diffraction is that the variation in this phase shift is of order one. This is the case when the modulation depth $y(x)$ is comparable to the de-Broglie wavelength of the incoming atom in the direction perpendicular to the surface, a condition which occurs when the contrast ε is small, since for normal conditions the de-Broglie wavelength of the atom is much smaller than the optical decay length q.

2.5.2 The effect of angle of incidence

Because the primary advantage of an evanescent wave reflection grating is its ability to produce large angle (well separated) diffraction orders using moderate laser power when the atoms approach the glass at grazing incidence, one would like to be able to obtain high diffraction efficiency at these angles. Unfortunately, the scalar model of diffraction predicts a rapid dropoff in the diffraction efficiency as the angle of incidence is decreased from normal. This decrease is related to the fact that, during the time the atom spends inside the interaction region, its classical trajectory will traverse a number of wavelengths of the standing wave which increases from zero at normal incidence as the angle of incidence is decreased. If the number of wavelengths traversed is much greater than one then all classical trajectories with the same incidence angle will acquire a similar phase shift due to the standing wave and hence diffraction will not be efficient. In essence, the rapid variation of the potential over the path of the atom tends to average out to zero.

This explanation shows why the 'softness' of the evanescent potential is important to take into account, since if the potential were infinitely steep, like a perfect optical mirror, then the time spent in the interaction region would be negligible and the atom would only see one point on the standing wave. In this case, efficient diffraction would occur for all incidence angles. Thus, as was mentioned in the introduction to this chapter, the analogy with an optical reflection grating is flawed and the 'thin phase grating' interpretation of Section 2.5.1 is a more accurate analogy.

2.5.3 Comparison with experiments

Experiments showing diffraction in the regime of scalar diffraction have been performed by the group at the Orsay Institut d'Optique [5]. In these experiments, trapped atoms were dropped at normal incidence onto an evanescent wave grating. They found a very good agreement with theory, although in the paper [5] the individual diffraction orders could not be resolved due to the fact that the incoming atoms were dropped at normal incidence and hence the diffraction angles were very small. The populations in the various diffraction orders could be varied by adjusting the ratio of the forward and retro-reflected intensities. As was suggested in Section 2.5.1, a high diffraction efficiency for the lowest orders was observed for a small contrast ϵ equivalent to a retroreflected beam with only 10^{-4} of the intensity of the forward beam.

2.6 The two-level model

The scalar model of atomic diffraction relies on the fact that the atom always remains in the dressed state $|1\rangle$ from Eq. (1.3). This may not always be the case, since resonant transitions can occur. In order to study this possibility, we must abandon the scalar model and introduce a model in which the atom has internal structure. As will be shown in the next section, a model incorporating a description of the full hyperfine structure of the transition is most useful for describing a high-efficiency beamsplitter. However, a simpler two-level model is useful for illustrative purposes and can be used to explain certain features of evanescent gratings such as absorptive doppleron resonances [44–48].

The atom is described by a ground state and an excited state, $|g\rangle$ and $|e\rangle$ respectively. The external motion of the atom is represented in the position basis in the y-direction and the momentum basis in the x-direction:

$$|\Psi(t)\rangle = \sum_n \int dy\, \Psi_n(y,t)\, |n\rangle\, |y\rangle\ . \tag{2.15}$$

Here $|n\rangle$ represents the outer product between x-momentum eigenstate with $p_x = p_{i,x} + n\hbar Q$ and the state $|g\rangle$ in the case of even n and $|e\rangle$ in the case of odd n. If the initial state of the atom is an eigenstate of the x-component of the momentum operator, then the periodicity of the potential in the x-direction ensures that the atom can only acquire momentum in packets of $\hbar Q$, and hence the state (2.15) gives a total description of the atomic motion. Thus the discrete expansion of the motion in the x-direction is justified.

We label the copropagating electric field component by the subscript 1 and the counterpropagating component by the subscript 2. The light field is then

given by:

$$E(\mathbf{r},t) = [E_1 e^{iQx} + E_2 e^{-iQx}]e^{-qy}e^{-i\omega_l t} + \text{H.c.}\,, \tag{2.16}$$

where E_1 and E_2 are the amplitudes of the copropagating and counterpropagating beams respectively, and ω_l is the laser frequency. Thus the positive frequency component of the light field is:

$$E^+(\mathbf{r}) = [E_1 e^{iQx} + E_2 e^{-iQx}]e^{-qy}\,. \tag{2.17}$$

In the interaction picture discussed in Section 1.1.1 (with $\hat{H}_0 = \hbar\omega_L |e\rangle\langle e|$), and using the rotating wave approximation, the Hamiltonian for the system is:

$$\hat{H} = \frac{\hat{p}_y^2}{2m} + \frac{\hat{p}_x^2}{2m} + \hat{H}_{\text{int}} + \hat{H}_{ED}\,, \tag{2.18}$$

where $\hat{p}_y^2/2m = -\hbar^2\nabla^2/2m$ is the kinetic energy in the y-direction,

$$\frac{\hat{p}_x^2}{2m} = \frac{1}{2m}\sum_n (p_{i,x} + n\hbar Q)^2 |n\rangle\langle n| \tag{2.19}$$

is the kinetic energy in the x-direction, and

$$\hat{H}_{\text{int}} = \sum_{n(\text{odd})} \hbar\Delta |n\rangle\langle n| \tag{2.20}$$

is the internal energy of the atom. $\hat{H}_{ED}$ is the electric dipole interaction of the atom with the light field, defined with reference to Section 1.1.1 as $\hat{H}_{ED} = d^+E^+(\mathbf{r}) + \text{H.c}$, where $\hat{d} = d^+ + \text{H.c.}$ is the electric dipole moment operator for the atom:

$$\hat{d}^+ = d\,|e\rangle\langle g|\,. \tag{2.21}$$

The light-dipole interaction $\hat{d}^+E^+(\mathbf{r})$ is thus given in our basis by:

$$\hat{d}^+E^+(\mathbf{r}) = d\,e^{-qy}\left[E_1 \sum_{n,\text{even}} |n+1\rangle\langle n| + E_2 \sum_{n,\text{odd}} |n+1\rangle\langle n|\right]\,. \tag{2.22}$$

To calculate the amount of diffraction into the various diffraction orders, one can take two distinct approaches: one can solve the stationary Schrödinger equation for boundary conditions corresponding to an incoming momentum eigenstate with a suitably vanishing or exponentially decaying wavefunction at the glass surface [40,46,49,50], or one can directly solve the time dependent Schrödinger equation for an incoming wavepacket [34,48]. The latter approach was used for the multi-level calculations presented in this chapter.

2.6.1 Adiabatic quasipotentials

A particularly useful interpretational description of the diffraction process can be gained by considering the *adiabatic quasipotentials* of the system [51]. These are the eigenstates of the Hamiltonian (2.18) minus the kinetic energy term $\hat{p}_y^2/2m$. Since the amplitude of the light field depends on y, the quasipotentials are a function of y.

The quasipotentials are different from normal potentials in that they include the x-component of momentum. Nonetheless, in the sense that they specify the energy of the atom as a function of y, they are conceptually no different from real potentials. In the quasipotential basis, the various quasipotentials for a given value of y are not coupled, since they result from diagonalising part of the Hamiltonian. However, the quasipotential basis changes as y is varied. This means that the motion of the atom in the y-direction can couple the quasipotentials. However, if this motion is slow enough, then the adiabatic theorem tells us that an atom travelling in a quasipotential will remain within that quasipotential.

The adiabatic quasipotentials for a purely reflective grating are shown in Fig. (2.3(a)). Several features are apparent. In the region to the right of the figure, where the intensity of the light field is negligible, the quasipotentials are given by the energies

$$\begin{aligned} E_{\infty,n(\text{even})} &= (1/2m)[p_{i,x}^2 + 2p_{i,x}n\hbar Q + n^2\hbar^2Q^2] \\ &= p_{i,x}^2/(2m) + n\hbar\Delta_D + n^2\hbar\Delta_R\,, \\ E_{\infty,n(\text{odd})} &= (1/2m)[p_{i,x}^2 + 2p_{i,x}n\hbar Q + n^2\hbar^2Q^2] + \hbar\Delta \\ &= p_{i,x}^2/(2m) + n\hbar\Delta_D + n^2\hbar\Delta_R + \hbar\Delta\,, \end{aligned} \tag{2.23}$$

where Δ_D and Δ_R are the Doppler and recoil shifts defined previously. As the atom approaches the grating, the ground state (n even) quasipotentials experience a repulsive potential whereas the excited state quasipotentials experience an attractive potential. Since, for normal conditions, the rate of change of the electric field experienced by the atom is much slower than its internal precession frequency, the atom will adiabatically remain in its initial quasipotential.

If we introduce a retroreflected beam, then the quasipotentials undergo a qualitative change, see Fig. (2.3(b)); at points where the excited state and ground state quasipotentials would normally cross, *avoided crossings* appear. These avoided crossings lead to non-adiabatic motion, resulting in a partial transfer of the atomic wavefunction from one quasipotential to another. The non-adiabatic motion is due to two factors: (a) the quasipotentials are nearly degenerate at the point where the crossing occurs, and (b) the slope of the quasipotentials is rapidly changing, so that the assumption that the atoms sees

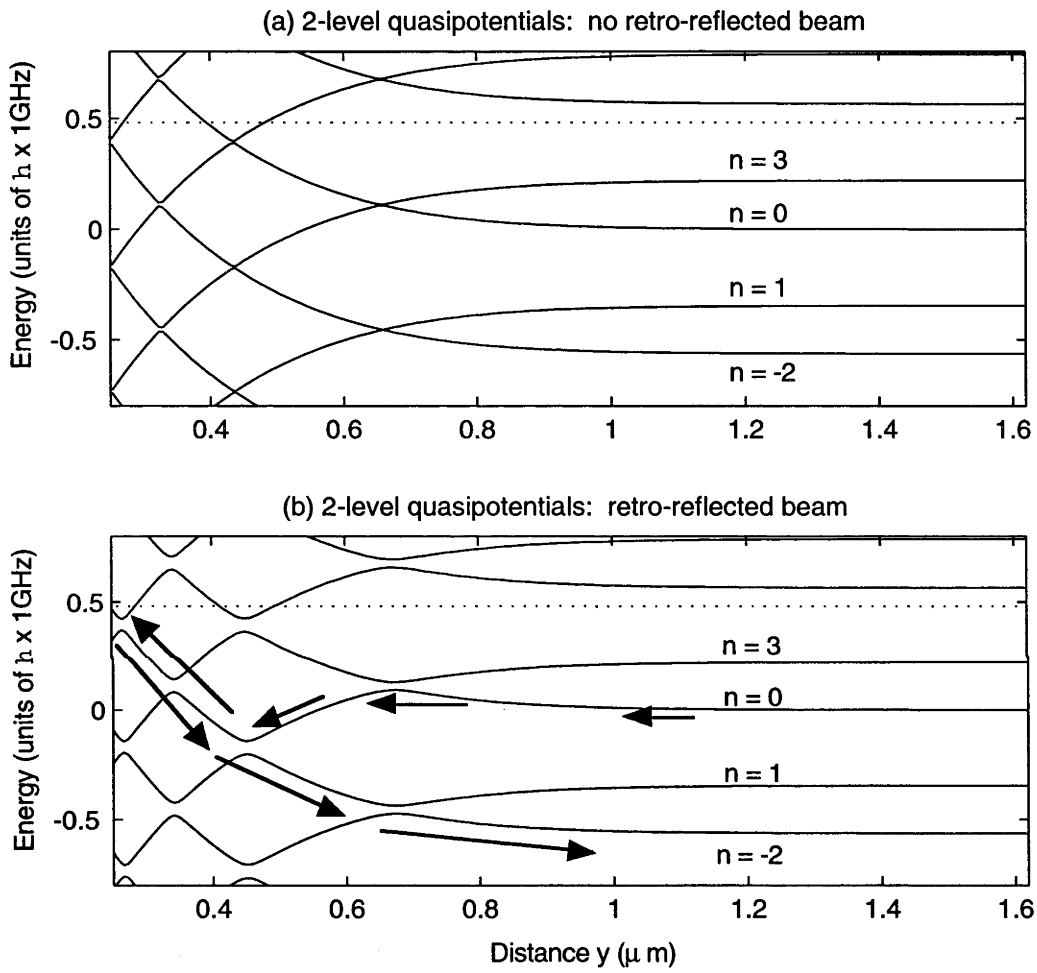

Figure 2.3: (a) Adiabatic quasipotentials for a two-level atom and a purely reflective grating. Atoms are incident at 25 ms^{-1} at an angle of 70 mrad. Laser detuning is 100 MHz. (b) The addition of a counterpropagating beam leads to resonant transitions between quasipotentials (avoided crossings). A possible route leading to $n = -2$ diffraction is shown by the arrows.

a slowly changing potential is no longer applicable and hence the adiabatic theorem no longer holds. This non-adiabatic behaviour is shown schematically in Fig. (2.4). The avoided crossings act as effective beamsplitters with variable transmission and reflection coefficients which depend on parameters such as the detuning and the ratio between the copropagating and counter-propagating beam intensities.

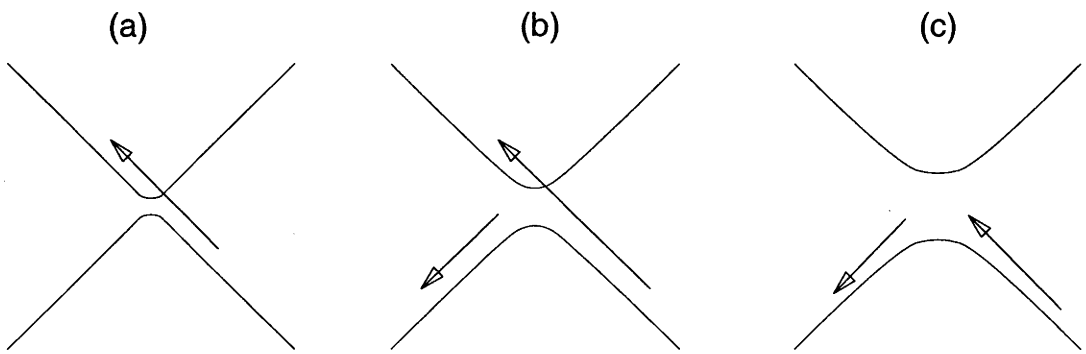

Figure 2.4: Schematic motion of the atom in an avoided crossing. Motion is shown by the arrows (a) Narrow crossing: mainly diabatic motion. (b) Medium crossing produces a beam-splitting effect. (c) Wide crossing: mainly adiabatic motion.

A mechanism for two-level diffraction can now be given. The atomic wavepacket approaches the glass surface and is split into partial waves by the avoided crossings. These partial waves propagate along the quasipotentials, splitting at each crossing, and are eventually either reflected or reach the glass surface. The reflected partial waves propagate back through the system and emerge in the various diffraction orders. For example, in Fig. (2.3), a possible atomic trajectory leading to $n = -2$ diffraction is shown.

In order to obtain ground state diffraction the partial wavepackets must traverse at least two avoided crossings. This is because there are no ground-ground crossings, only ground-excited crossings, and hence an excited state quasipotential must act as an intermediate state in the transfer of the wavefunction between two ground state quasipotentials. Furthermore, we are limited to paths where reflection occurs, meaning that at least the same number of crossings must be traversed on the return journey. In fact it can be shown (as is suggested by a careful study of Fig. (2.3(b))), that at least four crossings must be involved in the process of ground state diffraction [51]. It is shown in [51] that this condition means that the optimum diffraction efficiency into a ground state diffraction order is $0.5^4 \approx 6\%$.

This means that a diffraction grating operating on the principles outlined in this discussion of the two-level model will not function as an efficient beamsplitter. This is due to two fundamental problems: the requirement that the

excited state must function as an intermediary in the diffraction process and the necessity to obtain reflection even though the excited quasipotentials are attractive. In the next section, we will see that these problems can be overcome by taking advantage of the possibilities inherent in the full multi-level nature of atomic transitions. Furthermore, we shall show that the multi-level model is able to explain experimental results [41] which are not explained by the two-level model.

2.7 The multi-level model

In 1994 Christ *et. al.* [41] were able to observe diffraction in a slowed beam of metastable atoms. The parameters of the experiment are shown in Table (2.1). The two-level quasipotentials for these parameters are shown in Fig. (2.5(a)). It is immediately apparent from this figure and the discussion of the preceding section that this system will not exhibit diffraction; the crossings are so narrow that the atomic motion will be diabatic. The reason for this is made apparent when one looks at the parameters in Table (2.1). We see that the detuning Δ is some twenty times larger than the doppler shift $\Delta_D = p_{i,x}Q/m$. This means that the incoming $n = 0$ quasipotential crosses the $n = 21, 23, \ldots$ excited state quasipotentials. Any transfer into these orders would involve at least a 21 photon process and hence be an extremely narrow resonance [1]. This accounts for the narrowness of the crossings for the experimental parameters.

Nonetheless, the experiment [41] observed a diffraction efficiency into the $n = -2$ order of around 3%, half of the theoretical maximum possible for the two-level model, given ideal parameters. Clearly these results are not explained by the two-level model.

This discrepancy between experiment and theory can be resolved by taking into account the full multi-level nature of the relevant atomic transition. This multi-level structure takes into account the various magnetic sublevels of the atomic transition. As an example, we shall first consider the 3s[3/2]2 $\leftrightarrow$ 3p'[3/2]2 transition of metastable neon which is the transition relevant to the experiment [41]. Fig. (2.6) shows this transition schematically. The various magnetic sublevels of the ground and excited state are coupled by the components of the light field in a circularly polarised basis - for example, the $m_g = -2$ and $m_e = -1$ levels are coupled by the σ_+ (left circularly polarised) component

[1] For example, if we were to treat the coupling of the ground and excited state quasipotentials using perturbation theory, then this process would only appear at the 21st-order in the perturbation expansion. Hence the presence of the excited state will have a negligible effect on the system. In terms of the quasipotentials, this means that the motion at the crossing is almost entirely diabatic.

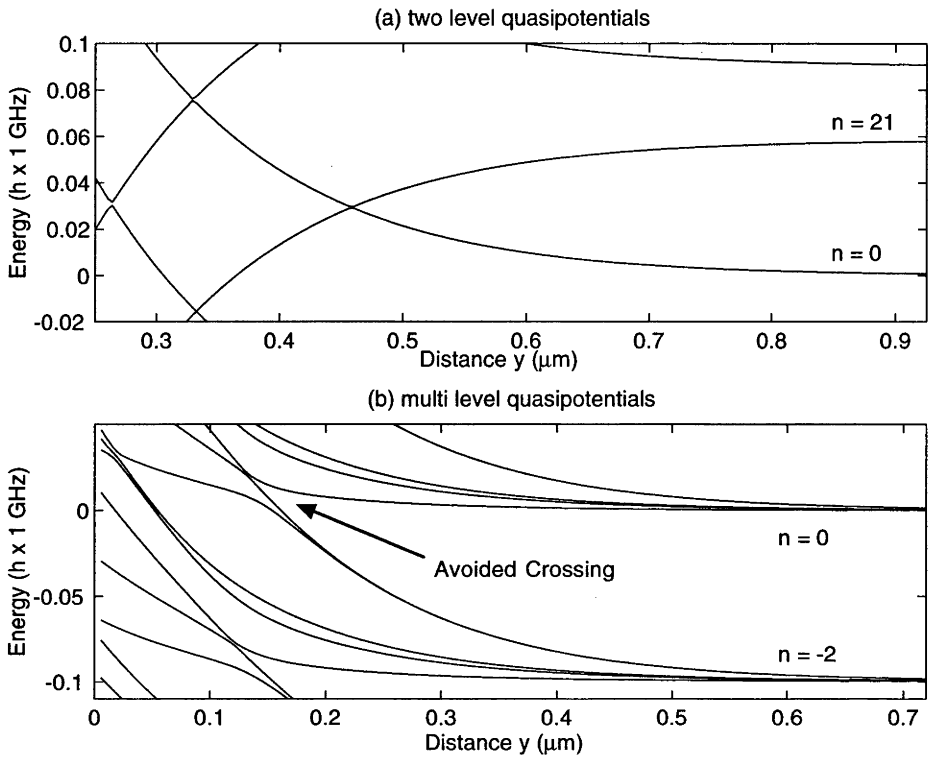

Figure 2.5: Quasipotentials for the parameters of the experiment [41] (see Table (2.1)). (a) Two-level quasipotentials (b) Multi-level quasipotentials for a laser polarisation angle of $5°$ away from p-polarisation (see Section (2.7.1)).

of the light field whereas the $m_g = -2$ to $m_e = -2$ sublevels are coupled by the π component. The complex nature of this transition has several consequences.

Firstly, each diffraction order n representing a particular value of the x-component of momentum outside the interaction region should be split into five quasipotentials by the light field. This is because each magnetic sublevel is coupled to the light field through a different Clebsch-Gordan coefficient, and also through different polarisation components of the field. Secondly, we see that by varying the polarisation components of the field we can vary the couplings to the various sublevels and thus should be able to change the behaviour of the quasipotentials inside the interaction region. Thus the polarisation of the incoming laser beams should allow us to have some control over the amount of diffraction into various orders.

Fig. (2.5(b)) shows the quasipotentials for this transition in metastable Neon. The excited state quasipotentials are omitted for clarity, but as in the two-level model Fig. (2.5(a)) their interaction with the ground state quasipotentials is negligible due to the large value of the detuning. We see that the

Table 2.1: Parameters used in experiment of Christ *et al.* [41].

Parameter	Value
Atom	Ne*
Atom mass	3.3×10^{-26} kg
Atomic velocity	25 ms^{-1}
Angle of incidence	36 mrad
Laser detunings	900 MHz
Transition wavelength	594.5 nm
k	1.058×10^{7} m^{-1}
Q	1.10×10^{7} m^{-1}
q	2.72×10^{6} m^{-1}

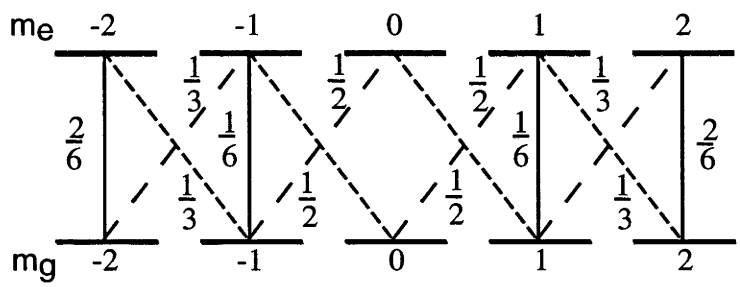

Figure 2.6: Schematic diagram of the atomic level structure used in the model. The squares of the Clebsch-Gordan coefficients for the transitions are shown.

various orders n are indeed split into five in the multi-level model. This figure suggests a mechanism for efficient multi-level diffraction. The wavepacket approaches the avoided crossing labelled in the figure where it is split into two partial wavepackets. Both of these partial wavepackets are subsequently reflected from the repulsive potential, and after passing through the avoided crossing once more they exit the field in the $n = 0$ and $n = -2$ diffraction orders. Assuming that all of the initial wavepacket can be made to enter the field in the particular quasipotential which sees the avoided crossing, a 50% transmission/reflection coefficient in the crossing will lead to a 50/50 ratio in the diffracted and reflected atomic beams. This latter assumption may be hard to guarantee in practice without careful optical pumping of the incoming atoms, however, it is often the case that several avoided crossings are involved in the interaction with the light field and thus most of the incoming wavepacket is

diffracted to some degree. In the limit where there are many avoided crossings of varying transmission/reflection ratios, the atoms are well and truly 'mixed up' by the interaction with the light field and a diffraction efficiency of close to 50% is likely to result.

This mechanism of diffraction solves the two problems mentioned in Section 2.6.1. The problem of obtaining reflection is overcome by the fact that all ground state sublevels remain reflective even where avoided crossings are involved, and the problem of requiring an intermediate excited state population to obtain ground state diffraction is not present in this model, since ground state quasipotentials can now quite easily cross due to the multiple splitting of each order n. These ground-ground crossings describe two (or four, six ...) photon transitions (Raman transitions). The excited state acts only as a virtual intermediate state in each particular transition; it is never in resonance and thus does not become permanently populated.

In what follows, we shall extend the theory of Section 2.6 to the multi-level model. In Section 2.7.2 we shall adiabatically eliminate the excited state sublevels from this model. Section 2.8 will extend the theory to more complex level structures involving several excited state manifolds. Numerical results for metastable Ne and Cs will be presented in Sections 2.11 and 2.12

2.7.1 Derivation of the multi-level Hamiltonian

Here we consider a case like that of metastable Neon, in which the transition is between ground and excited states each consisting of a manifold of magnetic sublevels for a single total angular momentum quantum number F. Later we shall see that the situation is greatly complicated when the excited state consists of a series of hyperfine levels - for example the case of the Cs 6s[3/2]2$\leftrightarrow$ 6p'[3/2]2 transition which is between a ground state with angular momentum F = 5 and an excited state manifold consisting of hyperfine levels with F = 5,4,3 and 2.

We use the spatial orientation given in Fig. (2.1) and build on the description of the two-level model presented in Section 2.6. Clearly, the condition that the momentum in the x-direction is discrete and takes the values $p_x = p_{i,x} + n\hbar Q$ still holds, so that we can use the description of state given by Eq. (2.15) with an additional discrete degree of freedom m denoting the magnetic sublevel:

$$|\Psi(t)\rangle = \sum_{n,m} \int dy\, \Psi_{n,m}(y,t)\, |n,m\rangle\, |y\rangle\ , \tag{2.24}$$

where m runs from $-F_g$ to F_g for the ground state (even n) orders and from

$-F_e$ to F_e for the excited state (odd n) orders, with F_g and F_e being the total angular momentum numbers for the ground and excited levels respectively. In order to simplify the Hamiltonian in what follows, we employ the following ansatz in order to shift the zero point of the energy so that the incoming $n = 0$ order has zero energy:

$$|\Psi(y,t)\rangle = \exp(-i\hbar p_{i,x}^2 t/2m) \sum_{n,m} \Psi_{n,m}(y,t)\,|n,m\rangle\ . \tag{2.25}$$

Since the transitions between the various sublevels now depend on the circular polarisation components of the evanescent light field, we must now take into account the polarisation of the evanescent field. We write

$$\mathbf{E}(\mathbf{r},t) = [\mathbf{e}_1 E_1 e^{iQx} + \mathbf{e}_2 E_2 e^{-iQx}]e^{-qy}e^{i\omega_l t} + \text{H.c.}\,, \tag{2.26}$$

where $\mathbf{e}_{1,2}$ are the field polarisation vectors for the copropagating and counterpropagating evanescent beams and E_1 and E_2 are their respective amplitudes, assumed real for convenience. The positive frequency component of the electric field is now defined as

$$\mathbf{E}^+(\mathbf{r}) = [\mathbf{e}_1 E_1 e^{iQx} + \mathbf{e}_2 E_2 e^{-iQx}]e^{-qy}\,, \tag{2.27}$$

and the negative frequency component is $\mathbf{E}^- = (\mathbf{E}^+)^*$.

Using the same interaction picture and RWA (rotating-wave approximation) as that used in Section 2.6, we have the Hamiltonian

$$\hat{H} = \frac{\hat{p}_y^2}{2m} + \frac{\hat{p}_x^2}{2m} + \hat{H}_{\text{int}} + \hat{V}_{AL}\,, \tag{2.28}$$

where, as before, we have that $\hat{p}_y^2/2m = -\hbar^2\nabla^2/2m$ is the kinetic energy in the y-direction,

$$\frac{\hat{p}_x^2}{2m} = \frac{1}{2m}\sum_n (p_{i,x} + n\hbar Q)^2\,|n\rangle\langle n| \tag{2.29}$$

is the kinetic energy in the x-direction, and

$$\hat{H}_{\text{int}} = \sum_{n(\text{odd})} \hbar\Delta\,|n\rangle\langle n| \tag{2.30}$$

is the internal energy of the atom. The term $\hat{V}_{AL}$ is more complicated than is the case for a two-level atom, due to the vector nature of the coupling between the hyperfine levels and the light field:

$$\hat{V}_{AL} = \mathbf{d}^+ \cdot \mathbf{E}^+ + \text{H.c.}\,, \tag{2.31}$$

where $\mathbf{d}^+$ is the positive frequency part of the electric dipole moment operator for the given transition:

$$\mathbf{d}^+ = \sum_{m_g,m_e} |m_e\rangle\langle m_e|\mathbf{d}|m_g\rangle\langle m_g|\,, \tag{2.32}$$

with m_g running from $-F_g$ to F_g and m_e from $-F_e$ to F_e.

We take the z direction as the quantisation axis and work with a spherical basis of polarisation vectors $\{\mathbf{u}_\pm, \mathbf{u}_0\}$ defined in terms of the Cartesian unit vectors by

$$\mathbf{u}_\pm = \frac{1}{\sqrt{2}}(\mathbf{u}_x \pm i\mathbf{u}_y), \quad \mathbf{u}_0 = \mathbf{u}_z\,. \tag{2.33}$$

In such a basis the components of $\mathbf{d}^\pm$ are components of a spherical tensor operator of rank 1 [52], and thus by applying the Wigner-Eckert theorem we can calculate their matrix elements up to a constant factor:

$$\langle m_e|d^q|m_g\rangle = \mathcal{D}\langle 2\ 1\ m_g\ q|2\ 1\ 2\ m_e\rangle\,, \tag{2.34}$$

where the term $\langle 2\ 1\ m_g\ q|2\ 1\ 2\ m_e\rangle$ is a Clebsch-Gordan coefficient and $\mathcal{D}$ is a reduced matrix element which does not depend on m_g or m_e. Hence it follows that

$$\begin{aligned}\hat{V}_{AL} &= \mathcal{D}e^{(-qy)} \sum_{q,m_g,m_e,n_g} \begin{array}{l} E_1\,\langle F_g 1 m_g q|F_g 1 F_e m_e\rangle\, e_{1,q}\,|m_e, n+1\rangle\langle m_g, n| \\ +\, E_2\,\langle F_g 1 m_g q|F_g 1 F_e m_e\rangle\, e_{2,q}\,|m_e, n-1\rangle\langle m_g, n| \end{array} \\ &+ \text{H.c.}\end{aligned} \tag{2.35}$$

For convenience we break up the Hamiltonian as follows:

$$\hat{H} = \hat{H}_A + \hat{V}_{AL}\,. \tag{2.36}$$

The energy of the atom excluding its interaction with the light field, $\hat{H}_A$, is:

$$\hat{H}_A = \frac{\hat{p}_y^2}{2m} + \sum_{n,m} W_n|nm\rangle\langle nm|\,, \tag{2.37}$$

with W_n defined by:

$$W_n = \begin{cases} (2n\hbar Q p_{i,x} + n^2\hbar^2 Q^2)\,|n\rangle\langle n| & \text{n even} \\ (2n\hbar Q p_{i,x} + n^2\hbar^2 Q^2 + \hbar\Delta)\,|n\rangle\langle n| & \text{n odd.} \end{cases} \tag{2.38}$$

The atom-field interaction term, $\hat{V}_{AL}$ is:

$$\hat{V}_{AL} = \sum_{q,m_g,m_e,n\text{even}} V_{(1)}^{qm_g m_e}|n+1\ m_e\rangle\langle n\ m_g| + \text{H.c.}$$

$$+ \sum_{q,m_g,m_e,n\text{even}} V_{(2)}^{q,m_g,m_e} |n-1\ m_e\rangle\langle n\ m_g| + \text{H.c.}\,, \tag{2.39}$$

where

$$V_{(1)}^{q,m_e,m_g} = E_1 e_{1,q} \langle 2\ 1\ m_g\ q|2\ 1\ 2\ m_e\rangle \tag{2.40}$$

and

$$V_{(2)}^{q,m_e,m_g} = E_2 e_{2,q} \langle 2\ 1\ m_g\ q|2\ 1\ 2\ m_e\rangle \tag{2.41}$$

are the matrix elements describing the coupling of the various states via the two laser fields.

The polarisation of the evanescent wave

We can use Fresnel equations [53] to determine the polarisation of the evanescent wave in the spherical basis as a function of the polarisation of the incoming laser beam. We have in Cartesian coordinates that

$$\begin{aligned} E_x &= \frac{2n^2 \cos\theta_b \sin\theta_b}{\cos\theta_l + in\sqrt{n^2\sin^2\theta_l - 1}} E_p\,, \\ E_y &= \frac{2in\cos\theta_l\sqrt{n^2\sin^2\theta_l - 1}}{\cos\theta_l + in\sqrt{n^2\sin^2\theta_l - 1}} E_p\,, \\ E_z &= \frac{2n\cos\theta_l}{n\cos\theta_l + i\sqrt{n^2\sin^2\theta_l - 1}} E_s\,, \end{aligned} \tag{2.42}$$

where θ_l is the angle of incidence for the incoming laser beam, n is the refractive index of the prism, and E_s and E_p are the s and p polarisation components of the incoming laser beam (s-polarisation is normal to the plane of incidence and p-polarisation is in the plane of incidence). E_x, E_y and E_z are the Cartesian polarisation components of the evanescent wave. Note that, unlike a usual plane wave, evanescent waves can have a polarisation component in the direction of propagation. For a retroreflected beam, the components are the same as the copropagating beam except that E_x picks up a minus sign. Finally, since we actually require the spherical polarisation components, we have:

$$\begin{aligned} E_\pm &= \frac{1}{\sqrt{2}}(\mp E_x + iE_y)\,, \\ E_0 &= E_z\,. \end{aligned} \tag{2.43}$$

From these relations we can easily determine the components e_q of the polarisation vector of the evanescent wave.

2.7.2 Adiabatic elimination of the excited states

We have seen that the diffraction of an atom in the multi-level regime can occur for a detuning much higher than the doppler shift, and indeed, that this is desirable. A high detuning leads to lower spontaneous emission rates and negligible diffraction into excited state orders.

For detunings much larger than the doppler or recoil shifts, we can adiabatically eliminate the excited states. This provides a great computational advantage (especially in the case of complex atoms such as Cesium), as well as making the essential physics of diffraction more transparent.

For the Hamiltonian (2.36) and with the ansatz (2.25), we can write down a set of coupled Schrödinger equations for the ground and excited sublevels:

$$\begin{aligned} i\hbar\frac{\partial}{\partial t}\Psi^{(g)}_{n_g,m_g}(t) &= \left(\frac{\hat{p}_y^2}{2m}+W_n\right)\Psi^{(g)}_{n_g,m_g} \\ &+\sum_{q,m_e}\left\{\begin{array}{c}\left(V^{q,m_e,m_g}_{(1)n_g+1,n_g}\right)^*\Psi^{(e)}_{n_g+1,m_e}\\ +\left(V^{q,m_e,m_g}_{(2)n_g-1,n_g}\right)^*\Psi^{(e)}_{n_g-1,m_e}\end{array}\right\}, \end{aligned} \tag{2.44}$$

$$\begin{aligned} i\hbar\frac{\partial}{\partial t}\Psi^{(e)}_{n_e,m_e}(t) &= \left(\frac{\hat{p}_y^2}{2m}+W_n\right)\Psi^{(e)}_{n_e,m_e} \\ &+\sum_{q,m_g}\left\{\begin{array}{c}V^{q,m_e,m_g}_{(1)n_e,n_e-1}\Psi^{(g)}_{n_e-1m_g}\\ +V^{q,m_e,m_g}_{(2)n_e,n_e+1}\Psi^{(g)}_{n_e+1m_g}\end{array}\right\}, \end{aligned} \tag{2.45}$$

where $\Psi^{(g)}_{n_g,m_g}(t)$ is the coefficient of the basis vector $|n_g,m_g\rangle$ where n_g is even, and $\Psi^{(e)}_{n_e,m_e}(t)$ is the coefficient of the basis vector $|n_e,m_e\rangle$ where n_e is odd.

Since the energies of the excited states are large compared to other energies in the system due to the large detuning Δ, we assume that the populations of the excited states are small compared to the populations of the ground states. Under such an assumption, the LHS and the term containing $\hat{p}_y^2/2m$ in (2.45) are ignored. This gives

$$\Psi^{(e)}_{nm_e} \approx -\frac{1}{W_n}\sum_{q,m_g} V^{q,m_e,m_g}_{(1)n_e,n_e-1}\Psi^{(g)}_{n_e-1,m_g}+V^{q,m_e,m_g}_{(2)n_e,n_e+1}\Psi^{(g)}_{n_e+1,m_g}\,. \tag{2.46}$$

Substituting this into (2.44) gives

$$i\hbar\frac{\partial}{\partial t}\Psi^{(g)}_{n_g,m_g}(t) = \left(\frac{\hat{p}_y^2}{2m}+W_n\right)\Psi^{(g)}_{n_g,m_g}$$

$$
-\sum_{q,q',m_e,m_g'}
\left\{
\begin{array}{l}
\left(
\begin{array}{l}
V_{(1)n+1,n}^{q',m_e,m_g'}\left(V_{(1)n+1,n}^{q,m_e,m_g}\right)^*/W_{n+1} \\
+V_{(2)n-1,n}^{q',m_e,m_g'}\left(V_{(2)n-1,n}^{q,m_e,m_g}\right)^*/W_{n-1}
\end{array}
\right)\Psi_{n,m_g'}^{(g)} \\
+\left(V_{(1)n+1,n}^{q',m_e,m_g'}\left(V_{(2)n+1,n+2}^{q,m_e,m_g}\right)^*/W_{n+1}\right)\Psi_{n+2,m_g'}^{(g)} \\
+\left(V_{(2)n-1,n}^{q',m_e,m_g'}\left(V_{(1)n-1,n-2}^{q,m_e,m_g}\right)^*/W_{n-1}\right)\Psi_{n-2,m_g'}^{(g)}
\end{array}
\right\}. \tag{2.47}
$$

Thus the Hamiltonian with adiabatically eliminated upper states is:

$$
\hat{H} = \hat{H}_A + \hat{V}_{AL}\,, \tag{2.48}
$$

where $\hat{H}_A$ is identical to Eq. (2.37) except that the odd (excited) values of n are excluded, and $\hat{V}_{AL}$ is now defined by

$$
\hat{V}_{AL} = -\sum_{\substack{n,q,q' \\ m_e,m_g,m_g'}}
\left\{
\begin{array}{l}
\left(
\begin{array}{l}
\dfrac{V_{1,n+1,n}^{q',m_e,m_g'}\left(V_{(1)n+1,n}^{q,m_e,m_g}\right)^*}{W_{n+1}} \\
+\dfrac{V_{2,n-1,n}^{q',m_e,m_g'}\left(V_{(2)n-1,n}^{q,m_e,m_g}\right)^*}{W_{n-1}}
\end{array}
\right)|n,m_g\rangle\langle n,m_g'| \\
+\left(\dfrac{V_{(1)n+1,n}^{q',m_e,m_g'}\left(V_{(2)n+1,n+2}^{q,m_e,m_g}\right)^*}{W_{n+1}}\right)|n,m_g\rangle\langle n+2,m_g'| \\
+\left(\dfrac{V_{(2)n-1,n}^{q',m_e,m_g'}\left(V_{(1)n-1,n-2}^{q,m_e,m_g}\right)^*}{W_{n-1}}\right)|n,m_g\rangle\langle n-2,m_g'|
\end{array}
\right\}, \tag{2.49}
$$

The first two terms in the expression above represent interactions which are diagonal in n and thus cannot lead to diffraction, but manifest as both the light shift due interactions involving cycles of absorption from the copropagating/counterpropagating beam followed by an emission into the same beam, and a mixing of magnetic sublevels m_g belonging to a given level n_g. The second two terms represent cycles of absorption from the copropagating (counterpropagating) beam followed by emission into the counterpropagating (copropagating) beam, resulting in the transfer of units of $2n\hbar Q$ of momentum in the x-direction; it is these terms which are responsible for diffraction.

As a verification of this Hamiltonian, we compare the adiabatic quasipotentials for the parameters of Fig. (2.5) calculated with and without adiabatic elimination of the excited states. This comparison is shown in Fig. (2.7), and is seen to be quite good. The validity of the adiabatic elimination has been further verified up by numerical simulation of the diffraction process (see Section 2.11).

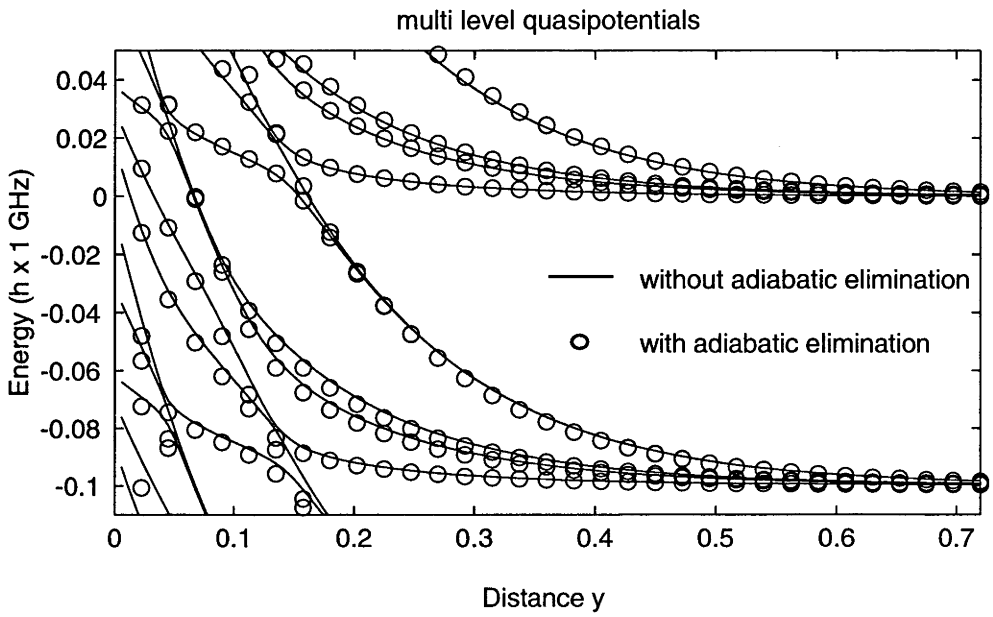

Figure 2.7: Comparison of adiabatic quasipotentials calculated with (circles) and without (solid line) adiabatic elimination of the excited state. Parameters are the same as Fig. (2.5). It can be seen that the comparison is quite good, and this fact has been backed up by direct numerical calculations of diffraction efficiency.

2.8 The case of Cesium: more complicated atoms

Many useful atomic transitions, such as the $6S_{1/2} \leftrightarrow 6P_{3/2}$ transition in Cesium 133, have a more complicated level structure than that of metastable neon. In what follows, we consider the $6S_{1/2} \leftrightarrow 6P_{3/2}$ Cs transition, however the theory is general and can be applied to other transitions.

The spin quantum number of the nucleus is $\frac{7}{2}$ and thus the ground ($6S_{1/2}$) state (with electronic angular momentum 1/2) will have total angular momentum quantum numbers F = 3 and 4 while the excited ($6P_{3/2}$) will have total angular momentum quantum numbers F = 2,3,4 and 5.

This can be seen in Fig. (2.8).

Since the hyperfine splitting between the F = 3 and F = 4 hyperfine levels of the ground state is large ($\approx$ 9GHz) while the hyperfine splitting between the excited hyperfine levels is small (of the order of 100 MHz), it is most accurate to consider the F = 4 ground state to F = 5,4,3,2 excited state transition. Atoms are prepared in this ground state and tend to remain in it due to a favourable branching ratio; those that do not will not be detected by the imaging system.

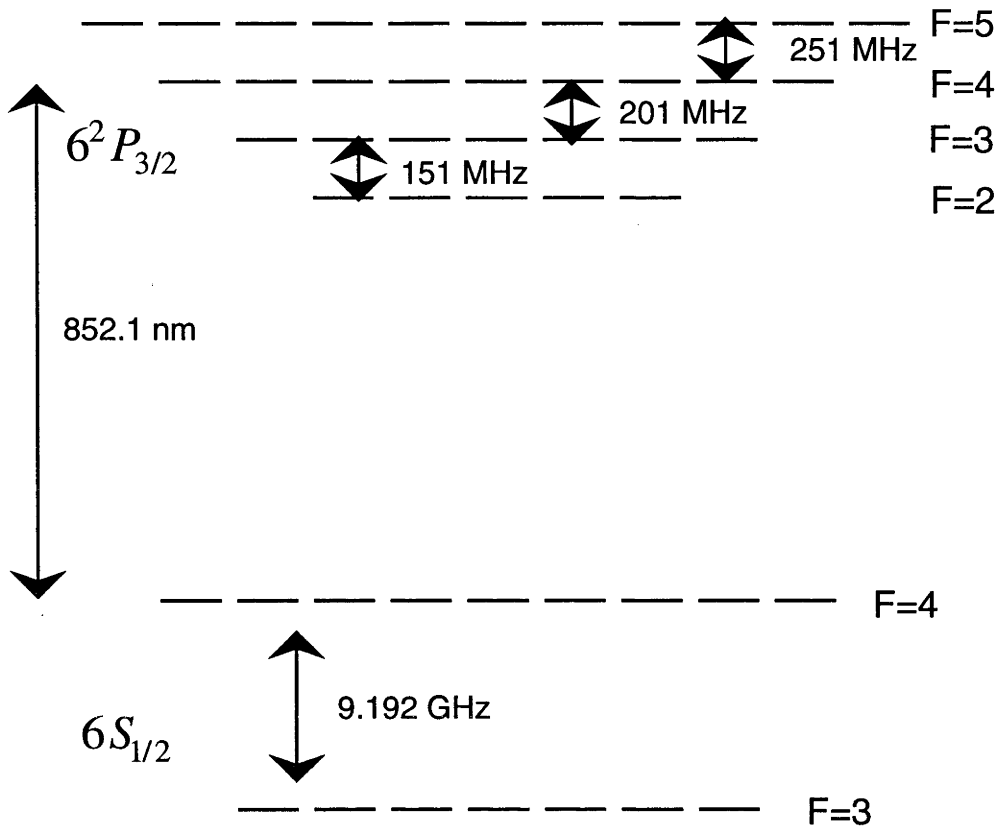

Figure 2.8: Schematic diagram of the $6S_{1/2} \leftrightarrow 6P_{3/2}$ Cs transition.

2.8.1 Calculating the matrix elements of the transition

The problem is now to calculate the matrix elements between the $F = 4$ ground state and the $F = 5, 4, 3$ excited states (the $F = 4$ to $F = 2$ transition is disallowed by the angular momentum selection rules). It is easy to calculate the Clebsch-Gordan coefficients between the $F = 4$ ground state and each excited state level taken individually. However, in order to obtain the correct splitting ratio for the various ground-excited transitions, we must perform a more complex calculation which takes into account the full angular-momentum structure of the transition by treating the nuclear and electric angular momentum separately.

We ultimately want to calculate the matrix elements $\langle F\ m_e|d^q|4\ m_g\rangle$. However, the laser field acts only on the electronic transition which is between $J_g = 1/2$ and $J_e = 3/2$. Thus we find dipole matrix elements in the basis of the electronic angular momentum quantum numbers and transform to the

basis of the total angular momentum quantum numbers:

$$\langle F\, m_e|d^q|4\, m_g\rangle = \sum_{m'_g m'_e m''} \left\{ \begin{array}{l} \langle 1/2\ 7/2\ m'_g\ m''|1/2\ 7/2\ 4\ m_g\rangle \\ \times\langle 3/2\ 7/2\ m'_e\ m''|3/2\ 7/2\ F\ m_e\rangle \\ \times\langle 3/2\ m'_e|d^q|1/2\ m'_g\rangle \end{array} \right\}. \qquad (2.50)$$

Here the top two terms in the curly braces are Clebsch-Gordan coefficients which express the change of basis between the basis consisting of a product space of electric and nuclear angular momentum and the basis consisting of the total angular momentum. The bottom term is the matrix element of the electronic transition (note that this transition is, of course, diagonal in the nuclear angular momentum). The nuclear spin is $7/2$ and the electric spin is $3/2$. The quantum number m'' gives the component of nuclear angular momentum in the direction of quantisation. The quantum numbers m'_g and m'_e give the components of the electric angular momentum in the direction of quantisation for the ground and excited states respectively. The Wigner-Eckert theorem can be applied to the last term above, and finally we have

$$\langle F\, m_e|d^q|4\, m_g\rangle = \sum_{m'_g m'_e m''} \left\{ \begin{array}{l} \langle 1/2\ 7/2\ m'_g\ m''|1/2\ 7/2\ 4\ m_g\rangle \\ \times\langle 3/2\ 7/2\ m'_e\ m''|3/2\ 7/2\ F\ m_e\rangle \\ \times\langle 1/2\ 1\ m'_g\ q|1/2\ 1\ 3/2\ m'_e\rangle \\ \times\mathcal{D} \end{array} \right\}, \qquad (2.51)$$

where $\mathcal{D}$ is a reduced matrix element which does not depend on the angular momentum quantum numbers.

The transition between the $F = 4$ ground state level and the $F = 2$ excited state is not allowed by the angular momentum selection rules, and this is indeed true for the formula given above.

2.9 Spontaneous emission

The interaction of atoms with light always carries with it the possibility of spontaneous emission. In the current context, the reflective potential is formed by a blue detuned laser field interacting with the atoms via the dipole force. This puts a fraction of the atomic population into the excited state and hence permits spontaneous emission.

In the following section, we estimate the spontaneous emission rates for atoms interacting with an evanescent wave laser field. We shall first consider the case of a purely reflective running wave field and then discuss the applicability of the results to the case of a partially standing wave and to the multi-level model.

2.9.1 Spontaneous emission for the scalar model

If the excited state population at time t is $p_e(t)$, then the spontaneous emission rate will be equal to γp_e, where γ is the excited state decay rate. Hence the proportion of atoms p_n which have not undergone spontaneous emission at time t satisfies the following differential equation:

$$\frac{d}{dt}p_n(t) = \gamma p_e(t)p_n(t)\ ,\ p_n(t_i) = 1, \tag{2.52}$$

which has the solution

$$p_n(t_f) = \exp\left(-\gamma \int_{t_i}^{t_f} p_e(t)\, dt\right) \tag{2.53}$$

For a two level atom moving adiabatically in a blue detuned laser field, we have from Eq. (1.3) that the excited state population is

$$p_e = \frac{1}{2}\left(1 + \frac{\Delta}{\sqrt{\Delta^2 + \Omega^2}}\right) \tag{2.54}$$

where it should be remembered that Δ is negative due to the blue detuning. If we assume that we are in the regime where p_e is small and hence adiabatic elimination of the excited state applies, then $\Delta \gg \Omega$ and hence we have

$$p_e \approx \frac{1}{4}\frac{\Omega^2}{\Delta^2} = \frac{d^2|E|^2}{\hbar^2\Delta^2}. \tag{2.55}$$

However, the scalar potential experienced by the atom is given by:

$$V(\mathbf{r}) = \frac{d^2|E(\mathbf{r})|^2}{\hbar\Delta} \tag{2.56}$$

and hence we have

$$p_e \approx \frac{V}{\hbar\Delta}. \tag{2.57}$$

For a scalar atom moving in such a potential, the classical trajectory is given by

$$y(t) = -\frac{1}{2q}\ln\left(\mathrm{sech}^2\left(\frac{qp_{0,y}t}{m}\right)\right). \tag{2.58}$$

This is the same as Eq. (2.13), except that the origin of the y-coordinate has been shifted to correspond with the classical turning point of the atom. At this point, the potential will have the value $p_{0,y}^2/(2m)$, and hence the potential is given by

$$V(y) = \frac{p_{0,y}^2}{2m}\exp(-2qy) \tag{2.59}$$

From this expression and Eqs. (2.57,2.59) we can deduce the excited state population as a function of t:

$$p_e(t) = \frac{p_{0,y}^2}{2m\hbar\Delta}\text{sech}^2\left(\frac{qp_{0,y}t}{m}\right) \tag{2.60}$$

and finally we integrate Eq. (2.53) from $t = -\infty$ to $t = \infty$ to obtain:

$$p_{n,\text{final}} = \exp\left(-\frac{\gamma p_{0,y}}{q\hbar\Delta}\right) \tag{2.61}$$

If we demand that this value be greater than, say e^{-1} then we obtain the condition that

$$\frac{\gamma p_{0,y}}{q\hbar\Delta} < 1 \tag{2.62}$$

in order for spontaneous emission to be limited to a reasonable level.

The physical significance of this expression is easy to interpret. If the momentum of the atom is large, then it penetrates further into the evanescent field and hence the spontaneous emission goes up. A small decay length $(1/q)$ corresponds to a sharp potential, which reflects the atom over a shorter timescale, thus reducing spontaneous emission. A large detuning also leads to a smaller amount of spontaneous emission, due to the inverse relationship between the excited state population and the detuning for a given potential.

2.9.2 Applicability to the multi-level model

This result clearly applies in the case of a running wave, when the excited state population is not too large. Indeed, it is quite clear that these results also apply to the case of Section (2.5), where the standing wave field is treated as a small perturbation on the running wave field.

It is less clear how these results apply to the two-level and multi-level theories of diffraction. However, in these cases it is clear from the discussions in this chapter that the atomic motion consists of adiabatic motion in various quasipotentials, which can be treated as scalar field except at points where adiabatic crossings occur. For example, referring to Fig. (2.5(b)), we see that the diffraction process involves two sets of quasipotentials (the $n = 0$ quasipotentials and the $n = -2$ quasipotentials), which are coupled by avoided crossings. For a coherent beamsplitter, we demand that the amount of spontaneous emission in both channels be sufficiently small.

In most circumstances, the process of diffraction takes place in two steps (see Fig. (2.5(b)). Firstly, as the atom travels toward the glass, it spends most of its time in the $n = 0$ reflection channel. After the classical turning point has

been reached, the diffracted part of the wavepacket travels outwards in the diffraction channel, and the reflected part returns along the reflection channel. To make this clearer, the diffracted atoms approach the glass in the reflection channel and return in the diffraction channel, whereas the reflected atoms approach and return in the reflection channel. Thus, to a reasonable approximation, the amount of spontaneous emission in the reflection channel will again be given by Eq. (2.61), whilst the spontaneous emission in the diffraction channel will be given by

$$p_{n,\text{final}} \approx \exp\left(-\frac{\gamma p_{0,y,\text{av}}}{q\hbar\Delta}\right), \tag{2.63}$$

where $p_{0,y,\text{av}}$ is the average y-momentum for the reflected and diffracted channels.

For negative order diffraction e.g. $n = -2$ diffraction, the diffraction angle is greater than the reflection angle and hence the diffracted channel will contribute most towards spontaneous emission.

2.9.3 Applicability to experiments

For the parameters of the Ne experiment, with a linewidth of 10 MHz, we find that approximately 20% of the atoms will experience at least one spontaneous emission event. However, the branching ratio in this transition was such that most of those atoms which experience spontaneous emission will not be detected [41].

For the Cs experiment, the linewidth is around 5 MHz. We have found that in some otherwise interesting parameter regimes, spontaneous emission will be a dominant factor. The spontaneous emission probabilities are discussed in detail in Section 2.12, but we shall remark here that we have found that spontaneous emission would be an important limiting factor in being able to construct a well functioning beam splitter for Cs.

2.10 Numerically solving the Schrödinger equation

2.10.1 Algorithm

We solve the Schrödinger equation with the Hamiltonian (2.36) by a well known numerical technique known as the split operator method [54]. As used in this instance, the method consists in splitting the unitary evolution operator into three parts:

$$U(t+\Delta t,t) \approx \exp\left(-\frac{i}{\hbar}\frac{\Delta t}{2}\hat{H}_A\right)\exp\left(-\frac{i}{\hbar}\Delta t\hat{V}_{AL}\right)\exp\left(-\frac{i}{\hbar}\frac{\Delta t}{2}\hat{H}_A\right), \quad (2.64)$$

where $\hat{H}_A$ and $\hat{V}_{AL}$ are defined by Eq. (2.36) or Eq. (2.48). The error in this expression goes as $(\Delta t)^3$.

In what follows we shall index the discrete degrees of freedom $\{n,m\}$ by a single index i, so that the wavefunction is stored as a series of vectors $\Psi_i(y_k)$, where i indexes values of the doublet $\{n,m\}$, and k labels the discretised values of y. Due to the fact that W_n is independent of y, the first term in the expression (2.64) can be expressed as

$$\exp\left(-\frac{i}{\hbar}\frac{\Delta t}{2}\hat{H}_A\right) = \exp\left(-\frac{i}{\hbar}\frac{\Delta t}{2}\frac{\hat{p}_y^2}{2m}\right)\exp\left(-\frac{i}{\hbar}\frac{\Delta t}{2}W_n\right). \quad (2.65)$$

A multiple data fast-Fourier transform (FFT) is applied to the y-dependence of the wavefunction $\Psi_i(y_k)$, transforming it into the momentum basis in the y-direction. The y-kinetic energy evolution operator $\hat{p}_y^2/2m$ is now diagonal in y, and by its definition (2.38) is diagonal in the discrete degrees of freedom i. This means that the operator (2.65) is easily calculated, and is diagonal in both y and i. The wavefunction is multiplied by this operator and is then Fourier transformed back into position space, completing the first part of the unitary evolution.

The operator $\hat{V}_{AL}$ is diagonal in y but not i. Because it is expressed in the form of a direct product $\hat{V}_{AL} = \hat{V}_{AL,i}\exp(-qy)$, where $\hat{V}_{AL,i}$ does not depend on y, the calculation of the term $\exp\left(-i\Delta t\hat{V}_{AL}/\hbar\right)$ can be accomplished by a single diagonalisation of the matrix $\hat{V}_{AL,i}$ which is used to accomplish the N_y calculations of $\exp(\left(-i\Delta t\hat{V}_{AL}(y)/\hbar\right)$, where N_y is the number of discretised values of y used. The wavefunction is multiplied by this operator and is then Fourier transformed back into the momentum basis, where a final $\Delta t/2$ timestep of evolution under $\hat{H}_A$ is accomplished. This completes one timestep of unitary evolution under the operator (2.64).

2.10.2 Implementation

The algorithm outlined above was implemented on a Fujitsu VPP2200 supercomputer in Fortran90. The NAG (Numerical Algorithms Group) routine c06frf was used to accomplish the multiple data FFT, and the routine f02abf was used in diagonalising the matrix $\hat{V}_{AL,i}$. Vectorisation was in excess of 99%. A typical runtime for the code mentioned above would be about 15 minutes to simulate the atomic dynamics for one set of parameters.

2.10.3 Validation

Several tests were applied to validate the numerical results.

The basic method had been previously tested for the two-level model by quantitative comparison with experiment [48]. This modelling predicted absorptive Doppleron resonances at certain values of the detuning, and was found to agree with the experiment [47]. The ultimate validation of the multi-level numerical results would come from a detailed comparison between experiment and theory in the multi-level regime over a range of parameters, however, such a comparison has so far not been possible due to a lack of detailed experimental evidence.

The timestep and grid sizes were set by verifying that increasing or decreasing these parameters did not affect the results too much. Relevant parameters were the spatial grid spacing and the timestep.

For the Ne* results presented in Section 2.11, the parameters of Table 2.1 were used. The timestep was 0.2 ns. In order to make comparisons in the what follows, we shall concentrate on the case where the polarisation is $5°$ from p-polarisation and the initial sublevel is $m = 2$.

For the Cs results and using the parameters discussed in Section (2.12) were used. The timestep was 20 ns, which is larger than the Ne* case because the different mass and incoming velocity result in a longer interaction with the evanescent field for Cs. For the purposes of the comparisons which are presented below, a laser polarisation of $50°$ from p-polarisation was selected.

The variation of the diffraction efficiency with timestep is shown below for Ne*

dt (ns)	$n = -2$ diffraction efficiency (%)
0.4	45.0
0.2	47.9
0.1	47.5

This table suggests that the timestep of 0.2 ns is sufficiently small to an accuracy at around the 1% level.

For Cs the corresponding results are given by:

dt (ns)	$n = -2$ diffraction efficiency (%)
40	38.2
20	38.2
10	38.3

Again, these results suggest that the timestep was small enough to give stability and accuracy of better than 1%.

The grid spacing in the y-direction was measured by the dimensionless pa-

rameter nq, which specified the number of grid points within one decay length of the evanescent field. It is not such a trivial matter to set the grid spacing as it is for the timestep, since following interaction with the evanescent wave, the wavefunction consists of several partial wavepackets travelling away from the glass at different velocities. One must ensure that all of these wavepackets have stopped interacting with the evanescent wave and yet all are contained within the grid at the time when the diffraction efficiencies are read off.

For the Ne* results, a value of $nq = 170$ was used. Increasing nq to 300 did not alter the diffraction efficiency (47.9%) to within three decimal places. Thus we conclude that the spatial grid was sufficiently small to give reliable results.

For Cs, a value of $nq = 400$ was used [2]. Increasing this value to $nq = 600$ did not change the diffraction efficiency (38.2%) to within three decimal places. Again, we can conclude that the spatial grid was adequate.

Another relevant numerical parameter was $n_{\max}$, the cutoff for the number of diffraction orders n used. For example, $n_{\max} = 6$ would correspond to values of n between $n = -6$ and $n = 6$. For the Ne* results a value of $n_{\max} = 6$ was used. Increasing this value to 10 changed the diffraction efficiency from 47.9% to 46.9%, showing that the inclusion of the extra levels did not affect the results above the 1% level.

For the Cs results, a value of 4 was generally used for $n_{\max}$. The complicated nature of the transition coupled with the range of parameters investigated makes it harder to specify the variation in the diffraction efficiency with $n_{\max}$, however, it was certainly true that in certain parameter regimes, the diffraction was found to be more dependent on $n_{\max}$ than were the Ne* results. This was due to the fact that the atoms penetrated deeper into the evanescent field, bringing higher diffraction orders into resonance. As an example of the kind of variation which was seen, the following table shows the diffraction efficiency in various orders for the parameters of Fig. (2.15):

$n_{\max}$	$n = -2$ (%)	$n = -4$ (%)	$n = -6$ (%)
4	13.5	4.2	1.6
6	15.1	5.6	1.9

The version of the program involving adiabatic elimination of the excited state was compared to the version with no adiabatic elimination. For the case of Ne* and for the parameters quoted above, introducing adiabatic elimination of the excited state was found to change the $n = -2$ diffraction efficiency from

[2]The Cs and Ne* values are different for a number of reasons, including different evanescent wave decay lengths, different values for the y-component of the incoming atomic velocity and practical considerations involving the need to avoid the wavefunction reaching the endpoint of the grid

47.9% to 47.0 %, showing both that the adiabatic elimination procedure was carried out correctly and that adiabatic elimination was valid for the relevant parameter regime. For the Cs model, it was impossible to directly test the effect of introducing adiabatic elimination, since the complicated level structure, with 27 excited state sublevels and 9 ground state sublevels made it unfeasible to model the system without adiabatically eliminating the excited states. However, the Ne results at least imply that there was nothing fundamentally flawed in the way the basic procedure of adiabatic elimination was carried out for Cs.

Finally, examination of the quasipotentials gives a good indication of the qualitative behaviour which would be expected from the system —for example, the presence of two avoided crossings predicts the double peaked structure seen in Fig. (2.9).

2.11 Numerical results for metastable Neon

In this section we consider the parameters of the experiment of Christ *et al.* This experiment reported the first observation of atomic diffraction by an evanescent wave. Up to 3% diffraction was reported in this experiment. The parameters of the experiment are shown in Table (2.1). The atoms were slowed by a Zeeman slower to a speed of 25m s^{-1} and were incident at an angle of grazing incidence of 36 m rad. As has been pointed out, the parameters of this experiment indicate that diffraction will not occur for two-level atoms but should occur for multi-level atoms with the structure shown in Fig. (2.6).

The model outlined in Section 2.7 predicts that polarisation will play an important part in controlling the diffraction efficiency. Numerical results of diffraction efficiency vs. the polarisation of the incoming beam are shown in Fig. (2.9). These particular results were calculated by averaging over an equal mixture of magnetic sublevels m_g[3]; this will not accurately represent the real situation if there has been any optical pumping or if there are stray magnetic fields present. For the conditions shown in this figure a maximum diffraction efficiency of around 18% is seen, for a polarisation angle of around 6°.

The double peaked structure of Fig. (2.9(b)) can be explained by noting that there are actually *two* avoided crossings involved in the diffraction process.

[3]Actually, the bulk of the points were calculated for an $m_g = 2$ incoming atom. However, only one of the five $n = 0$ quasipotentials is actually involved in the diffraction process. Because of this, it turns out that, irrespective of the laser polarisation, the amount of diffraction produced for each of the other four possible values of m_g will be in a constant ratio to the amount produced by $m_g = 2$. This has been verified for a range of laser polarisations. This allows us to infer the diffraction efficiency for a mixture of incoming sublevels m_g.

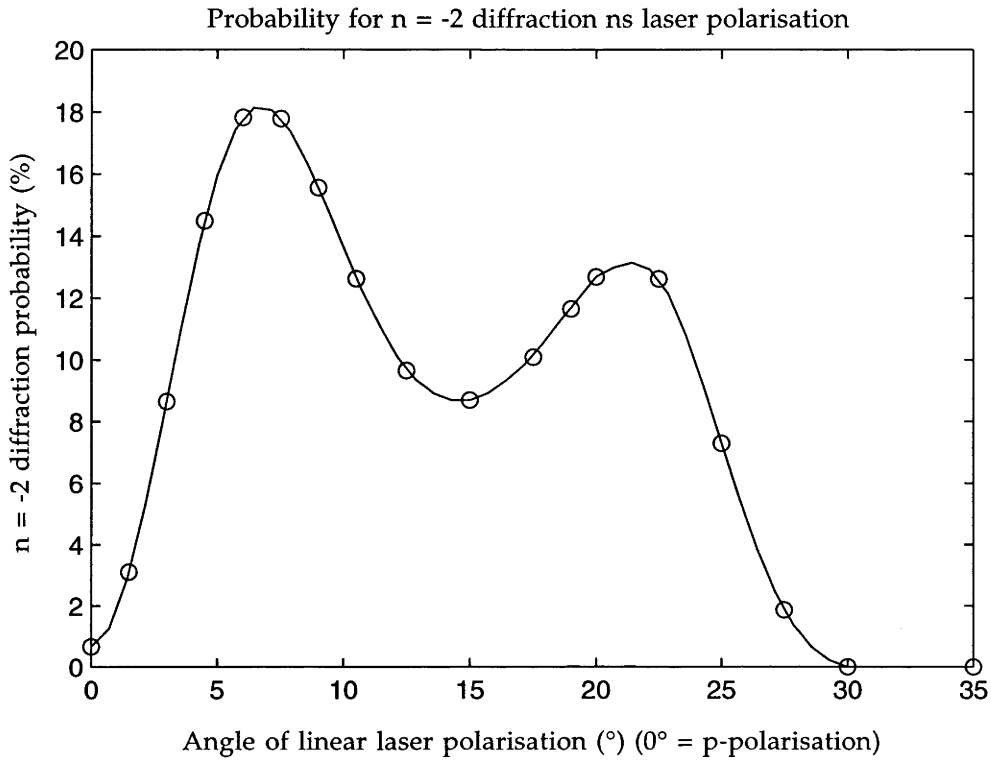

Figure 2.9: Percentage $n = -2$ order diffraction versus polarisation angle for an equal mixture of incoming sublevels. The percentage of diffraction is plotted versus the linear polarisation angle, in degrees, of the two laser beams from pure p-polarisation, 0°. The solid curve is a fit to the calculated points. Other parameters are as in Table 1.

This is shown in Fig. (2.5(b)); the first is indicated by an arrow and the second can be seen at the top left hand corner of the figure. The two peaks result from the fact that the two crossings do not achieve their optimum splitting efficiencies for the same parameters.

Unpublished experimental data [55] reported that there was some uncertainty in the polarisation of the laser beams, due to faulty components, but that the copropagating beam seems to have been polarised at 5° from p-polarisation and the counterpropagating beam at 10°. Here p-polarisation is used to indicate polarisation in the plane of incidence of the laser beams and s-polarisation perpendicular to the plane of incidence. For these conditions, we find a diffraction efficiency of 14%, close to the maximum value.

Other important parameters are the angle of incidence and the incoming velocity of the atoms. The main effect of increasing the angle of incidence is

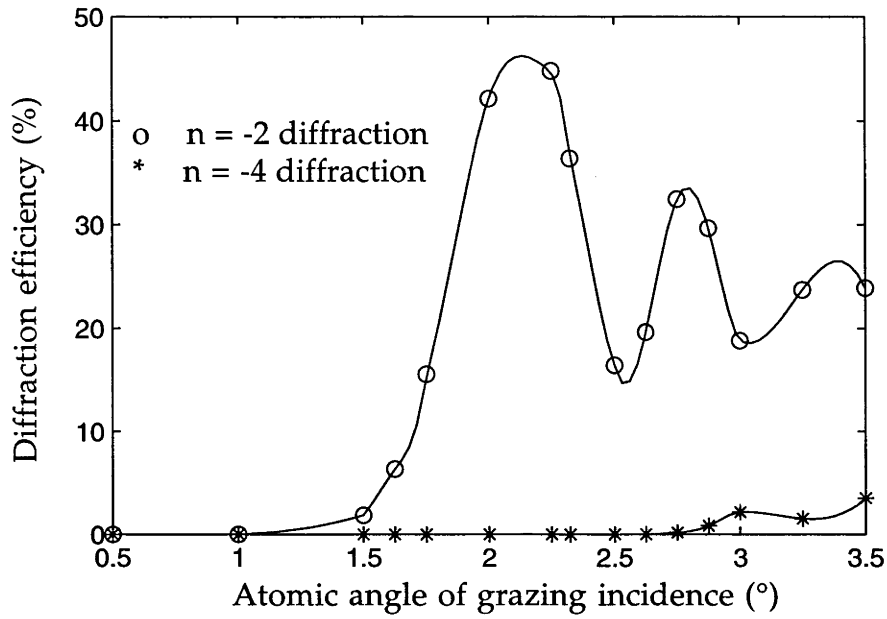

Figure 2.10: The effect of varying the angle of incidence on the diffraction efficiency. The parameters are those of Table (2.1), with a beam polarisation of 5° from p-polarisation.

to increase the initial kinetic energy in the y-direction [4]. This has the effect of raising the classical reflection point of the atom, so that it penetrates closer to the glass. If we imagine increasing the angle of incidence from zero, we should see the sudden appearance of diffraction at the point where the classical reflection point allows the atom to traverse the first quasipotential seen in Fig. (2.5(b)). Raising the angle of incidence further will bring other avoided crossings into resonance, thus affecting the diffraction efficiency. At a given angle, we should see the appearance of $n = -4$ diffraction at the point where the atom penetrates deeply enough into the light field to bring the $n = -4$ diffraction orders into resonance. This kind of behaviour is indeed seen in Fig. (2.10).

As the incoming atomic velocity is increased, the height of the classical turning point, which is proportional to the square of the velocity, will increase. However, this will be partially offset by the fact that the Doppler shift will also increase, meaning that the atom will need to travel further into the light field in order to bring transitions which lead to diffraction into resonance. This increase in the Doppler shift should also affect the shape of the avoided

[4]There is also a second order effect which decreases the doppler shift and therefore brings the various diffraction orders closer to one another (see Fig. (2.5(b))

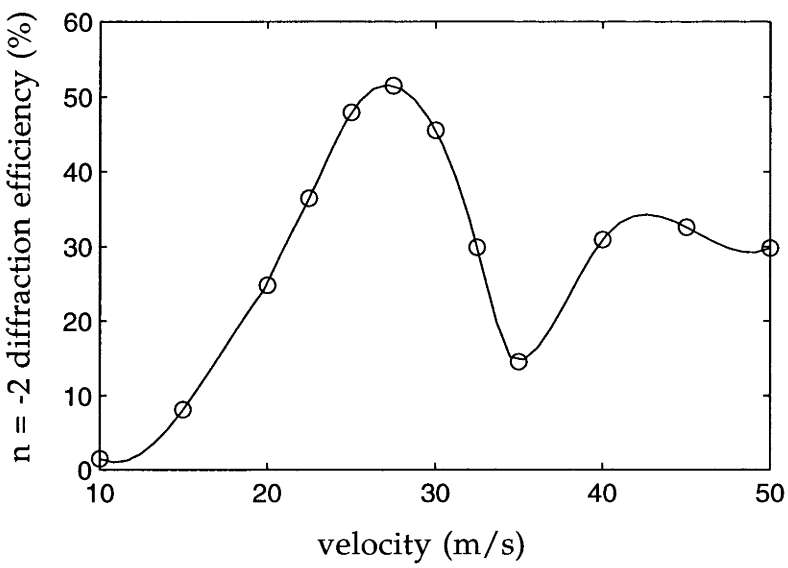

Figure 2.11: The effect of varying the incoming velocity on the diffraction efficiency. The parameters are those of Table (2.1), with a beam polarisation of 5° from p-polarisation.

crossings, and hence affect the diffraction efficiency. Using this reasoning, we would expect that an increase in velocity would show similar behaviour to an increase in the angle of incidence, but with a slower parameter dependence and differences in the shape of the diffraction efficiency curve. Numerical results which show the diffraction efficiency vs. the incoming velocity are shown in Fig. (2.11). We see that the system behaves as predicted.

The experiment also reported the condition that the ratio of the intensities of the copropagating and counterpropagating beams was fixed at 1.64. For the other conditions reported, we find that this condition gives a local maximum in the diffraction efficiency, although the dependence on this ratio is not strong.

One advantage of numerically solving the time-dependent Schrödinger equation is that 'movies' of the wavefunction evolution are available. Fig. (2.12) shows an initial $m_g = 2, n = 0$ probability density evolving to produce $n = -2$ order diffraction.

We conclude that, given the uncertainties in experimental parameters (especially the polarisation), our numerical results are consistent with the observations of the experiment whereas the two-level model is unable to explain these results. Unfortunately, detailed experimental results concerning polarisation etc. are not available, and so we are unable to give a more detailed comparison between experiment and theory.

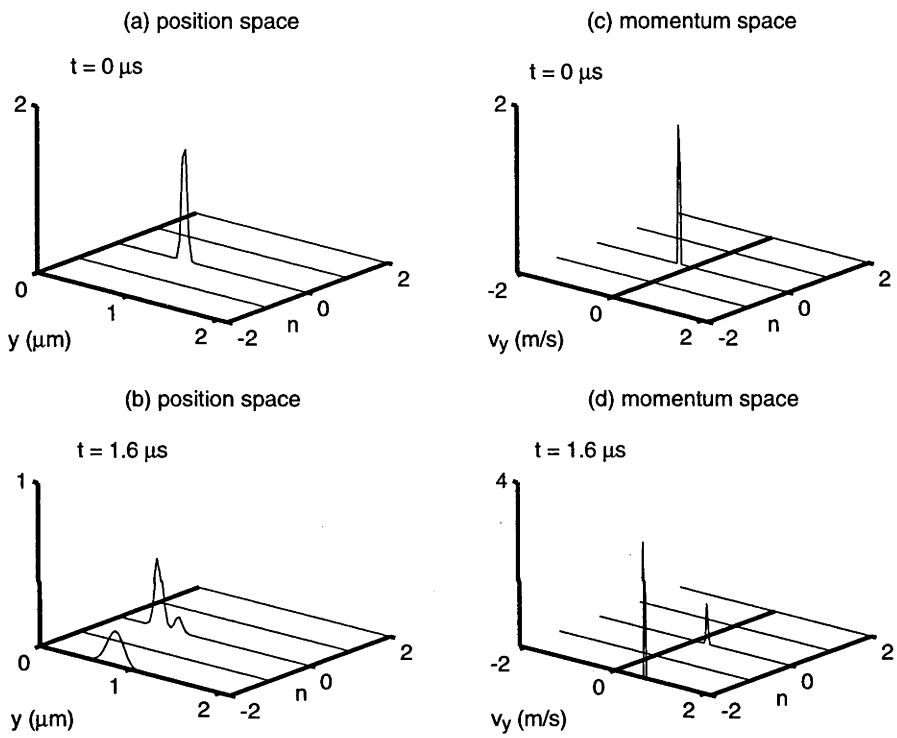

Figure 2.12: Probability densities in position and momentum spaces for an initial $m_g = 2$ state atom. The probability density $P_n = \sum_m |\Psi_{n,m}|^2$ is plotted against the diffraction order n and either the distance from the glass in microns (a) and (b), or the velocity perpendicular to the glass (c) and (d). In each case the top figure is the initial condition and the bottom figure is 1.6 μs later, after reflection. There is no probability in the orders not shown. Parameters are as in Table 1 with laser polarisations of 5° away from p-polarisation.

2.12 Numerical results for Cs

In the following section we present some numerical results for the case of the Cs transition shown in Fig. (2.8). We will ultimately compare the results of our calculations with the results of an experiment currently underway at the Australian National University; at the present time definitive results are not available for comparison, but initial indications suggest that the experiment may agree with our predictions of a sensitive dependence on polarisation, and with the dependence on detuning which will be discussed below [7].

The transition in question suffers from the peculiarity that if the lasers are detuned above the top ($F = 5$) level of the transition, then the various quasipotentials in each order are light shifted by a similar amount unless the polarisation of the two beams meets very particular criteria. This is in fact due to two effects: firstly, the $F = 4$ to $F = 5$ transition does not show a particularly large splitting under normal circumstances, and secondly, if the detuning is large compared to the splitting between the excited state hyperfine levels, then the all of the excited state hyperfine levels (except the $F = 2$ level, which is a forbidden transition) contribute to the transition, thereby destroying the splitting effect which would occur if each of the hyperfine levels was considered separately. The quasipotentials are shown in Fig. (2.13); this lack of good splitting between the quasipotentials can be seen in (a). It is clear from this figure that it will be hard to obtain the conditions needed for diffraction under such conditions, because there are no crossings between the quasipotentials for different diffraction orders which occur before the classical reflection point.

There are a couple of possible remedies to this situation. One could detune to *between* the $F = 4$ and $F = 5$ levels, so that the laser is actually *red* detuned relative to the $F = 5$ level but blue detuned relative to the other levels. The effect of the red detuned component is to pull the lowest quasipotentials downwards, since red detuning will lead to attractive potentials. This has the effect of increasing the splitting between the quasipotentials and restoring the conditions for diffraction. This is shown in Fig. (2.13(b)). At first sight, this situation seems to present ideal conditions for diffraction. We have calculated the diffraction vs. polarisation angle - the results are shown in Fig. (2.14).

Despite the fact that this regime allows a high degree of diffraction, there is a serious problem: spontaneous emission. Using the results of Section (2.9), we calculate that under the conditions of Fig. (2.14), only 30% of the reflected atoms and 7% of the diffracted atoms will survive without having undergone at least one spontaneous emission event. This is clearly unacceptable.

One could use a number of strategies to improve the situation. Detuning further away from the $F = 4$ transition is found to lead to a combination of repulsive and attractive quasipotentials. While this situation can certainly

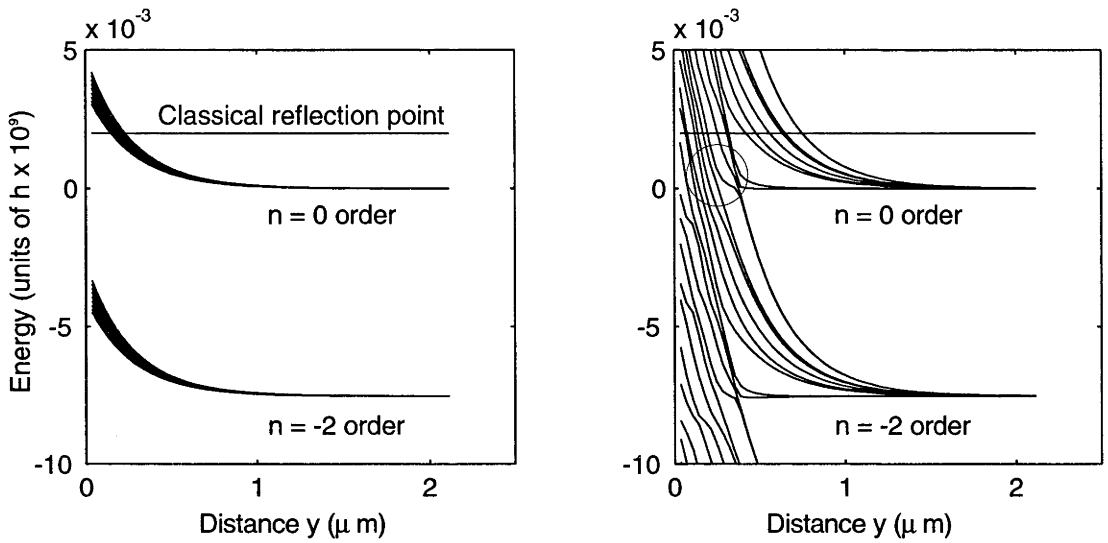

Figure 2.13: Quasipotentials for the Cs transition shown in Fig. (2.8). The atoms are incident at 5° grazing incidence with a speed of 0.5 m s^{-1}. The lasers are linearly polarised at an angle of 63° from p-polarisation. (a) shows the case for a detuning of 500 MHz above the top ($F = 5$) excited level; in this case the splitting between the quasipotentials is small and hence there are no crossings which could lead to diffraction. In (b) the lasers are tuned 220 MHz *below* the $F = 5$ level, i.e. *between* the $F = 4$ and $F = 5$ levels. In this case, the red detuned component due to the interaction with the $F = 5$ level increases the splitting between the quasipotentials, and hence the conditions for diffraction are restored.

lead to beamsplitting, there will probably be significant losses at the glass, and in general the system becomes so complex that a detailed modelling of its behaviour is probably not warranted. If one were to detune halfway in between the $F = 4$ and $F = 5$ hyperfine levels, the results of Section (2.9) suggest that 75% of the reflected atoms and 53% of the diffracted atoms would survive without undergoing any spontaneous emission events.

Decreasing the angle of incidence is not a particularly good strategy to use, since the angle of diffraction is largely left unchanged and hence there will still be large losses in the diffracted channel.

Decreasing the atomic velocity is another possibility. If the parameters of Fig. (2.14) were used, but with a velocity of 0.1 ms^{-1} and an angle of grazing incidence of 7°, then around 70% of the reflected atoms and 53% of the diffracted atoms would survive without having undergone spontaneous emission. For these parameters, we have found that a laser polarisation of 50° leads to an $n = -2$ diffraction efficiency of 14%.

There is a whole different strategy available whereby one would abandon

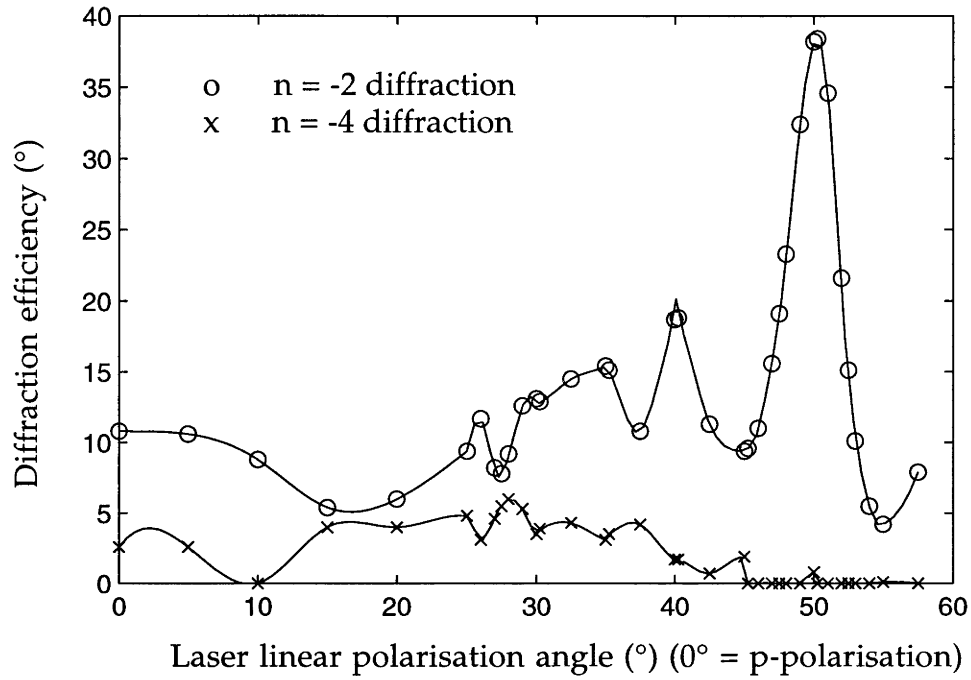

Figure 2.14: Diffraction efficiency vs. angle of linear polarisation of the incoming laser beam.

the whole idea of detuning in between the $F = 4$ and $F = 5$ sublevels, and simply try to find the right parameter combination which, despite the factors working against this, would allow diffraction to occur. This is not an easy task, due to the rather large parameter space and the fact that most parameter combinations do not lead to diffraction. It was found that visually assessing the behaviour of the quasipotentials was a great help in finding parameters which would lead to diffraction. For the parameters of Fig. (2.15), there is an 52% survival rate in the reflected channel and a 48% survival rate in the diffracted channel. However, these parameters are far from ideal in that the high angle of incidence coupled with the low incident velocity means that the angle of diffraction is not as large is it could be - about 5° as opposed to around 17° for the parameters of Fig. (2.14).

We have modelled the behaviour of this system as the angle of incidence is increased. The results are plotted in Fig. (2.15). The overall behaviour is similar to the case of Fig. (2.10), except that the diffraction into higher orders ($n = -4, n = -6 \ldots$) appears more rapidly. It is possible to further improve the conditions for diffraction by increasing the angle of internal reflection for the laser beams, and thereby altering the ratio between the σ_+ and σ_- polarisation components of the evanescent wave, but this would require replacing the prism in the case of the ANU experiment.

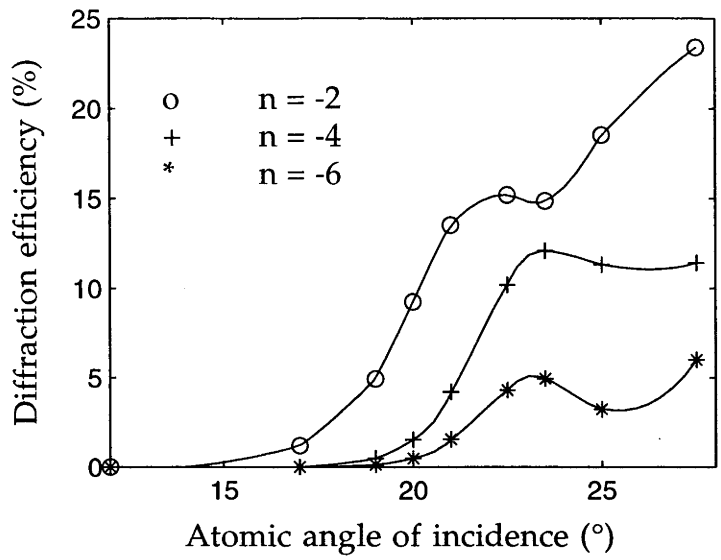

Figure 2.15: Diffraction efficiency vs atomic angle of grazing incidence. Diffraction is possible because of a very special combination of parameters: a detuning 100 MHz above the $F = 5$ transition, an incident velocity of 0.2ms^{-1}, an intensity ratio of 9 between the copropagating and counterpropagating beams, a polarisation angle of 55° from p-polarisation, and a phase shift of $\pi/2$ radians applied to the π component of the counterpropagating beam, so that the polarisation in this beam is in fact elliptical rather than linear.

2.12.1 Experimental results to date

At the time of writing, it is too early to present quantitative results of the ANU experiment, since experimental issues regarding signal to noise and stability need to be resolved. However, anecdotal evidence [7] suggests that the presence of diffraction appears to hinge on (a) having a particular polarisation of the laser beam, and (b) having a detuning between the $F' = 5$ and $F' = 4$ hyperfine levels. Thus there is some qualitative agreement between the experimental results and the modelling presented here. However, the presence of spontaneous emission certainly complicates the situation, and at present it would not be wise to draw too many conclusions.

Chapter 3

Introductory theory for Bose-Einstein condensation

From here on, this thesis will be concerned with dilute gas Bose-Einstein condensation in a trapping potential. In this chapter, we shall provide a brief review of the recent developments in the theory of trapped dilute gas BECs, and then go on to give some derivations of Bogoliubov theory in a form which will be used in later chapters of this thesis.

3.1 BEC theory literature

In the following section, we shall provide a very brief description of some important developments in the theory of dilute gas BEC. Due to the large number of theoretical papers and to the breadth of subject matter covered, we shall limit ourselves to considering work which deals with the most basic processes and experiments. Thus we shall omit work describing more particular experiments e.g. those involving two-species BECs, the interaction of BECs with light and so on. The list of references should not be considered to be comprehensive. In producing this summary, I have made frequent use of the review by Parkins and Walls [56], to which the reader is referred for greater detail.

The gross behaviour of the density profile of a trapped BEC is very well described by mean-field theory, which treats the condensate as a classical field. Mean-field theory can be used to find the ground state density profile of a condensate. The most common way of doing this is to solve the time-independent Gross-Pitaevskii equation [57]. This equation is a nonlinear Schrödinger equation. The nonlinearity is provided by the atom-atom interactions, which cause the condensate cloud to expand for repulsive interactions and to contract for attractive interactions. The time independent Gross-Pitaevskii equation has been solved for a trapped BEC by several groups, eg. [58–61].

Once the ground state density profile has been determined, the linearised excitation spectrum can be found by solving the Bogoliubov equations or sim-

ilar equations[1] eg. [23,24,63–66].

However, Bogoliubov theory is accurate only for small amplitude excitations. In order to examine the effect of large amplitude excitations as well as other dynamical processes in the evolution of the density profile, the time dependent Gross-Pitaevskii equation must be solved [59,63,67–70].

The whole area of mean field theory is usually formulated in terms of U(1) symmetry broken (coherent) states. Since these states are not eigenstates of the Hamiltonian, they undergo dynamical evolution in the form of a phase diffusion. This formally invalidates the linearisation around a classical field which is the hallmark of the Bogoliubov approach [71]. Recently Gardiner [72] and Castin and Dum [73] have presented modified theories which are particle number conserving, and thus allow a more systematic treatment of the validity of mean-field approaches, especially where dynamical processes such as condensate growth or a rapid evolution of the density profile are involved.

Processes involving the interplay between condensed and non-condensed atoms (most notably, the process of condensate growth) require a more sophisticated treatment than is given by mean field theory. Quantum kinetic theories which treat both the coherent and incoherent evolution have been developed by several groups [74–81].

The question of coherence in Bose-Einstein condensates has received a lot of theoretical attention, since coherence is one of the most useful properties of a BEC. Coherence is closely related to the existence of a condensate phase or relative phase between two condensates. The diffusion of this phase has been studied by several authors [82–87]. There has also been a good deal of interest in the way that a relative phase can be built up between two condensates by a process of measurement [84,88–92], since this topic deals with the question of the broken U(1) symmetry in condensates [2]

There are many other areas of theoretical investigation which have not been touched upon. Examples include the effects of finite temperature on the coherence and mean field properties of BECs, the interaction of BECs with light, microscopic treatment of atom-atom interactions etc. The rapid rate of experimental progress and the large number of possible applications for BECs will no doubt make them a 'hot topic' of theoretical research for years to come.

[1] for example, one can apply linear response theory to the time dependent Gross-Pitaevskii equation. Doing so gives a set of equations which are identical to the Bogoliubov equations [62]

[2] Strictly speaking, a single condensate cannot have broken U(1) symmetry and therefore does not have a phase. At first sight, this might appear to invalidate the basis of mean field theory, however, it can be shown that for most purposes a condensate can in fact be treated as if it had a phase.

3.2 Description of a trapped dilute-gas Bose-Einstein condensate

A dilute gas at low temperature can be described by the many-body Hamiltonian

$$\begin{aligned}\hat{H} &= \int d^3\mathbf{r}\,\hat{\psi}^\dagger(\mathbf{r})\left[\frac{\hat{\mathbf{p}}^2}{2m}+V_T(\mathbf{r})\right]\hat{\psi}(\mathbf{r}) \\ &+ \frac{1}{2}\int d^3\mathbf{r}_1\,d^3\mathbf{r}_2\,\hat{\psi}^\dagger(\mathbf{r}_1)\hat{\psi}^\dagger(\mathbf{r}_2)V(\mathbf{r}_1,\mathbf{r}_2)\hat{\psi}(\mathbf{r}_1)\hat{\psi}(\mathbf{r}_2)\,, \end{aligned} \tag{3.1}$$

where m is the mass of one atom, $\hat{\mathbf{p}}^2/(2m)$ is the kinetic energy operator and $V_T(\mathbf{r})$ describes the trapping potential. The term in the second integral describes the effects of collisions between one atom and another; if the density is not too high, then the effects of three and more body collisions may be ignored. The function $V(\mathbf{r}_1,\mathbf{r}_2)$ gives the precise two-body potential for an atom located at $\mathbf{r}_1$ and an atom located at $\mathbf{r}_2$. In dilute gas BECs, this term is usually negligible unless the two atoms are closer together than a distance (the scattering length) which is small compared to the other scales of the system, and thus the effect of the two-body potential can be well approximated by a delta function potential:

$$V(\mathbf{r}_1,\mathbf{r}_2)\approx U_0\delta(\mathbf{r}_1-\mathbf{r}_2)\,, \tag{3.2}$$

with $U_0 = 4\pi a\hbar^2/m$, where a is a length indicating the range of the interaction, termed the *scattering length*. The Hamiltonian then simplifies to the following well known form:

$$\begin{aligned}\hat{H} &= \int d^3\mathbf{r}\,\hat{\psi}^\dagger(\mathbf{r})\left[\frac{\hat{\mathbf{p}}^2}{2m}+V_T(\mathbf{r})\right]\hat{\psi}(\mathbf{r}) \\ &+ \frac{1}{2}U_0\int d^3\mathbf{r}\,\hat{\psi}^\dagger(\mathbf{r})^2\hat{\psi}(\mathbf{r})^2\,. \end{aligned} \tag{3.3}$$

3.3 Bogoliubov theory in a general basis

In the following section, we present a derivation of the time-independent Gross-Pitaevskii equation, which determines the lowest energy density profile, and the related Bogoliubov equations which determine the spectrum and shape of the small amplitude excitations around this density profile. We choose to present this derivation in a general basis rather than the position basis, as would be more usual, in the interest of generality, so as to provide a straight forward generalisation to the case of two-species or multi-species BECs, and finally because most of the numerical and analytical computations presented

in later chapters were not performed in the position basis. For a discussion of Bogoliubov theory/linear response theory in the position basis, see eg. [62].

3.3.1 The Hamiltonian

We work in a single particle basis described by the complete orthonormal set of wavefunctions $\phi_i(\mathbf{r})$, so that a general single particle wavefunction is described as $\psi(\mathbf{r}) = \sum_i \alpha_i \phi_i(\mathbf{r})$. In the second quantised picture we use a Fock-basis $|N\rangle_i$ which describes N atoms in the single particle wavefunction ϕ_i. We define a set of annihilation/creation operators $\hat{a}_i$, $\hat{a}_i^\dagger$ which annihilate/create an atom in the state ϕ_i:

$$\begin{aligned} \hat{a}_i |N\rangle_i &= \sqrt{N}\,|N-1\rangle_i \\ \hat{a}_i^\dagger |N\rangle_i &= \sqrt{N+1}\,|N+1\rangle_i \,. \end{aligned} \tag{3.4}$$

They fulfill the usual commutation relations

$$[\hat{a}_i, \hat{a}_j^\dagger] = \delta_{ij} \,. \tag{3.5}$$

The Hamiltonian can then be written as

$$\hat{H} = \sum_{ij} H_{ij}^0 \hat{a}_i^\dagger \hat{a}_j + \frac{1}{2} \sum_{ijkl} V_{ijkl} \hat{a}_i^\dagger \hat{a}_j^\dagger \hat{a}_k \hat{a}_l \,. \tag{3.6}$$

which is simply the general form for a second quantised Hamiltonian including two-body interactions. However, we must be able to obtain this form by making a change of basis from the position basis to our general basis, and hence comparison to Eq. (3.3) gives

$$H_{ij}^0 = \int d^3\mathbf{r}\, \phi_i^*(\mathbf{r}) \left[\frac{\mathbf{p}^2}{2m} + V(\mathbf{r}) \right] \phi_j(\mathbf{r}) \,, \tag{3.7}$$

$$V_{ijkl} = U_0 \int d^3\mathbf{r}\, \phi_i^*(\mathbf{r}) \phi_j^*(\mathbf{r}) \phi_k(\mathbf{r}) \phi_l(\mathbf{r}) \,. \tag{3.8}$$

We note that the matrix represented by H_{ij}^0 is Hermitian and that V_{ijkl} is symmetric under the interchange of indices 1 and 2 or 3 and 4 and Hermitian under the simultaneous interchange of indices 1 with 3 and 2 with 4, or 1 with 4 and 2 with 3. If we take the basis wavefunctions $\phi_i(\mathbf{r})$ to be real, then both H_{ij}^0 and V_{ijkl} are symmetric under any interchange of indices, a fact which allows certain expressions to be simplified considerably.

It is customary to use the so called 'grand canonical Hamiltonian' $\hat{K}$, defined by $\hat{K} = \hat{H} - \mu\hat{N}$, where $\hat{N} = \sum_i \langle \hat{a}_i^\dagger \hat{a}_i \rangle$ is the total number of particles, and μ is the chemical potential and can be considered as a parameter

to be determined later. The grand canonical Hamiltonian is used in statistical mechanics to describe a system interacting with a particle reservoir. Since $\hat{N}$ is a conserved quantity, the grand canonical Hamiltonian differs from the Hamiltonian by a constant energy shift and thus describes essentially the same physics.

The essence of the Bogoliubov approach is to assume that the condensate is in a coherent state, so that we have $\langle \hat{a}_i \rangle = \alpha_i = \sqrt{\hat{a}_i^\dagger \hat{a}_i}$. We now define a new set of operators $\hat{b}_i$ such that $\hat{a}_i = \alpha_i + \hat{b}_i$, i.e. we 'split' the operators $\hat{a}_i$ into c-number terms α_i and operator terms $\hat{b}_i$. It is obvious from this definition that $\langle \hat{b} \rangle = 0$, and in a sense $\hat{b}$ can be considered 'small'. We thus expand the grand canonical Hamiltonian in increasing powers of $\hat{b}$ and $\hat{b}^\dagger$, and neglect terms of third and fourth order in these operators:

$$\begin{aligned}
\hat{K} &= K_0 + \hat{K}_1 + \hat{K}_2 + \hat{K}_3 + \hat{K}_4 \\
K_0 &= \sum_{ij} H^0_{ij} \alpha_i^* \alpha_j - \mu \sum_i \alpha_i^* \alpha_i + \frac{1}{2} \sum_{ijkl} V_{ijkl} \alpha_i^* \alpha_j^* \alpha_k \alpha_l \\
\hat{K}_1 &= \sum_i \left[-\mu \alpha_i + \sum_j H^0_{ij} \alpha_j + \sum_{jkl} V_{ijkl} \alpha_j^* \alpha_k \alpha_l \right] \hat{b}_i^\dagger + \text{H.c.}
\end{aligned}$$

(here we have used the symmetry properties of H^0_{ij} and V_{ijkl}),

$$\begin{aligned}
\hat{K}_2 &= \sum_{ij} H^0_{ij} \hat{b}_i^\dagger \hat{b}_j - \mu \sum_i \hat{b}_i^\dagger \hat{b}_i \\
&+ \frac{1}{2} \sum_{ijkl} \left[V_{ijkl} \alpha_k \alpha_l \hat{b}_i^\dagger \hat{b}_j^\dagger + V^*_{ijkl} \alpha_k^* \alpha_l^* \hat{b}_i \hat{b}_j + 4 V_{ikjl} \alpha_k^* \alpha_l \hat{b}_i^\dagger \hat{b}_j \right] . \qquad (3.9)
\end{aligned}$$

The definition of the terms $\hat{K}_3$ and $\hat{K}_4$ is ommitted here, since in the Bogoliubov approach these terms are ignored.

We define terms H_0 and $\hat{H}_{1-4}$ as above but without including the terms proportional to μ. For convenience we rewrite $\hat{K}_2$ as follows:

$$\hat{K}_2 = \sum_{ij} P_{ij} \hat{b}_i^\dagger \hat{b}_j + Q_{ij} \hat{b}_i \hat{b}_j + Q^*_{ij} \hat{b}_i^\dagger \hat{b}_j^\dagger , \qquad (3.10)$$

with $P_{ij} = H^0_{ij} - \mu \delta_{ij} + \sum_{kl} 2 V_{ikjl} \alpha_k^* \alpha_l$ and $Q_{ij} = (1/2) \sum_{kl} V^*_{ijkl} \alpha_k^* \alpha_l^*$. Note that the matrix whose elements are P_{ij} is Hermitian, and the matrix Q_{ij} is symmetric.

3.3.2 The Gross-Pitaevskii equation(s)

To a good approximation, the term H_0 gives the energy of the BEC. The α_i's determine the single-particle condensate wavefunction. Minimising the value

of H_0 for a fixed particle number ($\sum_i \alpha_i^* \alpha_i - N = 0$) gives a very good approximation to the lowest energy state of the condensate. In this context, the parameter μ in the grand canonical Hamiltonian can be seen to function as a Lagrange multiplier which ensures fixed particle number. Solving for the stationary points of H_0 with respect to the α_i's and subject to the fixed particle number constraint gives the following equations.

$$\begin{aligned} \left[\sum_i H^0_{ni} + \sum_{ijk} V_{njki}\alpha_j^*\alpha_k - \mu\right]\alpha_i &= 0\,, \\ \sum_i \alpha_i^*\alpha_i - N &= 0\,. \end{aligned} \tag{3.11}$$

The former set of linear equations is equivalent to the Gross-Pitaevskii equation, or nonlinear Schrödinger equation. It can be seen that if these equations are satisfied, then the term $\hat{K}_1$ will vanish.

In the position basis, the Gross-Pitaevskii equation is:

$$\left(\frac{\hat{\mathbf{p}}^2}{2m} + V_T(\mathbf{r}) + NU_0|\psi(\mathbf{r})|^2\right)\psi(\mathbf{r}) = \mu\psi(\mathbf{r})\,, \tag{3.12}$$

where $U_0 = (4\pi a\hbar^2)/m$. Note that, in order to emphasise the similarity to the linear Schrödinger equation, we have used a different normalisation than was presented for the general basis Eq. (3.11): we have

$$\int d^3\mathbf{r}\,|\psi(\mathbf{r})|^2 = 1\,, \tag{3.13}$$

so that the particle number N must be included explicitly in the equation. In the two limits of very few atoms or very many atoms, we can find analytical approximations to the solution of this equation. The validity of such approximations may be checked self-consistently after they are made.

Small number of particles

In this limit, the term proportional to N may be ignored, and hence an approximation to the ground state density profile is given by the ground state solution to the linear Schrödinger equation for the trapping potential V_T

Large number of particles

In this limit, we may ignore the contribution of the kinetic energy. This approximation is known as the Thomas-Fermi approximation.

The Gross-Pitaevskii equation becomes

$$\left(V_T(\mathbf{r}) + NU_0|\psi(\mathbf{r})|^2\right)\psi(\mathbf{r}) = \mu\psi(\mathbf{r})\,, \tag{3.14}$$

or

$$|\psi(\mathbf{r})|^2 = \frac{\mu - V_T(\mathbf{r})}{NU_0}\,. \tag{3.15}$$

The chemical potential μ is fixed by the fact that the mean field wavefunction must be normalised:

$$\int d^3\mathbf{r}\,|\psi(\mathbf{r})|^2 = 1\,. \tag{3.16}$$

For the case of a cylindrically symmetric harmonic trapping potential we have

$$V_T(x,y,z) = \frac{m\omega_\perp}{2}(x^2 + y^2 + \lambda^2 z^2)\,, \tag{3.17}$$

where $\omega_\perp$ is the trap angular frequency in the x and y directions, perpendicular to the axis of symmetry, and $\lambda\omega_\perp$ is the angular frequency in the z direction. For such a potential, we find

$$|\psi(x,y,z)|^2 = \frac{1}{NU_0}\left[\mu - \frac{1}{2}m\omega_\perp(x^2 + y^2 + \lambda^2 z^2)\right]\,, \tag{3.18}$$

with

$$\mu = \frac{1}{4}\left[\frac{15\sqrt{2}\lambda NU_0(m\omega^2)^{3/2}}{\pi}\right]^{2/5}\,. \tag{3.19}$$

3.3.3 The Bogoliubov transformation

Once we have determined the density profile of the BEC by solving the Gross-Pitaevskii equation, the excitation spectrum can be also determined. This is done by making a unitary transformation so that the term $\hat{K}_2$, which is the leading term in the $\hat{b}$'s and $\hat{b}^\dagger$'s, takes the form of the Hamiltonian for a set of noninteracting particles.

Since $\hat{K}_2$ is quadratic in the creation and annihilation operators and we want the transformed term to be bilinear, we use the transformation

$$\begin{aligned}\hat{b}_i &= \sum_j u_{ij}\hat{c}_j + v_{ij}^*\hat{c}_j^\dagger\,,\\ \hat{b}_i^\dagger &= \sum_j u_{ij}^*\hat{c}_j^\dagger + v_{ij}\hat{c}_j\,,\end{aligned} \tag{3.20}$$

where the $\hat{c}$'s and $\hat{c}^\dagger$'s are assumed to obey the commutation relations $[\hat{c}_i, \hat{c}_j^\dagger] =$

δ_{ij}. The commutation relations for the $\hat{b}$'s then give the conditions

$$\sum_j u_{ij}u^*_{i'j} - v^*_{ij}v_{i'j} = \delta_{ii'} \tag{3.21}$$

and

$$\sum_j u_{ij}v^*_{i'j} - v^*_{ij}u_{i'j} = 0\,. \tag{3.22}$$

Since the transformation (3.20) expresses a linear relationship, we can write it in matrix form:

$$\begin{bmatrix} \hat{b} \\ \downarrow \\ \hat{b}^\dagger \\ \downarrow \end{bmatrix} = \begin{bmatrix} U & V^* \\ & \\ V & U^* \end{bmatrix} \begin{bmatrix} \hat{c} \\ \downarrow \\ \hat{c}^\dagger \\ \downarrow \end{bmatrix}. \tag{3.23}$$

Here we have used the notation

$$\begin{bmatrix} \hat{b} \\ \downarrow \\ \hat{b}^\dagger \\ \downarrow \end{bmatrix}$$

to denote the vector

$$\begin{bmatrix} \hat{b}_0 \\ \hat{b}_1 \\ \vdots \\ \hat{b}_0^\dagger \\ \hat{b}_1^\dagger \\ \vdots \end{bmatrix},$$

and U and V are the matrices of which u_{ij} and v_{ij} are the components.

Eqs. (3.21) and (3.22) then give the following matrix expression:

$$\begin{bmatrix} U & V^* \\ V & U^* \end{bmatrix} \begin{bmatrix} U^\dagger & -V^\dagger \\ -V^\mathsf{T} & U^\mathsf{T} \end{bmatrix} = I\,, \tag{3.24}$$

from which we deduce the inverse transformation

$$\begin{aligned} \hat{c}_i &= \sum_j u^*_{ji}\hat{b}_j - v^*_{ji}\hat{b}^\dagger_j\,, \\ \hat{c}^\dagger_i &= \sum_j v_{ji}\hat{b}_j - u_{ji}\hat{b}^\dagger_j\,. \end{aligned} \tag{3.25}$$

The commutation relations for the $\hat{c}$'s and $\hat{c}^\dagger$'s then give the following relations:

$$\begin{aligned} \sum_j u^*_{ji}u_{ji'} - v^*_{ji}v_{ji'} &= \delta_{ii'}\,, \\ \sum_j u^*_{ji}v^*_{ji'} - v^*_{ji}u^*_{ji'} &= 0\,. \end{aligned} \tag{3.26}$$

These relations along with the relations (3.21,3.22) express the completeness and orthonormality of the transformation.

We would like this transformation to take $\hat{K}_2$ to a form which looks like the Hamiltonian for non-interacting particles:

$$\hat{K}_2 = \sum_i \varepsilon_i \hat{c}^\dagger_i \hat{c}_i\,. \tag{3.27}$$

The commutation relations for the $\hat{c}$'s and $\hat{c}^\dagger$'s mean that we should have $[\hat{c}_i, \hat{K}_2] = \varepsilon_i \hat{c}_i$. In the basis of the $\hat{b}$'s, this equation leads to:

$$\sum_j P_{ji}u^*_{jn} + R_{ij}v^*_{jn} = \varepsilon_n u^*_{in}\,, \tag{3.28}$$

$$\sum_j -P_{ij}v^*_{jn} - R^*_{ij}u^*_{jn} = \varepsilon_n v^*_{in}\,, \tag{3.29}$$

where we have defined $R_{ij} = Q_{ij} + Q_{ji}$. This equation can be put into matrix form by defining the set $\{\mathbf{u}_n\}$ and $\{\mathbf{v}_n\}$ as consisting of vectors whose i'th components are u_{in} and v_{in} respectively. We then have:

$$\begin{bmatrix} P^* & R \\ -R^* & -P \end{bmatrix} \begin{bmatrix} \mathbf{u}^*_n \\ \mathbf{v}^*_n \end{bmatrix} = \varepsilon_n \begin{bmatrix} \mathbf{u}^*_n \\ \mathbf{v}^*_n \end{bmatrix}\,, \tag{3.30}$$

where P and R are the matrices whose components are P_{ij} and R_{ij} respectively, and we have used the fact that P is Hermitian. Thus performing the Bogoliubov transformation amounts to solving the eigenvector problem above. From the form of the matrix above, it can be seen that if $[\mathbf{u}^*, \mathbf{v}^*]^\mathsf{T}$ is an eigenvector for Eq. (3.30) with eigenvalue ε, then $[\mathbf{v}, \mathbf{u}]^\mathsf{T}$ will also be an eigenvector with eigenvalue $-\varepsilon$, reflecting the time-reversal symmetry of the problem (these extra eigenvectors are in fact analogous to the prediction of positrons as the antiparticles of electrons, etc.).

The 'particles' which appear in Eq. (3.27) are termed *quasiparticles*, since their creation operators consist of a linear combination of atom creation and annihilation operators. In a trapped condensate, it is possible to identify three classes of quasiparticles graded by increasing energy [24,77,93–95]. Those quasiparticles with lowest energy take the form of phonons i.e. their creation operators contain significant contributions of both particle creation and parti-

cle annihilation operators. They can be determined by solving the Bogoliubov equations as outlined above, or the largely equivalent Hartree-Fock equations in the random phase approximation [66]. In a band of somewhat higher energy, the quasiparticles are particle-like i.e. their creation operators contain only a very small contribution from particle annihilation operators. However, their spectrum *is* affected by the presence of the condensate. They can be found by solving the Hartree-Fock equations [66] which are simpler than the Bogoliubov equations. At even higher energies, the quasiparticle operators are identical to the particle operators, since the condensate does not affect particles with very high energy.

Chapter 4

Excitations and instability of a two-species BEC

In the following chapter, we extend the Bogoliubov theory described in the last chapter to the case of a two-species BEC consisting of a mixture of two hyperfine sublevels of a given atom condensed in a single trap. We find that the density profile of the system can undergo a spontaneous breaking of cylindrical symmetry as certain parameters of the system are changed, and that this symmetry breaking greatly affects the excitation spectrum of the system. This work was published in [35].

4.1 Introduction

A two-species BEC was first produced in the lab by Myatt *et al.* [28] in 1996. A two-species BEC is a condensate consisting of two different species of atoms - or alternatively, two interacting BECs composed of different species. We could have, for example, a Rb-Na mixture [96–98] or two hyperfine sublevels of the same atomic species [28–31, 35, 99]. At the time of writing, only the latter case has been achieved in the laboratory, with either the $|1,-1\rangle$ and $|2,2\rangle$ [28] or the $|1,-1\rangle$ and $|2,1\rangle$ [29–31] hyperfine sublevels of ^{87}Rb. Such two-species condensates allow many interesting experiments to be performed, especially since the two hyperfine sublevels can be coupled by means such as rf fields or laser driven Raman transitions. For example, one could perform experiments which demonstrate an effect analogous to the Josepson effect seen in other condensed systems [100–102], or one could investigate the dynamics of the relative phase between the two components [31, 82, 83, 85, 87]. One would certainly be interested in seeing how the complexity introduced by having two condensed components would affect the behaviour of the density profile and excitation spectrum of the two-condensate system. In this chapter, we examine this problem for the case of one experimentally relevant and interesting setup,

and find that instabilities in the system can lead to a spontaneous breaking of spatial cylindrical symmetry. The symmetry breaking takes the form of a discontinuous change to a different stable configuration (a phase change).

4.2 Properties of two-species BECs in ^{87}Rb

Magnetic trapping introduces the possibility that the two species may exist in traps which are vertically offset relative to one another. This will occur whenever the trapping potential in one species is not the same as that for the other species. The reason for this is that the gravitational field introduces a linear potential in one direction. Thus the potential in the vertical direction becomes

$$\begin{aligned} V_z &= \frac{1}{2}m\omega^2 z^2 + mgz \\ &= \frac{1}{2}m\omega^2\left(z + \frac{g}{\omega^2}\right)^2 - \frac{mg^2}{2\omega^2}, \end{aligned} \tag{4.1}$$

meaning that the trap center becomes offset, or 'sags' by a distance of g/ω^2. Unequal trap strengths for the two species will result in a different degree of 'sag' for each species, and hence the trap centres will be offset relative to one another. Such an offset was present in the first double condensate reported by Myatt *et al.* [28], which involved the $|1,-1\rangle$ and $|2,2\rangle$ hyperfine sublevels of ^{87}Rb. This density profile and excitations of this system have been studied by Esry *et al.* [103,104]. Such a system exhibits a certain degree of spatial separation between the components which is purely due to the gravitational sag, and thus it is not ideal for experiments in which the overlap between the components needs to be large.

It is also possible to condense the $|1,-1\rangle$ and $|2,1\rangle$ hyperfine sublevels of ^{87}Rb [29–31]. The magnetic dipole moments of these two sublevels are, to first order, equal. The trapping potential is also to some degree variable by adjusting the parameters of the TOP trap in which they are condensed [29]. It is possible to produce a two-species BEC in which the two species share the same trapping potential, and thus present the best chance of maximising spatial overlap. This situation is obviously interesting from the point of view of performing interference and internal Josephson coupling experiments, which utilise the mixing of the components.

In what follows, we shall refer to the two species as species A and species B.

The scattering lengths for the $|1,-1\rangle$, the $|2,-1\rangle$ and the $|2,2\rangle$ sublevels are all similar. For the case in which we are interested here, that of the $|1,-1\rangle$ (A)

and the $|2,-1\rangle$ (B) sublevels, the A-A scattering length describing collisions between two species A atoms is $a_{AA} = 5.68$ nm, the B-B scattering length is $a_{BB} = 5.36$ nm, and the A-B scattering length is $a_{AB} = 5.5(3)$ nm. At the time that this research was undertaken, this latter quantity was uncertain, and hence we used three different values (5.0 nm, 5.52 nm, 6 nm) for it. This also allows us to explore the effect of interspecies scattering length on spontaneous symmetry breaking. In general, if these scattering lengths differ from the each other by too much, then the system will exhibit a large loss rate due to inelastic collisions [28,105,106].

4.3 Previous work

Two-species BECs tend to behave analogously to two-fluid mixtures, for example oil and water or ethanol and water. If we first consider a free space two-species BEC as an illustration, and take the case where the intraspecies scattering lengths are equal, then the two components will preferentially mix together only if the interspecies scattering length is less than the intraspecies scattering lengths. If the interspecies scattering length is larger than the intraspecies scattering lengths, then the two components will preferentially separate out, like oil and water. This can be seen by comparing the energy due to atom-atom collisions for the case in which the two components are separated, with each taking up a volume V, and the case where the components are mixed, with the mixture taking up a volume $2V$. This separation has recently been studied systematically for a free space BEC by Timmermans [107].

Introducing a trapping potential complicates things somewhat, since the trap can act to force two otherwise immiscable components together. Ho and Shennoy [96] have used a generalisation of the Thomas-Fermi approximation to calculate the density profiles of the two-components. This approximation divides the density profile up into up to three volumes, the first containing only species A atoms, the second containing only species B atoms, and the third containing a mixture of the two. The precise configuration of the density profile of course depends on the details of the system, but in general the rule that an interspecies scattering length which is larger than the intraspecies scattering lengths leads to component separating holds. In fact it can be shown [108] that, in the Thomas-Fermi limit and equal mass for each species, component separation will occur for an interspecies scattering length a_{AB} which is greater than a critical value a_{AB}^c given by $a_{AB}^c = \sqrt{a_{AA}a_{BB}}$.

It is important to note, however, that the calculation used in this paper assumes cylindrical symmetry; as we will show here, this assumption may not always be warranted.

Pu and Bigelow [97] have gone beyond the Thomas-Fermi approximation and shown that in certain parameter regimes the Thomas-Fermi approximation can differ significantly from the actual ground state density profile even for a large number of atoms. This is because, in certain parameter regimes, the local energy density is more sensitive to the *total* density of atoms rather than to the individual density of each species, and thus the kinetic energy can play a role in determining the latter quantity. Esry *et al.* [66] have numerically calculated the density profile for the experimental case of Myatt *et al.* [28]; like the case treated here, this system is not spherically or cylindrically symmetric. Öhberg and Stenholm have treated the system in two dimensions using Hartree-Fock theory and have found similar breaking of spatial symmetry to that presented here.

The complicated behaviour of the density profile of such systems naturally increases the complexity of the collective excitations. The excitation spectrum has been analytically calculated in the Thomas-Fermi limit by Graham and Walls [109]. They consider a system in which the parameters are such that the two components form a homogeneous mixture throughout the trap. Under such circumstances, the excitation spectrum shows a doubling up as compared to that of the single-species excitation spectrum; there is one set of excitations which are identical to the corresponding single species system, and another set of excitations which are identical to the single species case except that all the frequencies have been scaled down by a factor which depends on the parameters of the system. If we take the simplest case, where there are equal numbers of atoms in each species and the intraspecies scattering lengths are equal, then this scaling factor goes to zero as the interspecies scattering length approaches the intraspecies scattering length from below.

It is easy to see what is going on here. The first 'normal' kind of excitations are due to the whole homogeneous mixture of two components oscillating in phase, as if it were a single species condensate; thus the excitation spectrum for this kind of oscillation resembles the single species case. The second 'scaled' excitations have the two components oscillating out of phase, so that when one component is moving one way, the other component is moving the other way. At the point of greatest amplitude of excitation, the components become somewhat separated. If the interspecies scattering length were greater than the intraspecies scattering lengths, then the components would want to stay separated from each other to some extent; in this case, the assumption that the ground state is a homogeneous mixture would be wrong. For interspecies scattering lengths which approach the intraspecies scattering length, we can see that this effect still tends to push the components apart somewhat and thus delay them coming back to their relaxed state as a homogeneous mixture.

Thus the period of the oscillation is increased. For all scattering lengths being equal, the oscillation period goes to infinity, marking the onset of instability in the density profile.

To investigate the excitation spectrum beyond the regime of homogeneously mixed components we must go beyond this analytical description. Esry and Greene [104], have calculated the excitation spectrum for the case of Myatt *et al.* [28] in which the two components are separated by gravity, and found various features such as avoided crossings in the excitation spectrum. Busch *et al.* [110] have taken an alternative approach and used a variational model to get the dynamics and the very lowest frequencies in the excitation spectrum. Pu and Bigelow [98] have numerically calculated the spectrum for a mixed Rb-Na two-species condensate in a spherically symmetric trap. They find that, as the interspecies scattering length approaches a certain critical value, the $n = 0, l = 1$ excitation, which represents a non-spherically symmetric oscillation, approaches zero, thus heralding the onset of the kind of instability discussed in this chapter. However, they do not investigate the breaking of spherical symmetry which would occur beyond this parameter regime.

4.4 The Hamiltonian for a two-species BEC

In the following section we shall derive the Gross-Pitaevskii and Bogoliubov equations for a two-species BEC.

For a two-species condensate, the second quantized grand canonical Hamiltonian is (eg. see [99]), in the position basis and using the delta function approximation,

$$\begin{aligned}
\hat{K} &= \int d^3\hat{\mathbf{r}}\, \hat{\psi}_A^\dagger(\mathbf{r}) \left[\frac{\hat{\mathbf{p}}^2}{2m} + V_A(\mathbf{r}) - \mu_A\right] \hat{\psi}_A \\
&+ \int d^3\hat{\mathbf{r}}\, \hat{\psi}_B^\dagger(\mathbf{r}) \left[\frac{\hat{\mathbf{p}}^2}{2m} + V_B(\mathbf{r}) - \mu_B\right] \hat{\psi}_B \\
&+ \frac{U_{AA}}{2} \int d^3\hat{\mathbf{r}}\, \hat{\psi}_A^\dagger(\mathbf{r})\hat{\psi}_A^\dagger(\mathbf{r})\hat{\psi}_A(\mathbf{r})\hat{\psi}_A(\mathbf{r}) \\
&+ \frac{U_{BB}}{2} \int d^3\hat{\mathbf{r}}\, \hat{\psi}_B^\dagger(\mathbf{r})\hat{\psi}_B^\dagger(\mathbf{r})\hat{\psi}_B(\mathbf{r})\hat{\psi}_B(\mathbf{r}) \\
&+ U_{AB} \int d^3\hat{\mathbf{r}}\, \hat{\psi}_A^\dagger(\mathbf{r})\hat{\psi}_B^\dagger(\mathbf{r})\hat{\psi}_A(\mathbf{r})\hat{\psi}_B(\mathbf{r}), \qquad (4.2)
\end{aligned}$$

where $\hat{\psi}_A(\mathbf{r})$ and $\hat{\psi}_B(\mathbf{r})$ are the field annihilation operators for species A and B respectively, $\mu_{A/B}$ are the chemical potentials for the two species, m is the

atomic mass (assumed here to be equal for species A and B), $V_{A/B}$ are the trapping potentials for the two species and the $U_{AA/BB/AB}$ are the strengths of the collisional interactions between two atoms of species A/two atoms of species B/an atom of species A and an atom of species B ($U_{pq} = (4\pi a_{pq}\hbar^2)/m$, where P and Q stand for A or B and the a_{pq} are the scattering lengths between an atom of species p and an atom of species q). We see in this expression that there are two chemical potentials, μ_A and μ_B. In the last chapter, it was shown that the chemical potential acts like a Lagrange multiplier to incorporate the constraint of a fixed number of particles; in the case here, the presence of two chemical potentials is due to the fact that we wish the number of atoms in *each* species to be fixed rather than simply the total number of atoms.

We wish to work in a general basis of harmonic oscillator eigenfunctions. As will be explained, the numerical technique which we employ means that these are not necessarily the single particle energy eigenstates of the trapping potential, but rather the energy eigenstates of some other fictitious trapping potential. We thus have a set of spatial modes $\phi_i^{A/B}(\mathbf{r})$. We use the operators $\hat{a}_i$ and $\hat{a}_i^\dagger$ to denote the annihilation and creation operators for an atom of species A in the mode $\phi_i^A(\mathbf{r})$ and $\hat{b}_i$ and $\hat{b}_i^\dagger$ to denote annihilation and creation operators for an atom of species B in the mode $\phi_i^B(\mathbf{r})$. In such a basis, we can write down the grand canonical Hamiltonian:

$$\begin{aligned}\hat{K} &= \sum_{i,j} H_{ij}^{0A}\hat{a}_i^\dagger\hat{a}_j + H_{ij}^{0B}\hat{b}_i^\dagger\hat{b}_j - \sum_i \mu_A\hat{a}_i^\dagger\hat{a}_i + \mu_B\hat{b}_i^\dagger\hat{b}_i \\ &+ \sum_{ijkl}\begin{pmatrix} \frac{1}{2}U_{AA}V_{ijkl}^{AA}\hat{a}_i^\dagger\hat{a}_j^\dagger\hat{a}_k\hat{a}_l \\ +\frac{1}{2}U_{BB}V_{ijkl}^{BB}\hat{b}_i^\dagger\hat{b}_j^\dagger\hat{b}_k\hat{b}_l \\ +U_{AB}V_{ijkl}^{AB}\hat{a}_i^\dagger\hat{b}_j^\dagger\hat{a}_k\hat{b}_l \end{pmatrix},\end{aligned} \tag{4.3}$$

where the $H_{nm}^{0A/B}$ are the matrix elements of the non-interacting Hamiltonian $p^2/2m + V_{A/B}(r)$ in our basis and the $V_{ijkl}^{AA/AB/BB}$ are the matrix elements of the two body potential:

$$V_{ijkl}^{pq} = \int d^3r\, \phi_i^{p*}(r)\phi_j^{q*}(r)\phi_k^p(r)\phi_l^q(r)\,, \tag{4.4}$$

where p and q denote the species of atom (A or B). In most cases we can assume that the members of the basis set $\{\phi_i\}$ are real, and thus the V_{ijkl}^{pq}'s are real. In such a case, V_{ijkl}^{AA} and V_{ijkl}^{BB} will be symmetric under any permutation of their indices and V_{ijkl}^{AB} will be symmetric under the interchange of the first and third, or second and fourth, indices. If we use the same spatial basis for each species, so that $\phi_i^A = \phi_i^B$, then V_{ijkl}^{AB} will be completely symmetric under the interchange of all indices. In such a case we would also have $V^{AA} = V^{BB} = V^{AB}$.

If we re-index our modes so that the mode index also includes the species index (A or B), then this Hamiltonian will take the same form as the single species Hamiltonian of the last chapter and thus we should be able to immediately write down the Gross-Pitaevskii equations and the Bogoliubov transformation. However, this is in practice rather confusing, so we shall outline the derivation below.

First we make the identification $\hat{a}_i = \alpha_i + \tilde{\hat{a}}_i$ and $\hat{b}_i = \beta_i + \tilde{\hat{b}}_i$, just as we did for the case of a single species condensate. In what follows, we shall abandon the tilde above the operators $\tilde{\hat{a}}$ and $\tilde{\hat{b}}$ and simply write them as $\hat{a}$ and $\hat{b}$, since we shall not again refer to the original operators of Eq. (4.3).

4.5 The two-species Gross-Pitaevskii equations

The energy functional is obtained by replacing the operators in Eq. (4.3) by their c-number equivalents, so that $\hat{a}_i$ is replaced by α_i and $\hat{b}_i$ by β_i, and likewise for the complex conjugates.

$$\begin{aligned} K_0 &= \sum_{i,j} H_{ij}^{0A}\alpha_i^*\alpha_j + H_{ij}^{0B}\beta_i^*\beta_j - \sum_i \mu_A\alpha_i^*\alpha_i + \mu_B\beta_i^*\beta_i \\ &+ \sum_{ijkl}\begin{pmatrix} \frac{1}{2}U_{AA}V_{ijkl}^{AA}\alpha_i^*\alpha_j^*\alpha_k\alpha_l \\ +\frac{1}{2}U_{BB}V_{ijkl}^{BB}\beta_i^*\beta_j^*\beta_k\beta_l \\ +U_{AB}V_{ijkl}^{AB}\alpha_i^*\beta_j^*\alpha_k\beta_l \end{pmatrix}. \end{aligned} \tag{4.5}$$

Taking the derivative of this quantity with respect to the α_i^* and β_i^*'s gives the coupled two-species Gross-Pitaevskii equations:

$$\begin{aligned} \sum_j H_{ij}^{0A}\alpha_j + \sum_{jkl} U^{AA}V_{ijkl}^{AA}\alpha_j^*\alpha_k\alpha_l + \sum_{jkl} U^{AB}V_{ijkl}^{AB}\beta_j^*\alpha_k\beta_l &= \mu_A\alpha_i \\ \sum_j H_{ij}^{0B}\beta_j + \sum_{jkl} U^{BB}V_{ijkl}^{BB}\beta_j^*\beta_k\beta_l + \sum_{jkl} U^{AB}V_{jilk}^{AB}\alpha_j^*\beta_k\alpha_l &= \mu_B\beta_i\,. \end{aligned} \tag{4.6}$$

The constraint of fixed particle number leads to the following additional conditions

$$\begin{aligned} \sum_i \alpha_i^*\alpha_i &= N_A\,, \\ \sum_i \beta_i^*\beta_i &= N_B\,, \end{aligned} \tag{4.7}$$

where N_A and N_B are the number of particles in species A and species B respectively.

Thus we see that solving the Gross-Pitaevskii equation amounts to solving a set of many coupled nonlinear equations in the α's, the β's and the μ's. However, what we are really interested in is the *minimum* of the energy functional H_0 subject to the constraints of particle number conservation; the solutions of the Gross-Pitaevskii equations only give its stationary points, irrespective of whether they are minima, maxima, or saddle points. This is typically not a problem, since in a numerical algorithm one would usually start with an analytic guess to the ground state which would then converge to the real ground state. However, as we shall see, it is possible for the global minimum of the energy functional for a two-species condensate to turn into a saddle point or a local maximum as the parameters of the system are smoothly varied, and thus solutions of the Gross-Pitaevskii equations can suddenly become unstable. Thus simply solving the Gross-Pitaevskii equation in the usual way will not guarantee a stable solution. In such a case, it is better to directly minimise the energy functional (4.5). This can be done by a variety of methods which will be discussed in Section 4.7.

4.6 The Bogoliubov equations

We can also generalise the Bogoliubov equations written down in the previous chapter to the case of a two-species BEC. We first write down the 2nd order grand canonical Hamiltonian $\hat{K}_2$:

$$\begin{aligned}
\hat{K}_2 &= \sum_{ij} H_{ij}^{0A}\hat{a}_i^\dagger\hat{a}_j + H_{ij}^{0B}\hat{b}_i^\dagger\hat{b}_j - \sum_i \mu_A\hat{a}_i^\dagger\hat{a}_i + \mu_B\hat{b}_i^\dagger\hat{b}_i \\
&+ \frac{1}{2}\sum_{ijkl} U^{AA}\left[V_{ijkl}^{AA}\alpha_k\alpha_l\hat{a}_i^\dagger\hat{a}_j^\dagger + V_{ijkl}^{AA*}\alpha_k^*\alpha_l^*\hat{a}_i\hat{a}_j + 4V_{ikjl}^{AA}\alpha_k^*\alpha_l\hat{a}_i^\dagger\hat{a}_j\right] \\
&+ \frac{1}{2}\sum_{ijkl} U^{BB}\left[V_{ijkl}^{BB}\beta_k\beta_l\hat{b}_i^\dagger\hat{b}_j^\dagger + V_{ijkl}^{BB*}\beta_k^*\beta_l^*\hat{b}_i\hat{b}_j + 4V_{ikjl}^{BB}\beta_k^*\beta_l\hat{b}_i^\dagger\hat{b}_j\right] \\
&+ \sum_{ijkl} U^{AB}\left[\begin{array}{l} V_{ijkl}^{AB}\alpha_k\beta_l\hat{a}_i^\dagger\hat{b}_j^\dagger + V_{klij}^{AB}\alpha_k^*\beta_l^*\hat{a}_i\hat{b}_j + V_{ikjl}^{AB}\alpha_k^*\alpha_l\hat{a}_i^\dagger\hat{a}_j \\ +V_{kijl}^{AB}\alpha_k^*\beta_l\hat{b}_i^\dagger\hat{a}_j + V_{iklj}^{AB}\beta_k^*\alpha_l\hat{a}_i^\dagger\hat{b}_j \\ +V_{kilj}^{AB}\alpha_k^*\alpha_l\hat{b}_i^\dagger\hat{b}_j + V_{ikjl}^{AB}\beta_k^*\beta_l\hat{a}_i^\dagger\hat{a}_j \end{array}\right]. \qquad (4.8)
\end{aligned}$$

With reference to the discussions of the previous chapter, we can write this expression as:

$$\begin{aligned}
\hat{K}_2 &= \sum_{ij} P_{ij}^{AA}\hat{a}_i^\dagger\hat{a}_j + P_{ij}^{BB}\hat{b}_i^\dagger\hat{b}_j + P_{ij}^{AB}\hat{a}_i^\dagger\hat{b}_j + P_{ij}^{BA}\hat{b}_i^\dagger\hat{a}_j \\
&+ Q^{AA}\hat{a}_i\hat{a}_j + Q_{ij}^{BB}\hat{b}_i\hat{b}_j + 2Q_{ij}^{AB}\hat{a}_i\hat{b}_j
\end{aligned}$$

$$+ \quad Q_{ij}^{AA*}\hat{a}_i^\dagger\hat{a}_j^\dagger + Q_{ij}^{BB*}\hat{b}_i^\dagger\hat{b}_j^\dagger + 2Q_{ij}^{AB*}\hat{a}_i^\dagger\hat{b}_j^\dagger \,. \tag{4.9}$$

With the Hamiltonian in this form we can make the straightforward generalisation for the matrix to be diagonalised:

$$\begin{bmatrix} P_{AA}^\mathsf{T} & P_{AB}^\mathsf{T} & R_{AA} & R_{AB} \\ P_{BA}^\mathsf{T} & P_{BB}^\mathsf{T} & R_{BA} & R_{BB} \\ -R_{AA}^* & -R_{AB}^* & -P_{AA} & -P_{AB} \\ -R_{BA}^* & -R_{BB}^* & -P_{BA} & -P_{BB} \end{bmatrix}, \tag{4.10}$$

where similar to the single species case the matrices P_{AA}, Q_{AA} etc. have the components P_{ij}^{AA}, Q_{ij}^{AA} and so on, and the matrices R are defined by $R = Q + Q^\mathsf{T}$. For completeness, we shall list these components:

$$\begin{aligned}
P_{ij}^{AA} &= H_{ij}^{0A} - \mu_A\delta_{ij} + \sum_{kl} 2U^{AA}V_{ikjl}^{AA}\alpha_k^*\alpha_l + U^{AB}V_{ikjl}^{AB}\beta_k^*\beta_l \,, \\
P_{ij}^{BB} &= H_{ij}^{0B} - \mu_B\delta_{ij} + \sum_{kl} 2U^{BB}V_{ikjl}^{BB}\beta_k^*\beta_l + U^{AB}V_{kilj}^{AB}\alpha_k^*\alpha_l \,, \\
P_{ij}^{AB} &= \sum_{kl} V_{iklj}^{AB}\beta_k^*\alpha_l \,, \\
P_{ij}^{BA} &= \sum_{kl} V_{kijl}^{AB}\alpha_k^*\beta_l \,, \\
R_{ij}^{AA} &= \sum_{kl} V_{ijkl}^{AA*}\alpha_k^*\alpha_l^* \,, \\
R_{ij}^{BB} &= \sum_{kl} V_{ijkl}^{BB*}\beta_k^*\beta_l^* \,, \\
R_{ij}^{AB} &= \sum_{kl} V_{klij}^{AB}\alpha_k^*\beta_l^* \,, \\
R_{ij}^{BA} &= \sum_{kl} V_{jikl}^{AB}\alpha_k^*\beta_l^* \,.
\end{aligned} \tag{4.11}$$

In most cases it will be possible to make several simplifying assumptions - for instance, V_{ijkl}^{pq}'s can usually be assumed to be real. Furthermore, in many cases it is possible to assume some kind of spatial symmetry, which means that it is often possible to rewrite the matrix (4.10) in block diagonal form, leading to large reductions in the time needed to compute the eigenvalues and eigenvectors.

4.7 Details of the algorithm

The major problem in solving for the density profile and excitations of a two-species BEC is that the number of basis vectors needed in three dimensions is large. If spatial symmetries exist (and at the time of writing this all BECs

made so far have been produced in cylindrically symmetric traps), then it is usually possible to greatly reduce the number of basis vectors by turning the problem into a one or two-dimensional problem. However, in such cases, one cannot keep the assumption of symmetry when calculating the excitations of the condensate, because if one does then the antisymmetric modes will be lost.

Unfortunately we cannot even assume cylindrical symmetry in the density profile for the current problem, even though the two species are assumed to exist in cylindrically symmetric traps. The reason for this is the spontaneous breaking of cylindrical symmetry discussed in the introduction to this chapter. If one chooses a basis which exhibits cylindrical symmetry, then one will find solutions which appear to be stable in this basis but which are in fact unstable to antisymmetric perturbations. This is important, because many papers on two species BECs have in fact made this assumption of cylindrical symmetry.

Bearing in mind that we will be dealing with completely anisotropic density profiles, we choose as our basis the basis of Cartesian normal modes for a harmonic oscillator potential. Thus we put

$$\psi_i^{A/B}(x,y,z) = \sqrt{(\lambda_x^{A/B}\lambda_y^{A/B}\lambda_z^{A/B})}\Phi_i\left(\frac{x}{\lambda_x^{A/B}}, \frac{y}{\lambda_y^{A/B}}, \frac{z}{\lambda_z^{A/B}}\right). \tag{4.12}$$

Here we have used the single subscript i to denote the triplet of quantum numbers (i_x, i_y, i_z) required by the normal modes representation. The $\Phi_i(x,y,z)$ are the modes of the single particle Hamiltonian with the trapping potential experienced by the BEC:

$$\Phi_{(i_x,i_y,i_z)}(x,y,z) = \phi_{i_x}(x)\phi_{i_y}(y)\phi_{i_z}(z), \tag{4.13}$$

where

$$\phi_{ix}(x) = 2^{-i_x/2}(i_x!)^{-1/2}\left(\frac{m\omega_x}{\hbar\pi}\right)^{1/4}\exp\left(\frac{m\omega_x}{2\hbar}x^2\right)H_{i_x}\left(\sqrt{\frac{m\omega_x}{\hbar}}x\right) \text{ etc.} \tag{4.14}$$

The λ's are scaling factors which give the factor by which our basis vectors differ from the basis of eigenfunctions of the single particle Hamiltonian without collisions.

4.7.1 The expanded basis set method

We have written our basis in this way so that we can employ a numerical method which we have called the expanded basis set method. The usual basis set method consists in minimising the energy functional H_0 using as a basis the trap eigenfunctions [62]. We have generalised this method so that our ba-

sis consists of scaled trap eigenfunctions, i.e. the λ's in Eq. (4.12) differ from 1. The value of the λ's is determined by minimising the energy functional with respect to variations in λ as calculated with a basis which is truncated after the lowest energy eigenfunction. In other words, we scale our basis vectors according to the Gaussian trial wavefunction which best approximates the lowest energy solution to the Gross-Pitaevskii equation. This method allows one to obtain a reasonable approximation to the ground state using fewer basis vectors —for example, in the extreme case where we use only one basis vector, this method is equivalent to the variational method of Fetter [65].

However, as the number of basis vectors increases, the scaling factors λ as determined by the variational method above do not necessarily remain the most efficient choice in determining the density profile and excitations. In such a case, is often better to scale back towards the original trap eigenfunctions and let the extra basis vectors provide the expansion in the size of the condensate cloud. Precisely how to scale the basis to give the most efficient performance for a given number of basis vectors seems to be a case of experimentation, but we have found that a good choice can be easily made if one knows the value of the λ's given by the variational method. Doing this allows one to obtain reasonable results using fewer basis vectors, an important consideration when dealing with completely anisotropic wavefunctions. Typically we have been able to obtain good results using about 200 basis vectors.

4.7.2 Symmetries in the problem

If we know by previous experience that the breaking of cylindrical symmetry will occur in a given direction, then we can use this knowledge to restore a degree of symmetry back into the problem. For instance, in the calculations presented here, the trap is shaped like a pancake, meaning that the radial frequency is less than the axial frequency. In this case, it turns out that the cylindrical symmetry is broken in a direction across a diameter of the 'pancake'. It is obvious that the particular orientation of this diameter is of no consequence, and hence we can choose a basis which considers only even basis vectors in the axial (z) direction, only even basis vectors in one of the radial directions (say x) and both even and odd basis vectors in the other radial direction (y), thus greatly reducing the number of basis vectors necessary for the problem. We have compared our results with assumed symmetry to results where no symmetry is assumed, and found that the essential results are the same except that the axis around which the symmetry was broken was somewhat random in the latter. This seemed to cause some numerical problems, due to the fact that there was no single point at which an energy minimum occurred.

4.7.3 Choosing the basis vectors

Our basis is composed of all basis vectors whose energy (as determined by the trap frequencies) is less than a certain maximum permissible energy. This means that there are less normal mode basis vectors $\phi_{iz}(z)$ in the axial direction, since the trap frequency in this direction is greater than in the radial direction. As the number of atoms in a condensate is increased, the cloud will expand due to repulsive atom-atom interactions. This expansion will be greatest in the direction which is most loosely confined, and hence this choice of basis vectors makes sense. Seen another way, the lowest energy basis vectors are preferentially populated.

4.7.4 Minimising the energy functional

Once we have determined a basis, the next step is to minimise the energy functional (4.5) subject to the fixed particle number constraints (4.7). This problem is a nonlinear minimisation problem with a large number of basis vectors and nonlinear constraints. We have solved it by using the NAG E04UCF library, which is part of a proprietary package provided by NAG (Numerical Algorithms Group). This routine employs the sequential quadratic programming (SQP) method of minimisation.

4.7.5 Finding the excitations

After solving the Gross-Pitaevskii equation, the final step is to find the excitations by calculating the eigenvectors and eigenvalues of the matrix (4.10). This is done using the NAG F02AXF package. We must use a larger basis to calculate the excitations than was used to find the mean field wavefunction, since we need to take into account antisymmetric excitations even in directions for which the wavefunction is symmetric. However, the symmetry of the wavefunction is still an asset since it means that many of the components of the matrix (4.10) are zero. We make use of this symmetry to write this matrix in block diagonal form and therefore greatly reduce the time and memory needed to compute the eigenvalues and eigenvectors.

4.7.6 Other considerations

There are other considerations which we will only briefly mention.

The V_{ijkl}'s as given in Eq. (4.4) are calculated using Gauss-Hermite quadrature. Although analytic expressions are available for these coefficients [62], this method turns out to by more efficient and stable, and can in fact be made

exact by using a certain number of quadrature points. The calculation of the coefficient V_{ijkl}^{AB} must take into account the scaling factors λ^A and λ^B, since these can be different for the two species. The other parameters, such as V_{ijkl}^{AA}, V_{ijkl}^{BB} and the H^0s depend on the λs only through constant scaling factors.

The program was carefully tuned to eliminate any redundant calculations by taking account of every symmetry in the problem. It was also vectorised to run efficiently on the Fujitsu VPP2200 at the Australian National University Supercomputer Facility (ANUSF).

4.7.7 Validation

Several tests were applied in order to validate the code.

If we consider the single condensate case[1], it is possible to derive analytical results for the excitation frequencies in the high particle number limit (see Stringari [111]). Firstly, it should be remarked that, if the particle number is high enough so that the Thomas-Fermi approximation is valid, then the excitation frequency should not depend on the particle number. This is clearly seen in Fig. (4.4(a)), where the excitation frequencies appear to reach assymptotic values. The horizontal ($|m| = 1$) excitation at $\omega_{||}$ (i.e. 16.6 Hz) is found not to change as the particle number is varied; this is in line with the analytical results of Stringari as well as other numerical calculations eg. those of Edwards *et al.* [23]. The pair of excitations ($|m| = 0$ and $|m| = 2$), which at low values of the particle number have a frequency of 2×16.6 Hz, are shifted downwards from this value as the particle number is increased. Stringari's calculation gives asyptotic values of $1.4\omega_{||}$ and $1.8\omega_{||}$ for parameters applicable to Fig. (4.4(a)). For the calculation used for Fig. (4.4(a)), the excitations appear to reach asymptotic values which are found to be $1.42\omega_{||}$ and $1.84\omega_{||}$, giving a relative error for these values of less than 3% as compared to the analytical results of Stringari. This calculation provides good circumstantial evidence that, at least in the single condensate case, the program is functioning correctly.

In another test, we have reproduced the parameters of Edwards [23]. Although the calculations could have been performed more efficiently and accurately with a code designed for single-species rather than two-species BECs, we have used the two-species code, since this calculation is a validation of this code. The excitation spectrum for this system is shown in Fig. (4.1) and may be compared to the graph in [23].

[1]Numerical calculations for the single condensate case were carried out simply by setting the parameter a_{AB} to zero, so that there was no interaction between the two clouds. It is possible to write much more efficient code when there is only one condensate to be considered, but in the current case this was unwarranted since we were primarily interested in the two-condensate case.

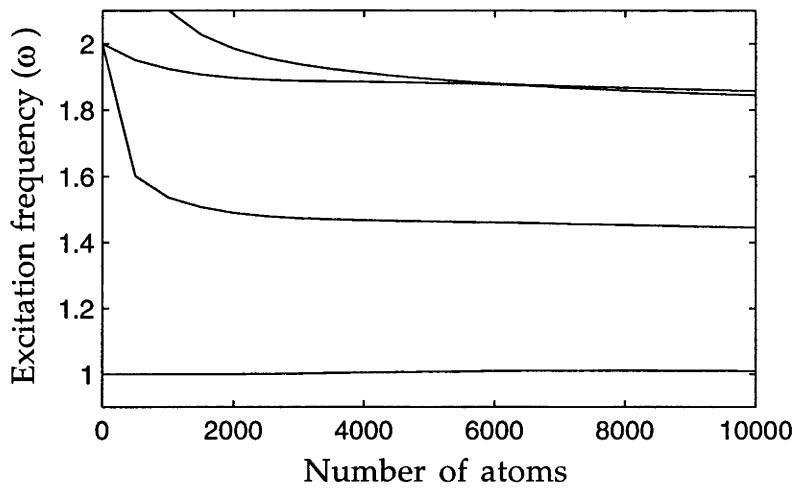

Figure 4.1: A plot of the single species $|m| = 1$ (lowest) and $m = 0$, $|m| = 2$ excitation frequencies for the parameters of [23].

It was also verified that the number of basis vectors was in a regime in which varying this number did not affect the results too much. To give an example of the kind of accuracy we were able to achieve, Fig. (4.2) shows the excitation spectrum for the parameters of Fig. (4.7), with two different basis sizes used. It can be seen that the results are fairly close for the low energy excitations, but begin to diverge for the higher frequency excitations, especially for the results calculated using 60 basis vectors.

Interestingly, the precise particle number at which the phase transition to a symmetry broken state was found to be very insensitive to the number of basis vectors used, so long as the population in the highest energy basis vectors did not become to large. The expanded basis method was found to be an important factor in maintaining this condition. As an extreme example of this, the program was run for only ten basis vectors. The phase transition was found to take place at the same atom number, to within the tolerance provided by the numerical parameters (which was approximately 5%).

Finally, the large atom number excitation spectrum was compared to the analytical results derived by Graham and Walls [109]. As an example, for the approximate parameters of Fig. (4.4)[2], the results of Graham and Walls [109] would give a lowest excitation frequency of 0.22×16.6 Hz. Our numerical

[2]To make a strict comparison, we would need to consider the case $a_{AA} = a_{BB}$. However, the difference is minor

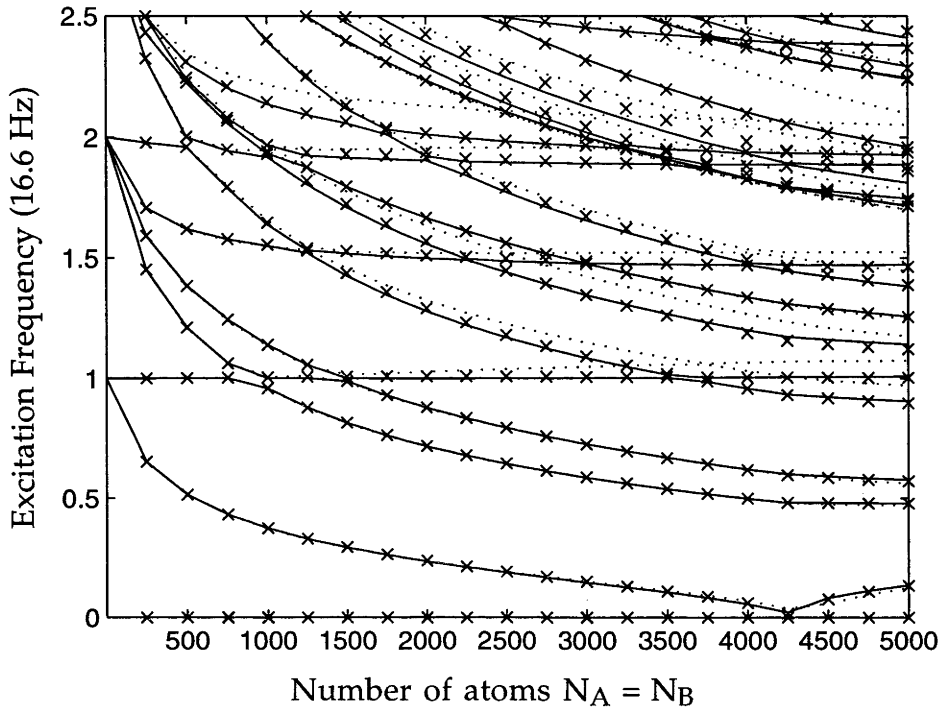

Figure 4.2: A comparison between the excitation spectrum calculated with 60 basis vectors (dotted line), 110 basis vectors (x's) and 172 basis vectors (solid line) Parameters are the same as those used for Fig. (4.7).

results give a value of 0.29×16.6 Hz, however, the asymptotic limit has clearly not yet been reached. A visual estimate of the asymptotic limit for the numerical results suggests a value of around 0.25×16.6 Hz, which is in reasonably good agreement with the analytical results.

4.8 Results

We consider here equal trapping potentials for species A and B. This situation has been experimentally achieved for ^{87}Rb atoms in the $|F, M_F\rangle = |1, -1\rangle$ and $|2, 1\rangle$ hyperfine sublevels which we label $|A\rangle$ and $|B\rangle$ [29]. We consider trap frequencies of $f_x = f_y = 47/\sqrt{8}$ Hz, $f_z = 47$ Hz which are relevant to these experiments in a TOP trap. The intraspecies scattering lengths are: $a_{AA} = 5.68$ nm, $a_{BB} = 5.36$ nm, and we consider three values (5.0 nm, 5.52 nm and 6.0 nm

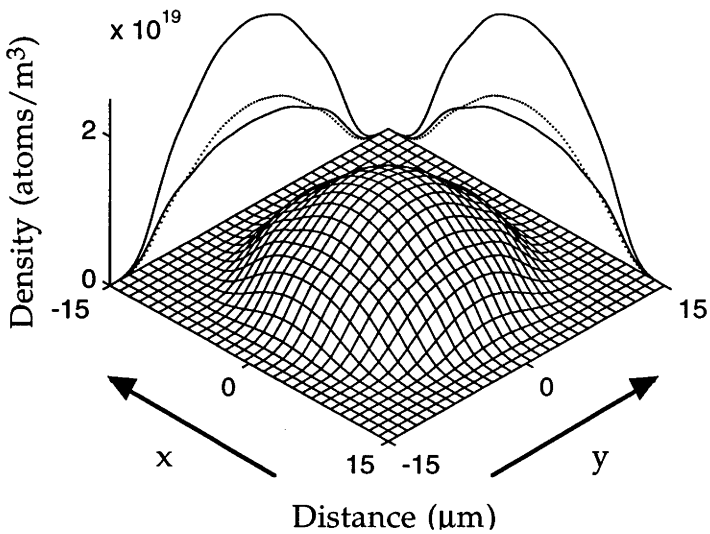

Figure 4.3: Radial cross section through the density profile for the parameters $a_{AB} = 5.0$ nm and $N_A = N_B = 15000$ atoms. The cross section is taken through the minimum of the trapping potential in the longitudinal direction. The mesh plot shows the maximum density for species A and B, and the line plots show the densities along the x and y axes of the combined density (upper plots) and species A and B densities (solid and dotted lines respectively). In this case, the scattering length a_{AB} is small enough compared to the two single species scattering lengths that the two species show no tendency to form separate clouds.

for a_{AB}

As shown by Ho and Shennoy [96], a binary condensate in the high particle number (Thomas-Fermi) limit can contain volumes in which only one species is present (giving two single particle phases, one for each species) and volumes in which both species coexist (binary phase) separated by phase boundaries. As an example, a condensate for which all parameters except the interspecies scattering length are the same for each species will exist as a single binary phase cloud only if $U_{AB} < U_{AA/BB}$. If we discard the Thomas-Fermi assumption, then this single species phase / binary phase picture is only approximate since the kinetic energy term in the Hamiltonian precludes the existence of sharp phase boundaries. However, a two-species BEC can still undergo phase transitions in the sense that a solution to the Gross-Pitaevskii equation may become unstable as parameters are varied, and the condensate will then undergo collapse to some other stable solution.

Fig. (4.3) shows a radial cross section through the density profile for $a_{AB} =$

5.0 nm and $N_A = N_B = 15000$ atoms. We see that in this case the two-species condensate exists as two highly overlapping clouds with no tendency to repel each other. The corresponding excitation spectrum is shown in Fig. (4.4 (b)), and Fig. (4.4 (a)) shows a single species condensate with $a = \sqrt{a_{AA}a_{BB}}$. We see that, as predicted by Graham and Walls [109], the excitation spectrum of the two-species condensate undergoes a doublet splitting as compared to the case of a single species condensate. We have compared our results to the high atom number limit derived by Graham and Walls for a spherically symmetric two-species condensate and found agreement to within a few percent for the lowest lying excitations with less than two hundred basis vectors.

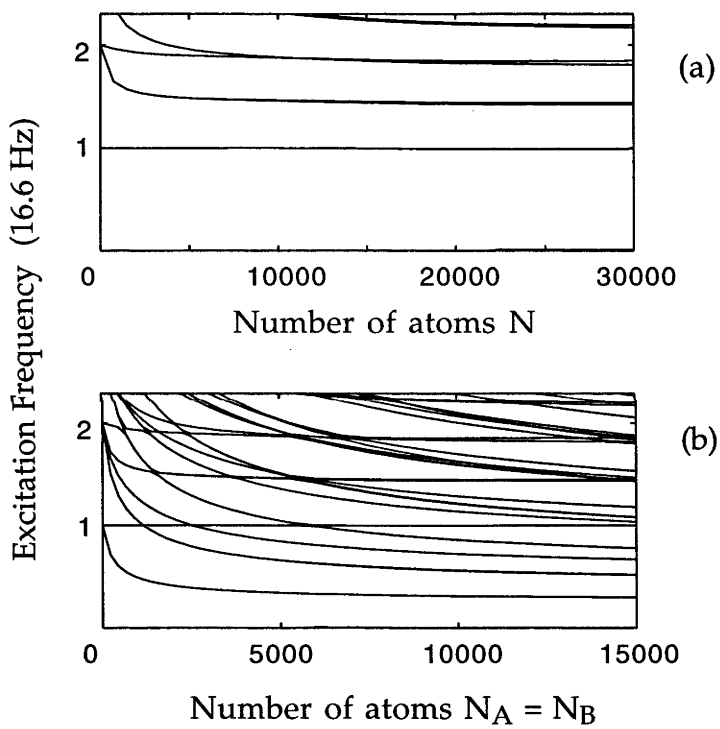

Figure 4.4: (a) Excitation spectrum for a single species BEC with $a_{AB} = 5.52$ nm. Parameters were chosen to approximate (b) as closely as possible. (b) Excitation spectrum for the parameters of Fig. (4.3).

Fig. (4.5) shows what happens when a_{AB} is increased to $\sqrt{a_{AA}a_{BB}} = 5.52$ nm. We see that at high atom number, the lowest energy eigenvalue approaches closer to zero frequency than in the case of Fig. (4.4), suggesting that we are near a region of phase instability in parameter space.

Indeed, in the case $a_{AB} = 6.0$ nm, the single phase solution to the GP equation becomes unstable at a critical atom number of around 4000. The minimum of the energy functional is given by a different density profile, as shown in

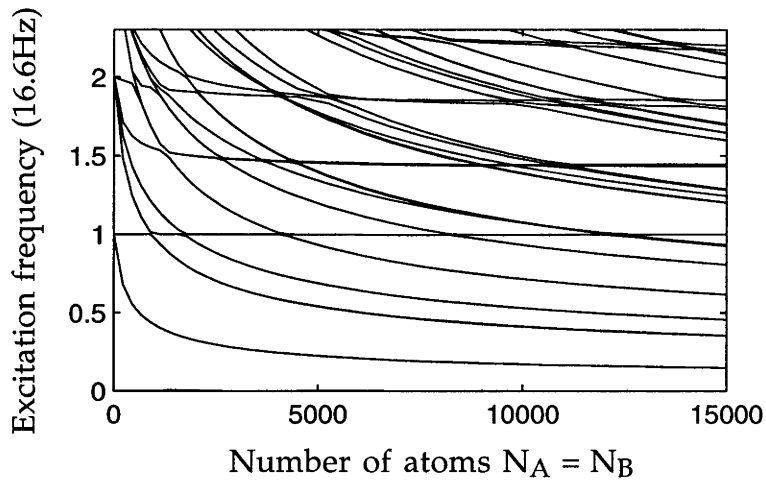

Figure 4.5: Excitation spectrum for $a_{AB} = 5.52$ nm.

Fig. (4.6). It can clearly be seen that the cylindrical symmetry is spontaneously broken by the two condensates' mutual repulsion. This effect was also seen by Öhberg and Stenholm [99] in a two dimensional calculation. It illustrates the danger in assuming spherical or cylindrical symmetry when solving for the density profile of a binary condensate, since in this case such an assumption leads to a state which is unstable with respect to certain antisymmetric perturbations.

The excitation spectrum for the parameters of Fig. (4.6) is shown in Fig. (4.7). We can clearly see that, for low atom numbers, the lowest (antisymmetric) excitation frequency goes to zero, suggesting the increasing instability of the condensate to antisymmetric perturbations[3]. This is indeed the case, as is shown by the breaking of cylindrical symmetry seen in Fig. (4.6). When $N \approx 4000$ is reached, the condensate undergoes a phase transition to an asymmetric ground state and the lowest energy eigenvalue increases again to an asymptotic limit.

One further interesting feature of this excitation spectrum is the persistence of excitations which look like the single condensate case even after the phase transition is reached - for example, the nearly horizontal excitation at 16.6 Hz which is hardly modified after the phase transition point. We interpret this as being due to the fact that, in the region above the phase transition, the *combined* density profile of the two species looks very much like a single species condensate, even though the individual density profiles of each species are greatly

[3]If we examine the symmetric state in the regime in which spontaneous symmetry breaking occurs, we find that the lowest energy eigenvalue has become imaginary. In such a case linear response theory suggests that a perturbation to such a state will grow exponentially in time instead of oscillating, as would be the case for a stable configuration

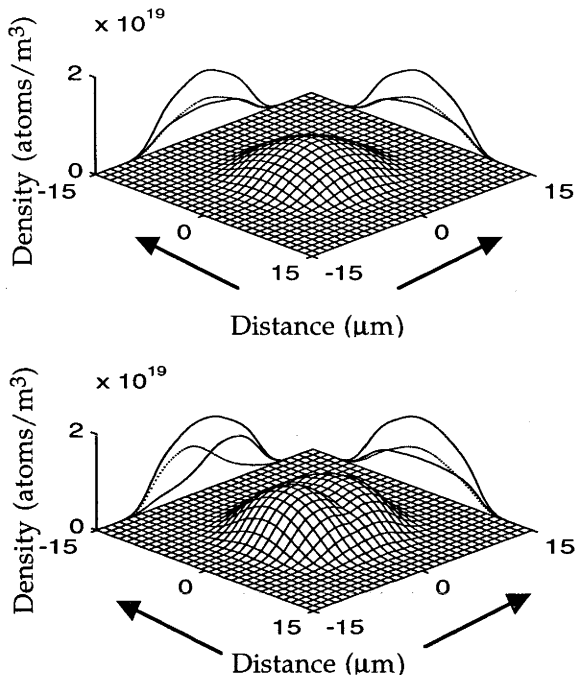

Figure 4.6: Density profile for $a_{AB} = 6.0$ nm. The top plot shows the densities for $N = 3000$ and the bottom plot shows the densities for $N = 4500$. The spontaneous breaking of cylindrical symmetry is seen in the latter case.

modified (see Fig. (4.6). The excitations in question are then interpreted as the normal single species type of excitations for this combined density profile.

We have also investigated the way that the critical atom number where symmetry breaking occurs varies with the intraspecies scattering length a_{AB}. Fig. (4.8) is a phase diagram which shows the region of broken symmetry.

4.9 Conclusion

By examining a realistic two-species BEC configuration, we have shown that it is possible for the spatial symmetry of such systems to be spontaneously broken in certain parameter regimes, and that this symmetry breaking is manifested in the excitation spectrum. It would be useful to know more generally the conditions under which such symmetry breaking occurs. Recently, Esry and Greene [108] have systematically investigated the spontaneous symmetry

breaking described by the author [35] and by Öhberg and Stenholm [99], and in particular have produced a phase diagram showing the regions of symmetry breaking in parameter space for a mixed Rb-Na condensate. Importantly, this phase diagram shows that if the other parameters of the system are kept constant and particle number is increased, then symmetry breaking will occur, as is found here. However, for even higher particle numbers, the system will again make a phase transition back to a symmetry preserving state in which one species forms a 'shell' around the other species.

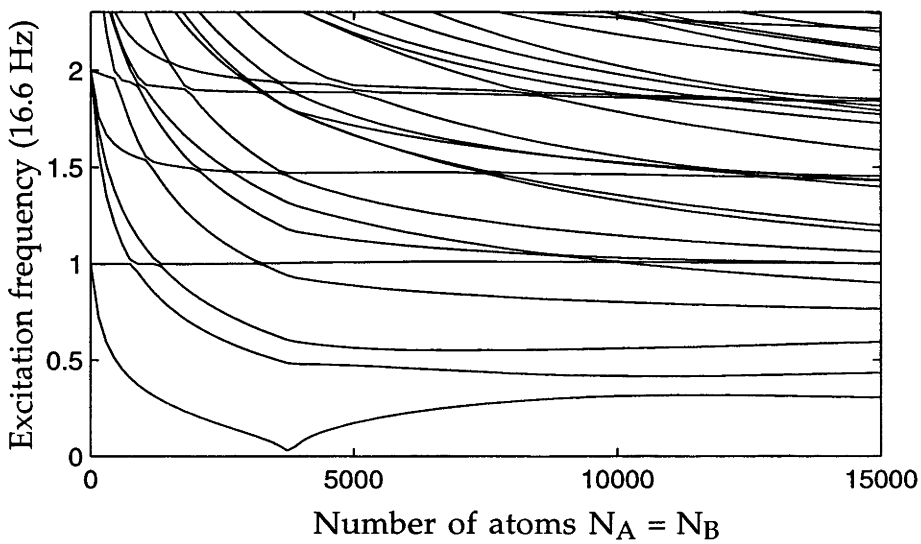

Figure 4.7: Excitation spectrum for $a_{AB} = 6.0$ nm. The onset of phase instability can be seen at around $N = 4000$ and is characterized by the lowest excitation frequency approaching zero. Following a phase transition to a symmetry broken state, the lowest energy eigenvalue increases again, tending towards an asymptotic limit.

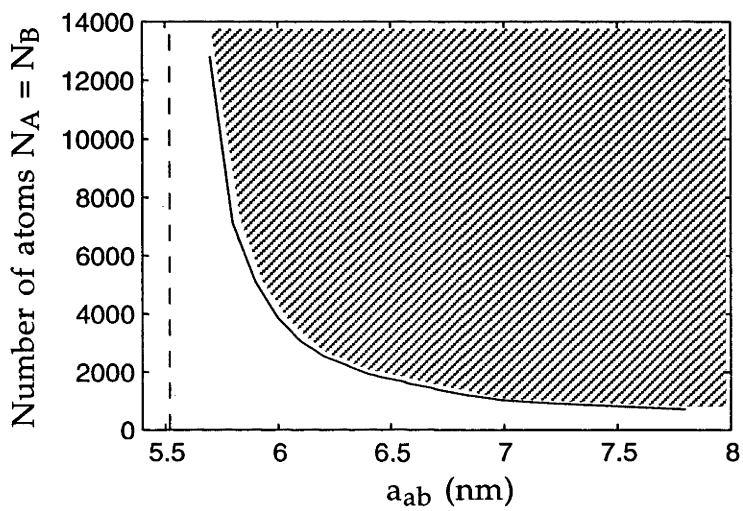

Figure 4.8: A phase diagram showing the region of broken symmetry (hatching). The dashed line denotes the value of a_{AB} below which no symmetry breaking can occur, i.e. $a_{AB} = \sqrt{a_{AA}a_{BB}}$.

Chapter 5

Creating Schrödinger cat states using Bose-Einstein condensates

5.1 Introduction

In the early days of quantum mechanics, Erwin Schrödinger [112] proposed a peculiar thought experiment designed to bring to light in the most dramatic way possible one of the supposed conflicts between the Copenhagen interpretation of quantum mechanics on one hand and everyday reality on the other hand. A cat is kept in a sealed container where it is unable to be observed by the outside world. Also in the container is a mechanism containing an atom of some radioactive material, a device to measure the radioactive decay of this atom, and a device to release a poisonous gas whenever the decay is detected. The decay of the atom is supposedly governed by quantum mechanics, so that after an amount of time equal to one half life has elapsed, the atom should be in a 50-50 superposition between having decayed and not having decayed. But if that is the case, then the presence of the poison-release device means that the cat should be in a superposition between being alive and being dead. On the other hand, if the cat is observed then according to the measurement postulate the wavefunction should collapse and the cat will be either alive or dead. Various questions then arise about what constitutes an observation, and for whom - the so-called measurement problem. For example, surely the cat observes itself, but does this also collapse the wavefunction for the outside observer?

One important factor in these questions is the macroscopic, everyday nature of the cat. We are regularly unconcerned with the thought that an atom can be in a superposition between several different states, but when the concept of superposition is brought to the level of cats and dogs then we begin to feel worried. This was the point Schrödinger was trying to make when he put

forward his thought experiment [1]. Moreover, a reductionist viewpoint would like to explain the process of measurement as simply bringing the quantity being measured to the macroscopic level, and therefore one could argue that the measurement postulate is intimately connected with the behaviour of quantum mechanics at a macroscopic level. The view that quantum superpositions cannot exist at a macroscopic level is known as *macroscopic realism.*

The relationship between quantum mechanics, measurement, and macroscopic realism is one of the important, as yet unanswered, philosophical questions posed by quantum mechanics. Macroscopic realism asserts that a system with several macroscopically distinguishable states available to it will always be in one of these states. This is incompatible with quantum mechanics, which permits superpositions of different states [114]. Von Neumann proposed [115] that as we increase the size of our system, or make a measurement, an irreversible reduction of the state vector into a classical mixture of the eigenstates of the observable being measured takes place.

As necessary as it might seem to be in order to explain our observations, such a postulate perhaps introduces more puzzles than it solves. For example: exactly what is the nature of this state vector reduction? Is there some unknown physics which describes it, or is it simply a natural result of applying quantum mechanics to very large, complex systems. Precisely when does it happen, and by what process? Is the process of measurement simply a way of entangling the world of the very small with the macroscopic world in a precise way (increasing the size of a quantum system), or is the conscious act of observing the outcome of a measurement important?

Broadly speaking, there are two main positions held today. One view says that state vector reduction is a real physical process which would be explainable only by modifying our physical theories. Proponents of this view include Karolhazy [116], Komar [117], Ghirardi *et. al.* [118,119], Diosi [120], Pearle [121] and Penrose [3,122]. For example, one particularly popular viewpoint proposes that the collapse of the state vector would be triggered when variations in the gravitational self energy reached a certain level. Under such views, a quantum theory of gravity would fully explain the process of state vector reduction [3,116,117,120,122].

In contrast to the 'reduction is real' view discussed above, there is a program which seeks to explain state vector reduction using only (unitary) quantum mechanics, possibly in conjunction with ideas involving consciousness.

[1] Schrödinger's own view was basically that of the *hidden variable* view of quantum mechanics, in which the quantum mechanical description of reality is only a single viewpoint of a larger whole, and the change that takes place upon measurement is merely a change in viewpoint - see [113]

There are several different viewpoints which fit into this category.

The main problem encountered here is the linearity of quantum mechanics. If we accept that quantum physics describes the whole of reality, then we must accept the fact that making a measurement of a quantum mechanical system which is in a superposition will put the measuring aparatus, and hence the macroscopic world, into a superposition.

The 'many worlds' interpretation of quantum mechanics, put forward by Everett [123] and DeWitt [124] holds that this is precisely what happens. Superpositions are allowed to propagate forever, with the wavefunction of the whole universe 'splitting' whenever quantum mechanics so dictates. The problem now is to explain why we percieve reality as consisting of classical branches of the universe - in other words, why we only experience single branches of this infinitely branched universe. There are really two questions here: why do we percieve the world as classical, and why do we percieve only one branch [125]? It is difficult to be precise about such questions, since they refer naturally to our perception or consciousness, a subject which physicists are generally somewhat uncomfortable with addressing.

The theory of decoherence due to entanglement with the environment attempts to explain, if not the process of state vector reduction, then at least the emergence of classical physics from the quantum world, without introducing any new physics [125]. Under such a view, the quantum nature of reality is preserved at all levels. However, it is always impossible to completely isolate any quantum system from its environment: there is always some degree of interaction present. A measuring aparatus, when it collects information about any open quantum system, is forced to ignore the information contained in the entanglement of the system with the environment. Decoherence shows that in such circumstances, coherences between possible outcomes of the measurement will decay as the degree of entanglement with the environment increases, and thus the system will appear to be in a classical mixture of states rather than a quantum superposition. Thus the reduction proposed by Von-Neumann [115] takes place as a natural consequence of entanglement with the environment, and not due to some other mysterious mechanism.

However, this in itself does not explain the apparent collapse of the state vector i.e. the fact that we always observe one particular outcome for each measurement. At its most fundamental level, decoherence does not deny superpositions at all levels, but only says that they do not matter. Zurek [125] attempts to explain our failure to perceive superpositions by invoking a combination of the decoherence of our own brain states and natural selection [2] -

[2]Natural selection would apply in the sense that there would be no evolutionary advantage in perceiving superpositions between classical states

thus again bringing the ultimate question down to one of consciousness.

Recently there have been several experiments performed in which two-species Bose-Einstein condensates are created and manipulated [28–31]. These experiments have involved two-species BECs in which the two species consist of two hyperfine sublevels of ^{87}Rb - the $|F, m_f\rangle = |1, -1\rangle$ and $|2, 2\rangle$ sublevels in the case of [28] and the $|1, -1\rangle$ and $|2, 1\rangle$ sublevels in the case of [29–31]. Such a configuration has the advantage that the two species can be coupled to one another via an internal Josephson-type coupling realized by a multi-photon transition, allowing a rich variety of experiments to be performed.

Cirac *et al.* [2] have shown that if the two species are Josephson coupled, then in certain parameter regimes the ground state of the Hamiltonian is a superposition of two states involving a particle number imbalance between the two species. Such a state represents a superposition of two states which are macroscopically (or mesoscopically) distinguishable, and hence can be called a Schrödinger cat state. Using the scheme described in [2], the production of such a state would involve the adiabatic transfer of the double condensate to the ground state of the Josephson coupling Hamiltonian. Ruostekoski *et al.* [126] have also shown that such states can be created by a mechanism involving the coherent scattering of far-detuned light fields. Their model neglects the collisional interactions between particles.

In this chapter, we use a two-mode model to investigate the quantum state dynamics of such a system, including both inter-species and intra-species two-body collisions between atoms. We show that the interplay between the atom-atom collisions and the Josephson coupling can lead to evolution which results in macroscopic superposition states of the type discussed in Cirac *et al.* [2] and Ruostekoski *et al.* [126]. The 'size' of the Schrödinger cat can be adjusted by changing the strength of the Josephson coupling. Our scheme for producing cat states differs from [2] in that the macroscopic superposition is produced by the normal dynamic evolution of the system rather than by adiabatic transfer to the ground state of the Josephson coupling Hamiltonian. Indeed, in the parameter regimes we investigate, the ground state shows squeezing in the relative particle number [127], and is thus certainly not a Schrödinger cat state.

Our scheme may be compared to a typical experiment in quantum optics, where a coherent light beam is passed through a nonlinear crystal. During the time it takes for one photon to traverse the length of a crystal, the quantum state of the beam is modified by the nonlinearity - for example, squeezing or second-harmonic generation could take place. In the situation which we describe here, the nonlinearity is provided by the various collisional interactions modified by the Josephson coupling. We envisage preparing the initial state and then turning on the Josephson coupling for some amount of time. The

period during which the Josephson coupling is active is analogous to the time spent by the light field in the crystal; after the Josephson coupling is turned off, the quantum state of the system will have been modified. In the example here, the end result will be a Schrödinger cat state.

Although the production of such states would no doubt involve considerable experimental difficulty, we believe that it would be worthwhile, since the investigation of the boundary between the quantum (microscopic) world and the everyday macroscopic world is sure to provide fertile ground for new discoveries.

5.2 Schrödinger cat states

There is frequently some confusion over the relationship between Schrödinger cat states and other kinds of superposition states. For example, two-species BECs contain some atoms in one state and some in another state, and this is sometimes described as being a superposition between the two states. The popular description of a BEC as a 'super-atom' coupled with a confusion between single particle and multi-particle superpositions can lead to a tendency to describe such superpositions as 'a BEC in state A superposed with a BEC in state B'. However, if, under normal conditions, the states of several atoms were to be detected, then some would be measured in state A and some in state B, and so this picture is wrong. Normally, the N-particle wavefunction of the system will be something similar to the suitably normalised wavefunction $(|A\rangle + |B\rangle)^N$. This is very different from a superposition between a BEC in state A and one in state B, which looks more like the suitably normalised state $|A\rangle^N + |B\rangle^N$.

This latter state could be called a Schrödinger cat state, since it describes a system which is a superposition of two macroscopically distinguishable states. In such a case, making a measurement of the system by detecting the species of a single atom will be enough to collapse the wavefunction to one of these two states. In contrast, for the former case above, detecting a single atom will not greatly change the state of the system.

5.3 Schemes for creating Schrödinger cat states

There have been several schemes proposed for creating these states, all with their various plusses and minuses. In what follows, we shall discuss three such schemes, bearing in mind our interest in Bose-Einstein condensates. We shall also discuss some experimental work that has been done in demonstrat-

ing mesoscopic quantum superpositions. The first scheme is the well known Yurke-Stoler, or Y-S scheme [128]. This scheme was originally discussed in the context of quantum optics, but the model used applies very naturally to the case of BEC. The second and third schemes relate directly to the case of BEC. The second was proposed by J. Ruostekoski *et. al.* [126] and relies on the stimulated scattering of light, and the third was proposed by Cirac *et. al.* [2] and relies on cooling to the ground state of a given Hamiltonian.

5.3.1 The Yurke-Stoler scheme

The Yurke-Stoler scheme [128] for creating Schrödinger cat states relies on the simple single mode Hamiltonian

$$H = \hbar\omega\hat{N} + \hbar\Omega\hat{N}^k, \tag{5.1}$$

where $\hat{N} = \hat{a}^\dagger\hat{a}$, and $\hat{a}^\dagger$ and $\hat{a}$ are the creation and annihilation operators for the single mode. The term proportional to Ω represents a nonlinearity, perhaps introduced by the passage of light through a nonlinear crystal in the quantum optics case.

Transforming to an interaction picture in which the linear rotation due to the term $\omega\hat{N}$ is eliminated, the unitary evolution operator can immediately be written down as $\exp(-i\Omega\hat{N}^k t)$. Applying this to an initial coherent state $|\alpha\rangle$ and putting $t = \pi/2\Omega$ leads to the final state $(1/\sqrt{2})(\exp(-i\pi/4)\,|\alpha\rangle + \exp(i\pi/4)\,|-\alpha\rangle)$ for even k. This is a superposition between two coherent states with different phases.

The low nonlinearity of nonlinear optical crystals means that the creation of such states by this scheme could be particularly hard. Improvements can be made by employing feedback systems [129].

The Hamiltonian (5.1) can also be applied to the case of a BEC. The mode described by $\hat{a}$ and $\hat{a}^\dagger$ refers to the condensate mode, and the system is described in the single mode approximation, explained later in this chapter. The term proportional to Ω, with $k = 2$, describes atom-atom collisions.

5.3.2 The scheme of Sanders

A two mode analog to the Yurke-Stoler scheme was suggested by Sanders within the context of quantum optics [130]. This scheme is of interest here because the nonlinear interactions present in a condensate mean that it could be conceivably useful for producing cat states in a two-species BEC. It is also relevant to this chapter in the sense that it uses the same Hamiltonian as the scheme proposed here, apart from a term describing the Josephson coupling

of the two species. However, the precise mechanism by which the cat state is formed is different. In the case of Sanders [130], the cat state is formed by a rephasing of the relative phase between the two modes. This rephasing takes place on a timescale $t_r/2$, where t_r is the revival time for the relative phase [82]. Since t_r is in general very long compared to the kinds of experiments which can be done with BECs, this scheme could prove experimentally unfeasable. However, if in the future condensates can be formed in which the collapse and revival of the phase can be observed, then this scheme would be an excellent candidate for forming cat states, since the states formed exhibit particularly good coherence properties. Perhaps the best possibility for such experiments would come from condensates formed in smaller, tighter traps, since the revival time would be smaller[3].

Due to its relevance to the work presented in this chapter, we shall discuss the details of this scheme more thoroughly in a later section.

The next two schemes discussed in this section were designed specifically for BECs.

5.3.3 The scheme of Ruostekoski *et al.*

This scheme is interesting because it relies on the scattering of light to produce cat states. This is possible because the presence of BECs and the associated effects of Bose-enhancement allow the light to be coherently, rather than incoherently, scattered.

The setup consists of two untrapped Bose-condensed clouds moving toward each other with velocities k_0 and $-k_0$. At some time the clouds will overlap with each other. A beam of far-detuned monochromatic light is shone onto the overlap region, in a direction perpendicular to the motion of the Bose-condensed clouds.

Two different kinds of coherent scattering processes can now occur. By coherent scattering, we mean scattering in which the atom off which a photon is scattered ends up back in one of the Bose-condensed clouds. Such processes will be favoured over incoherent scattering processes because of the action of Bose-enhancement.

In the first kind of scattering, a photon is scattered off an atom in one cloud, which then ends up back in the same cloud. Since the final momentum of the atom is then equal to the initial momentum, this scattering process can occur only in the forward direction and hence simply represents the effects of the

[3]The 'size' of the cat state would also be smaller, but this could be seen as an advantage, since creating a cat state with thousands or even millions of atoms could be seen as over ambitious, at least in the medium term

refractive index of the clouds.

In the second kind of scattering, however, an atom is transferred from one cloud to another, thus undergoing a momentum change of $2\hbar k_0$. The scattered photon therefore undergoes the same momentum change, and thus is deflected from the path of the forward beam, either to the left or the right depending on which direction the momentum transfer occurred.

Thus behind the region of scattering we should see three light beams - one in the forward direction, one to the left, and one to the right. The forward beam is now ignored, and the left and right beams are recombined at a beam-splitter/combiner after which point the two beams are detected.

Since detected photons could have come from either the left or the right beam and thus been brought about by the transfer of an atom from the $-k_0$ cloud to the $+k_0$ cloud or vice versa, after one such scattering event the system will be in a superposition between having an excess of one atom in the $-k_0$ cloud and having an excess of one atom in the $+k_0$ cloud. Modeling of the effects of scattering many photons by means of a master equation then shows [126] that the system will be gradually driven towards a Schrödinger cat state consisting of a superposition of a state containing an excess of atoms in the $-k_0$ cloud and one containing an excess in the $+k_0$ cloud. Eventually the two clouds will spatially separate, leading to a spatial Schrödinger's cat state. The fact that the two beams are recombined before detection ensures that superpositions, rather than mixtures, are produced, since the detection of a photon in the recombined beam does not give any information about which particular scattering process it originated from.

5.3.4 The scheme of Cirac *et al.*

This scheme relies on cooling to the many-body ground state of a Hamiltonian describing a two-species BEC of the kind described in the last chapter which are coupled by a beam or a series of beams (which could, for example, be a pair of Raman laser beams or a microwave/rf two photon transition [29–31]) which are tuned to the transition between the two-species. Such a setup permits an exchange of atoms between the two species, and is therefore similar to the case of Josephson coupling where a barrier of a given potential permits a flow of particles between the regions on either side of the barrier. In fact the former case is known as the *internal Josephson effect*, because it is between two internal states of the particles in question rather than two externally (spatially) separated states.

The idea behind the scheme is fairly simple. It is well known that for a double well potential, the actual ground state is a superposition between the localised state in which the particle is located mainly to the left of the barrier

and the localised state in which it is mainly located to the right of the barrier. Thus the ground state of the quantum double well differs greatly from the ground states of the corresponding classical system, in which the particle is located in either one well or the other. If we want to construct an approximation to the quantum solution using classical solutions, then we are best off taking a superposition of the two degenerate classical superpositions.

The system examined by Cirac *et. al.* shows analogous behaviour. The full many-body Hamiltonian is invariant under the interchange of the two species types i.e. $A \leftrightarrow B$ interchanges, and hence the ground state should show the same symmetry. But in certain parameter regimes, this is not true of the corresponding classical (mean field) approximation to the solution, which can have degenerate ground states in which one species contains an excess of atoms. A better approximation to the real ground state solution is made by taking a superposition between the case where there are more atoms of species A and the case where there are more atoms of species B. Such a state is a Schrödinger cat state.

Cirac *et. al.* [2] examine this system in varying degrees of approximation. Firstly, they look at a two-mode model, in which the spatial dependence of the system is not taken into account, both from the point of mean field theory and exact numerical solutions. They find that in most regions the mean field theory is fairly accurate. Secondly, they look at the mean field theory for the case in which the spatial variation of the condensate is taken into account. They find a similar picture, except that the two states, 'cat alive' and 'cat dead' in their Schrödinger cat state exhibit differences in density profile as well as in particle number. This is made more apparent because of a technical feature of their model. In order to obtain Schrödinger cat states, the interspecies scattering length must be greater than the intraspecies scattering length, and thus the system is in a regime where the two components will preferentially spatially separate out from one another. Finally, they present a variational calculation which goes beyond mean field theory by allowing wavefunction components with different numbers of atoms to have different spatial density profiles (within the constraints of the variational method) and find essentially the same results.

In order to make Schrödinger cat states using this scheme, it is necessary to cool close to the *many body* ground state of the Hamiltonian in question. This is because the Schrödinger cat state of their theory arises as precisely the many-body ground state of the system, and thus in order to have a large population in the cat state it is necessary to have a large population in the many-body ground state. This is a far greater restriction than simply demanding Bose-Einstein condensation, or off-diagonal long range order. This latter demand

simply means that each atom is mainly in the ground state of the *single particle* Hamiltonian. For example, if 80% of the N atoms are in the single body ground state, then the population of the many body ground state will only be 0.8^N. Using this reasoning, it is easy to show that if $N-1$ out of N atoms are in the single particle ground state, then a fraction $1/e$ will be in the many-body ground state, which is of the order of $1/2$. Hence if many more than one particles are not in the single particle ground state, then we will not be able to observe the effects of the cat state.

5.3.5 Experimental Work

SQUID rings and CBJs

A SQUID ring (Superconducting QUantum Interference Device) is a superconducting ring interrupted by a weak Josephson junction. If an external magnetic flux is applied through the ring, then for some range of values of the applied flux, the total magnetic flux through the ring is found to exhibit metabistability [131]. The flux is then found to undergo stochastic transitions between the two stable states. At high temperatures, these transitions are found to be consistent with thermal hopping between the two states and thus to depend on temperature. However, at temperatures corresponding to energies lower than the potential energy barrier between the two minima, the temperature dependence should disappear, and only transitions consistent with macroscopic quantum tunelling across the barrier should occur [132]. The concept of macroscopic tunelling is interpreted to be consistent with the existence of macroscopic superpositions [114, 132], since these will presumably exist during the process of tunelling. Experimental evidence confirms this picture eg. [133].

A CBJ (Current Biased Junction) is a similar device made by cutting the SQUID ring and applying a fixed current across the junction. Similar experiments which also show the effects of macroscopic quantum tunelling have been performed [134].

Microwave cavity experiments

A mesoscopic superposition has been demonstrated by Brune *et. al.* [135] using a high-Q microwave cavity through which was passed a Rydberg atom in a superposition between two states, $|g\rangle$ and $|e\rangle$. During its traversal of the cavity, the atom interacts with the field inside the cavity only through dispersive frequency shifts, since the field in the cavity is detuned relative to the transition between the two levels. The nonlinearity introduced by the atom-field interaction results in a superposition state $(1/\sqrt{2})(|e, \alpha\exp(i\phi)\rangle + |g, \alpha\exp(-i\phi)\rangle)$,

where $\alpha \exp(i\phi)$ describes a coherent state of size α and phase ϕ. This state is rather similar to the kind of state produced by the Yurke-Stoler scheme, except for the entanglement of the field to the state of the single atom. Since, in the experiment of Brune *et. al.*, the cavity contained only a few quanta of the radiation field, the superpositions generated were rather small.

5.4 The model

By nature, any investigation of Schrödinger cat states will need to go beyond the mean field description of a BEC, since by definition a Schrödinger cat state can be approximated by a superposition of two classical (mean field) states. Our proposal for cat states uses a process of unitary evolution. Solving the time dependent problem for even a moderate number of atoms, including the full spatial structure as well as the effects of quantum statistics would be a formidable and probably prohibitive task except for a few special cases. Thus we have simplified the problem by adopting a two-mode Hamiltonian, as used in the first part of Cirac *et. al.* [2].

Our system consists of a two species BEC of the type discussed in the last chapter. Just as in the case of Cirac *et. al.*, the two species are coupled by a series of laser/microwave/r-f fields which we term the Josephson coupling beams.

We work in a basis which is chosen as follows. The condensate modes for species A and B are those wavefunctions which satisfy the coupled two-species Gross-Pitaevskii equations i.e. they are those spatial modes for species A and B which are macroscopically occupied. We also include a set of non-condensate modes such that we have a complete orthonormal basis $|\phi_i\rangle$ (such modes could be determined by the Hartree-Fock equations [66]).

In such a basis, the second quantized Hamiltonian is:

$$\begin{aligned} H &= \sum_{i,j} H^A_{ij} \hat{a}^\dagger_i \hat{a}_j + H^B_{ij} \hat{b}^\dagger_i \hat{b}_j + \frac{1}{2}\lambda_{ij}(\hat{a}^\dagger_i \hat{b}_j + \hat{b}^\dagger_j \hat{a}_i) \\ &+ \sum_{i,j,k,l} \frac{1}{2} W^{AA}_{ijkl} \hat{a}^\dagger_i \hat{a}^\dagger_j \hat{a}_k \hat{a}_l + \frac{1}{2} W^{BB}_{ijkl} \hat{b}^\dagger_i \hat{b}^\dagger_j \hat{b}_k \hat{b}_l + W^{AB}_{ijkl} \hat{a}^\dagger_i \hat{b}^\dagger_j \hat{a}_k \hat{b}_l \,. \end{aligned} \tag{5.2}$$

The $H^{A(B)}_{ij}$ are the matrix elements of the single particle Hamiltonian in our basis:

$$H^{A(B)}_{ij} = \langle \phi_i | \hat{\mathbf{p}}^2/(2m) + V^{A(B)}(\hat{\mathbf{r}}) | \phi_j \rangle \,. \tag{5.3}$$

The λ_{ij} are the matrix elements describing the Josephson coupling between the

two species, which for a position independent coupling is defined by

$$\lambda_{ij} = \Lambda \int d^3\mathbf{r}\, \phi_i^A(\mathbf{r})\phi_j^B(\mathbf{r})\,, \tag{5.4}$$

where Λ describes the strength of the coupling and the ϕ's are taken to be real. The W_{ijkl}^{pq} are the matrix elements of the two-body potentials describing collisions between an atom of species p and an atom of species q, where p and q stand for A or B:

$$W_{ijkl}^{pq} = U_0^{pq} \int d^3\mathbf{r}\, \phi_i^p(\mathbf{r})\phi_j^q(\mathbf{r})\phi_k^p(\mathbf{r})\phi_l^q(\mathbf{r})\,. \tag{5.5}$$

The U_0^{pq} are the two-body interaction parameters as defined in the previous chapter:

$$U_0^{pq} = 4\pi a_{pq}\hbar^2/m\,, \tag{5.6}$$

where a_{pq} is the scattering length for a two-body collision between an atom of species p and an atom of species q, and m is the mass of the atom.

The two mode approximation consists in neglecting all modes except the condensate modes. At zero temperature, this amounts to ignoring the atoms which have left the condensate mode due to the two-body potentials. The validity of this approximation is discussed in Section 5.8.

Under this approximation the Hamiltonian becomes

$$\begin{aligned}\hat{H} &= E_A\hat{a}^\dagger\hat{a} + E_B\hat{b}^\dagger\hat{b} + \frac{1}{2}\lambda(\hat{a}^\dagger\hat{b} + \hat{b}^\dagger\hat{a}) \\ &+ \frac{W_{AA}}{2}\hat{a}^{\dagger 2}\hat{a}^2 + \frac{W_{BB}}{2}\hat{b}^{\dagger 2}\hat{b}^2 + W_{AB}\hat{a}^\dagger\hat{b}^\dagger\hat{a}\hat{b}\,,\end{aligned} \tag{5.7}$$

where $E_{A(B)} \equiv H_{00}^{A(B)}$, $W_{pq} \equiv W_{0000}^{pq}$, $\lambda = \lambda_{00}$, $\hat{a} \equiv \hat{a}_0$, $\hat{b} \equiv \hat{b}_0$ and the condensate modes have the index 0.

As an example, if we consider the case where there are an equal number of particles in each species, equal cylindrically symmetric harmonic trapping potentials for each species, and scattering lengths satisfying $a_{AA} = a_{BB}$ and $a_{AB} \leq a_{AA}, a_{BB}$, then we find that the components will not spatially separate (see Chapter 4) and hence by symmetry the ground state solution to these equations has $\phi_0^A(\mathbf{r}) = \phi_0^B(\mathbf{r})$. In such a case we can easily solve the coupled Gross-Pitaevski equations for the condensate wavefunction in the Thomas-Fermi limit. Doing so yields

$$W_{pq} = \frac{2\cdot 15^{\frac{2}{5}}}{7}\left(\frac{m\omega_\perp^6\lambda_a^2\hbar^4}{N^3(a+a_{AB})^3}\right)^{\frac{1}{5}} a_{pq}\,, \tag{5.8}$$

where we have set $a_{AA} = a_{BB} = a$, $\omega_\perp$ is the trap angular frequency of the trap perpendicular to the axis of cylindrical symmetry, λ_a is the trap anisotropy i.e. the ratio $\omega_{||}/\omega_\perp$, where $\omega_{||}$ is the angular frequency parallel to the axis of cylindrical symmetry.

5.4.1 Angular momentum basis

We find it convenient to use operators satisfying the usual angular momentum commutation relations:

$$\begin{aligned} \hat{J}_x &= \frac{1}{2}(\hat{b}^\dagger \hat{a} + \hat{a}^\dagger \hat{b}), \\ \hat{J}_y &= \frac{i}{2}(\hat{b}^\dagger \hat{a} - \hat{a}^\dagger \hat{b}), \\ \hat{J}_z &= \frac{1}{2}(\hat{a}^\dagger \hat{a} - \hat{b}^\dagger \hat{b}), \end{aligned} \tag{5.9}$$

for which the Casimir invariant is $\hat{J}^2 = \hat{N}(\hat{N} + 1/2)$, where $\hat{N} = (1/2)(\hat{a}^\dagger \hat{a} + \hat{b}^\dagger \hat{b})$. Note that, for the Hamiltonian (5.7), $\hat{N}$ is a constant of motion. We shall limit ourselves to working with eigenstates of this operator. Hence we make the substitution $\hat{N} \to N$ in what follows. We use as a basis for the state of the system the eigenstates of the operator $\hat{J}_z$. Such a restricted basis contains $2N + 1$ basis vectors defined by

$$\hat{J}_z |m\rangle = m |m\rangle , \tag{5.10}$$

where m runs from $-N$ to N.

In terms of the operators (5.9) and neglecting terms which simply describe a shift in the zero-point of the energy, the Hamiltonian (5.7) is

$$H = \alpha \hat{J}_z + \beta \hat{J}_z^2 + \lambda \hat{J}_x , \tag{5.11}$$

where we have defined $\alpha = E_A - E_B + \left(N - \frac{1}{2}\right)(W_{AA} - W_{BB})$ and $\beta = (W - W_{AB})$, with $W = (W_{AA} + W_{BB})/2$. We can see from the structure of this Hamiltonian that we lose no generality by considering the case $W_{AA} = W_{BB} = W$, since the term proportional to $W_{AA} - W_{BB}$ can be compensated for by changing the values of E_A and E_B. In the case where $E_A - E_B + (N - 1/2)(W_{AA} - W_{BB}) = 0$, which holds if both traps are identical and the two species have equal intraspecies scattering lengths, the first term in the Hamiltonian is zero and the expression is formally the same as the Hamiltonian considered by Milburn *et al.* [101] in their analysis of the double well system. Note however the parameter dependence of the second term, which can be close to zero for realistic experimental parameters [31]. In such a case the decay time of

the relative phase between the two species approaches infinity, an effect noted by Law *et al.* [85] with a macroscopic model of collapse and revival and by Villain *et al.* [87] with a fully quantum-field model. The system will then exhibit purely sinusoidal Rabi-type Josephson oscillations.

In our chosen basis we have the following:

$$\begin{aligned}
\hat{J}_x|m\rangle &= \frac{1}{2}\left(\sqrt{(N-m)(N+m+1)}|m+1\rangle + \sqrt{(N+m)(N-m+1)}|m-1\rangle\right), \\
\hat{J}_y|m\rangle &= \frac{i}{2}\left(\sqrt{(N+m)(N-m+1)}|m-1\rangle - \sqrt{(N-m)(N+m+1)}|m+1\rangle\right), \\
\hat{J}_z|m\rangle &= m|m\rangle, \qquad (5.12)
\end{aligned}$$

so that it can be seen that the matrix representing H is tridiagonal. In the limit of zero Josephson coupling, H is diagonal so that the unitary evolution matrix can immediately be written down, and the dynamics solved. For non-zero Josephson coupling we need to first diagonalise a real tridiagonal matrix, which is in general the simplest kind of diagonalisation to perform numerically. The time needed to perform such a diagonalisation scales as N^3, and we have solved for values of N up to a few thousand.

5.5 The Bloch states and the Bloch Q-function

We can get a better idea about the quantum state by looking at the Q-function on the Bloch-sphere [127, 136]. This function is defined in terms of the so called Bloch states, or atomic coherent states, of which the states (5.17) are a particular case. They are defined in our basis as:

$$|\theta,\phi\rangle = (\cos(\theta/2))^{2N} \sum_m \sqrt{\binom{2N}{N-m}} \tan^{(N-m)}(\tfrac{1}{2}\theta) \exp(i(N-m)\phi)|m\rangle\,. \quad (5.13)$$

The parameter θ fixes the number of particles in each species, with $\theta = \pi/2$ giving equal numbers of particles in each species. The parameter ϕ describes the relative phase between the two species. θ and ϕ can be thought of as spherical coordinates, and hence each Bloch state $|\theta,\phi\rangle$ can be represented as a point on a sphere, called the *Bloch sphere*. Rotations of the Bloch sphere are accomplished by the unitary transformations consisting of products of the operators $\exp(i\alpha\hat{J}_q)$, where q takes the values x, y, z, and α is the angle of rotation around the q axis. Thus any Bloch state is isomorphic to any other Bloch state under a given rotation of the Bloch sphere.

The Bloch Q-function is defined as

$$Q(\theta,\phi) = |\langle\psi|\theta,\phi\rangle|^2 . \tag{5.14}$$

or equivalently

$$Q(\theta,\phi) = \langle\theta,\phi|\,\hat{\rho}\,|\theta,\phi\rangle \tag{5.15}$$

where $\hat{\rho}$ is the density operator for the state.

The PDE which governs the evolution of the Q-function can be derived by considering the master equation for the evolution of the density matrix in the basis formed by the eigenstates of J_z. In the case where the Josephson coupling is zero, Sanders [130] has given a derivation for this evolution in terms of a stereographic projection of the Bloch-sphere onto the complex plane. We choose not to use this stereographic projection, since it does not preserve the symmetry between an interchange of species and so creates problems of interpretation. In terms of the coordinates θ and ϕ, we find after a great deal of tedious algebra that the Q-function obeys the equation[4]

$$\begin{aligned}\frac{\partial}{\partial t}Q(\theta,\phi) &= \beta\left(-2N\cos(\theta)\frac{\partial}{\partial\phi} + \sin(\theta)\frac{\partial^2}{\partial\theta\partial\phi}\right)Q(\theta,\phi) \\ &+ \lambda\left(\cos(\phi)\cot(\theta)\frac{\partial}{\partial\phi} + \sin(\phi)\frac{\partial}{\partial\theta}\right)Q(\theta,\phi)\end{aligned} \tag{5.16}$$

The term proportional to β is essentially the same as that given by Sanders [130]. The term proportional to λ describes the effects of the Josephson coupling. The most obvious difference between these two terms is that the Josephson term depends explicitly on the coordinate ϕ. This makes physical sense, since in the absence of Josephson coupling, the behaviour of the system should be invariant under U(1) transformations. It is only the addition of an external phase reference, provided by the Josephson lasers, which breaks the U(1) symmetry.

5.6 Quantum dynamics

Before considering the creation of Schrödinger cat states, it is interesting to consider the evolution of some basic expectation values. We shall consider in turn the limits of zero Josephson coupling, small Josephson coupling and large Josephson coupling. For simplicity we shall also assume that the two

[4] we have neglected terms which lead to a constant rotation of the phase difference between the two-species

condensates are in the same trap and that the intraspecies scattering lengths are equal, so that we have $E_A = E_B$ and $W_{AA} = W_{BB} = W$.

5.6.1 Initial state

In current experiments, the two-species BEC is created by coupling two hyperfine sublevels with electromagnetic fields [28–31]. If we start with all $2N$ atoms in state A and apply a strong $\pi/2$ pulse (strong in the sense that the pulse duration is smaller than the timescale characterizing the dynamics of the system), then we will end up with the state

$$|\psi\rangle = 2^{-N} \sum_{m=-N}^{N} \exp(i(N-m)\phi)\sqrt{\binom{2N}{N-m}}|m\rangle\,, \tag{5.17}$$

where $\phi = \pi/2$ for the situation described here. This becomes clearer when we consider the Bloch states. The initial state has all the atoms in one species, and thus is defined by the Bloch state at one of the poles of the Bloch sphere. A $\pi/2$ pulse corresponds to the application of the operator $\exp(-i\pi/2\hat{J}_x)$ which is a rotation of the Bloch sphere by $\pi/2$ around the J_x axis. This brings the state to the point at which the J_y axis intersects the Bloch sphere, which is the Bloch state $|\pi/2, \pi/2\rangle$. This process is shown graphically in Fig. (5.1).

In what follows, we will need to consider a range of values of ϕ other than $\phi = \pi/2$ in Eq. (5.17)—in particular, the $\phi = 0$ state will be shown to evolve into a Schrödinger cat state. One way of varying ϕ would be to apply a strong pulse (such as a highly detuned intense light field) to one or both of the species, in order to shift the zero-point of their energy. Providing that the pulse interacts with each species with different coupling strengths, this will result in fast phase evolution which will change the relative phase between the two species.

Another scheme for changing the relative phase between the two components involves shifting the phase of the light fields providing the Josephson coupling. We imagine applying the $\pi/2$ pulse to create the initial state, and then switching to Josephson coupling beams with a different relative phase than that of the original $\pi/2$ pulse. If we remain in our original basis, then this change of phase will result in complex laser-dipole coupling coefficients and hence will show up as complex matrix elements for the Josephson coupling term:

$$\begin{aligned} H_{JOS} &= \frac{1}{2}(\lambda \exp(i\delta\phi)\hat{b}^\dagger\hat{a} + \lambda \exp(-i\delta\phi)\hat{a}^\dagger\hat{b}) \\ &= \lambda \hat{J}'_x\,, \end{aligned} \tag{5.18}$$

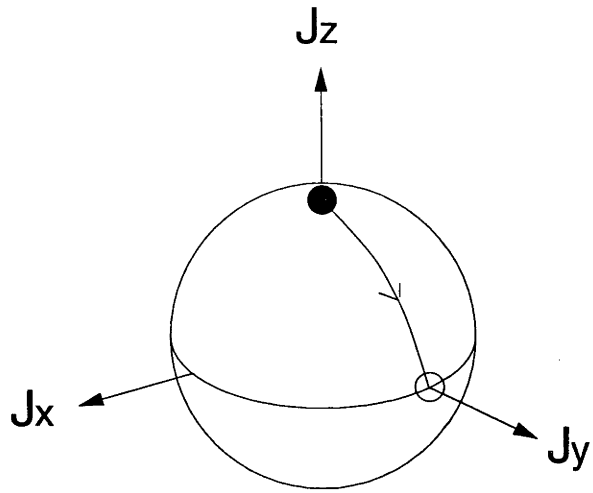

Figure 5.1: A schematic diagram of the Bloch sphere. The initial state has all atoms belonging to one species, and is a maximal eigenstate of J_z. It is located at the north pole of the Bloch sphere (the small black filled circle), with coordinates π, ϕ. A $\pi/2$ pulse is represented by the operator $\exp(-i\pi/2\hat{J}_x)$, which rotates the state by an angle of $\pi/2$ around the J_x axis. This brings it to the position of the small open circle, which is the Bloch state $|\pi/2, \pi/2\rangle$.

where $\hat{J}'_x = (1/2)(\exp(i\delta\phi)\hat{b}^\dagger\hat{a} + \exp(-i\delta\phi)\hat{a}^\dagger\hat{b})$, and $\delta\phi$ is the change in relative phase for the Josephson coupling beams relative to the beams which supplied the original $\pi/2$ pulse. This operator can be obtained from J_x by a unitary transformation corresponding to the unitary operator $\exp(-i\delta\phi\hat{J}_z)$. Since J_z commutes with this operator, it remains unchanged. Thus, if we apply this unitary transformation to the new Hamiltonian which has complex Josephson coupling matrix elements, we will end up with a Hamiltonian which again looks like the original Hamiltonian (5.11). However, in making our change of basis we must also apply this unitary transformation to the state vector; doing so is found to rotate the relative phase between the two species by an amount $\delta\phi$. Thus, in summary, if we change the phase of our Josephson coupling beams immediately following the initial $\pi/2$ pulse, and then imagine a certain unitary change of basis, the system will be unchanged except that the relative phase between the two species will appear to have been rotated.

5.6.2 Quantum dynamics in the absence of Josephson coupling

In this case, as has been remarked, the Hamiltonian is diagonal and is given by

$$H = \beta \hat{J}_z^2 . \tag{5.19}$$

Clearly the phase ϕ of the initial state (5.17) does not affect the quantum dynamics, since changes in ϕ correspond to rotations of the state around the J_z axis on the Bloch sphere. Such rotations are represented by the unitary operator $\exp(-i\phi\hat{J}_z)$, which commutes with the Hamiltonian.

The dynamics can be immediately solved and is given by

$$\langle m|\psi(t)\rangle = \exp\left(-\frac{i}{\hbar}\beta m^2 t\right)\langle m|\psi(0)\rangle . \tag{5.20}$$

For the initial state (5.17) with $\phi = 0$, the expectation value of the operator $\hat{a}^\dagger\hat{b} = \hat{J}_x + i\hat{J}_y$ is given by:

$$\begin{aligned}\left\langle (\hat{a}^\dagger\hat{b})(t)\right\rangle &= 2^{-2N}\sum_{m=-N}^{N-1}(N-m)\begin{pmatrix} 2N \\ N-m \end{pmatrix} \\ &\times \exp\left(-\frac{2i}{\hbar}(W - W_{AB})m\, t\right) ,\end{aligned} \tag{5.21}$$

where we have neglected a rotation which is constant in time. The real part of this equation gives the expectation value of $\hat{J}_x$ and the imaginary part gives the expectation value of $\hat{J}_y$. The operator $\hat{a}^\dagger\hat{b}$ can be considered to describe the relative phase between the two condensates: for large N, the state (5.17) is approximately an eigenstate of this operator with eigenvalue $N\exp(-iN\phi)$, and for a product of two coherent states in species A and B, the expectation value of $\hat{a}^\dagger\hat{b}$ is precisely this value. We can see from the expression (5.21) that its expectation value for the state (5.17) evolving under the Hamiltonian (5.19) consists of a sum of sinusoids with periods $T_m = \hbar\pi/(m\beta)$. Such a system exhibits collapse and revival of the relative phase between the two components. As in the single condensate calculation of [56], the collapse time can be calculated by considering the spread in frequency over the spread in relative particle number of the state, and for the case of (5.21) is given by

$$T_C \approx \frac{2\pi\hbar}{|\beta|\sqrt{2N}} . \tag{5.22}$$

It is apparent that the collapse time will go to infinity in the case $W = W_{AB}$, and indeed the system will exhibit no dynamics other than the normal rotation of the phase of the entire wavefunction. This effect has been noted by Law *et*

al. [85] and Villain *et al.* [87].

At the time given by

$$T_R = \frac{2\pi\hbar}{|\beta|} \tag{5.23}$$

the quantum state will be equal to its initial value, and hence a revival of the relative phase will occur. At $T_R/2$, the quantum state will be equal to the initial state, except that the relative phase between the two components will have been rotated through an angle of π

This collapse and revival is analogous to the collapse and revival of the phase of a single mode system eg. [56, 128]. Another feature of the single mode system which has an analogy in the system considered here is the formation of a superposition of two coherent states at time $T_R/2$, an effect which is the basis of the Yurke-Stoler scheme for creating macroscopic superpositions in single mode systems. In the current case of a two-mode system, we find that at time $T_R/4$ the state of the system is given by

$$\langle m|\psi(T_R/4)\rangle = \langle m|\psi(0)\rangle \times \left\{ \begin{array}{ll} 1 & ,m \text{ even} \\ i & ,m \text{ odd} \end{array} \right\}. \tag{5.24}$$

For the initial state (5.17), which is the Bloch state $|\pi/2, \phi\rangle$, we find that at $t = T_R/4$ the state has evolved into the state $(|\pi/2, \phi\rangle + (-1)^N i\,|\pi/2, \phi + \pi\rangle)/\sqrt{2}$, which is a superposition between two Bloch states, each containing equal numbers of atoms in each species, but differing by π in the phase difference between the two species.

A short Josephson coupling pulse can be used to tranfer this relative phase difference into a particle number difference. In the case of a $\pi/2$ pulse which has the right phase relative to atomic phases, it is possible to end up with the superposition state $(|N\rangle + |-N\rangle)/\sqrt{2}$, which consists of a superposition between N atoms in the state A and N atoms in the state B - a maximal cat state.

This scheme was investigated by Sanders [130] as a way of producing cat states in quantum optical systems. For Bose-condensed systems, the state has a number of advantages and drawbacks.

The primary advantage of this scheme over the scheme proposed here is that it produces a superposition between two Bloch states. These states are well behaved with regard to techniqes such as quadrature phase measurements, which are used to show that the states produced are in fact cat states, and not simply a classical probability mixture.

However, the time needed to produce such states scales as the revival time of the relative phase. This is approximately a factor of $\sqrt{N}$ longer than the collapse time of the relative phase, and is far beyond the lifetime of current

condensates. For example, if we consider the parameters used in this chapter, then it would take some 10 minutes to create such a superposition state as opposed approximately 5 seconds for the scheme put forward in this chapter. The time can be made less by increasing the parameter β, which could be accomplished by using very small, tight trapping potentials (perhaps formed by the wells in an optical crystal, for example.

The other disadvantage of this scheme, for the case of Bose-Einstein condensates, is the fact that the cat states produced are maximal in the sense that they consist of superpositions of two states lying at opposite sides of the Bloch sphere. At first glance, this factor is an advantage in the sense that the 'cat' is as big as possible. However, the experimental investigation of cat states is likely to be an evolution from the production of very small cat states to larger and larger cat states - hence the present scheme is probably in some sense too ambitious, and would be too sensitive to dissipation.

The problems of long revival time and the size of the cat state would both be overcome if the scheme were applied to a very small condensate held in a very small, tight trap - a 'nano-condensate'. Judging by the pace of recent experiments, such a situation will possibly achievable in the near future. If such a situation were in fact achieved, then this scheme would probably be a very promising way of performing realistic experiments with cat states.

5.6.3 The effect of Josephson coupling

The Hamiltonian of the system, including a term describing Josephson coupling, is basically the same as that described by Milburn *et al* [101], since under the conditions $E_A = E_B$ and $W_{AA} = W_{AB} = W$, the Hamiltonian (5.11) is formally the same as that considered by these authors. Milburn *et al.* [101] consider the evolution of $\langle J_z \rangle$ (i.e. the particle number difference between the species) from an initial state in which all the atoms are of the same species. In terms of the notation and physical system used in this thesis, they find that there exists a critical value of the Josephson coupling parameter λ given by

$$\lambda_C = \frac{N}{2}\beta . \tag{5.25}$$

For $\lambda \gg \lambda_C$, the system oscillates in a Rabi-type manner between all particles being species A and all particles being species B. These oscillations are eventually 'damped' by the phase diffusion in the system, and also exhibit partial revivals due to the finite particle number.

For $\lambda < \lambda_C$, the particle number difference oscillates, but incompletely, so that for λ appreciably less than λ_C most of the particles remain in the initial

species for all times. This effect describes a kind of self trapping, and is due to collisional terms in the Hamiltonian. Smerzi *et al.* [100] have found the same effect in their mean-field calculations, which neglect the quantum statistical effects in the system, but take into account the spatial variation of the wavefunction.

Fig. (5.2) shows the behaviour of the initial state (5.17) with $\phi = \pi/2$ under the Josephson coupling Hamiltonian. Under these conditions, there is no self trapping as such, because the initial condition has an equal number of particles in each species. However, it is the same mechanism which leads to self trapping which is responsible for the incomplete osscilations seen in Fig. (5.2(b)).

It is interesting to note that the presence of even weak Josephson coupling can have a large effect on the phase dynamics of the system, even when the expectation value of J_z remains constant or nearly constant. This is illustrated for an initial state (5.21) with $\phi = 0$ in Fig. (5.3). Such a state is not expected to exhibit Josephson oscillations due to the zero phase difference between the two species, however the state vector is affected by the Josephson coupling, greatly modifying the picture of collapse and revival.

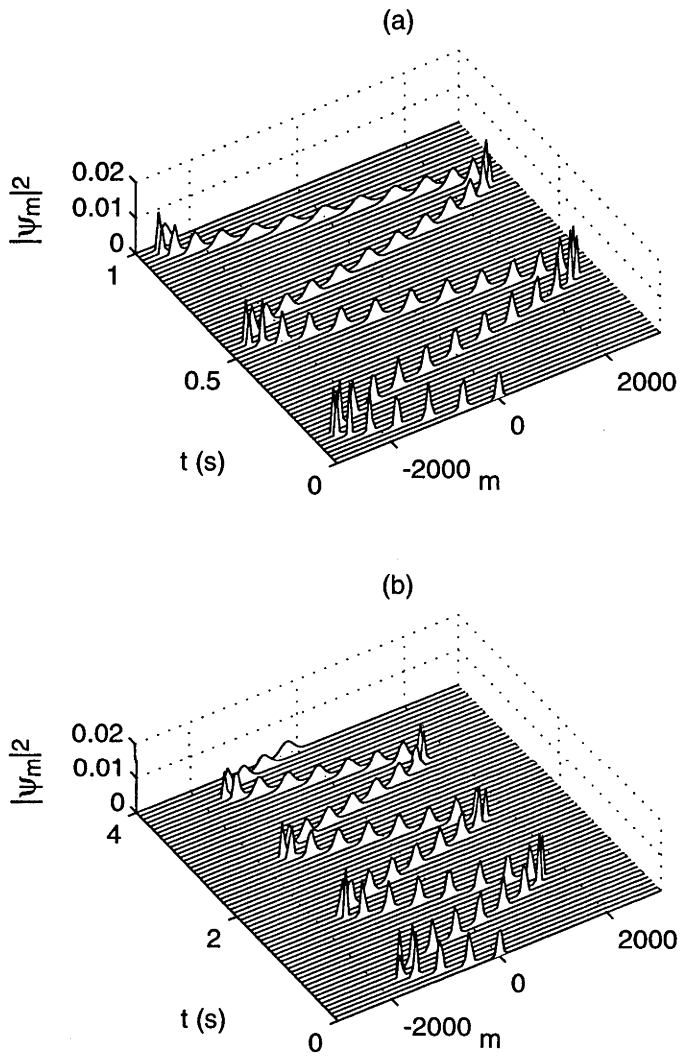

Figure 5.2: The evolution of the state vector under strong Josephson coupling. The initial state is given by (5.17) with $\phi = \pi/2$. All parameters except for λ are the same as those given in Fig. (5.3); as before we have $\lambda_C = 3.9\hbar\ \mathrm{s}^{-1}$. ψ_m denotes the m component of the state vector. (a) $\lambda = 12\hbar\ \mathrm{s}^{-1} > \lambda_C$. The Rabi-like Josephson oscillations can be seen to be due to a highly coherent wavepacket motion back and forth. Some wavepacket spreading is evident; this is due to the presence of collisional terms in the Hamiltonian and will eventually lead to a collapse of the oscillations. (b) $\lambda = 2.5\hbar\ \mathrm{s}^{-1} < \lambda_C$. The oscillations are seen to be incomplete; this is due to the same self-trapping mechanism discussed in Milburn *et al.* [11].

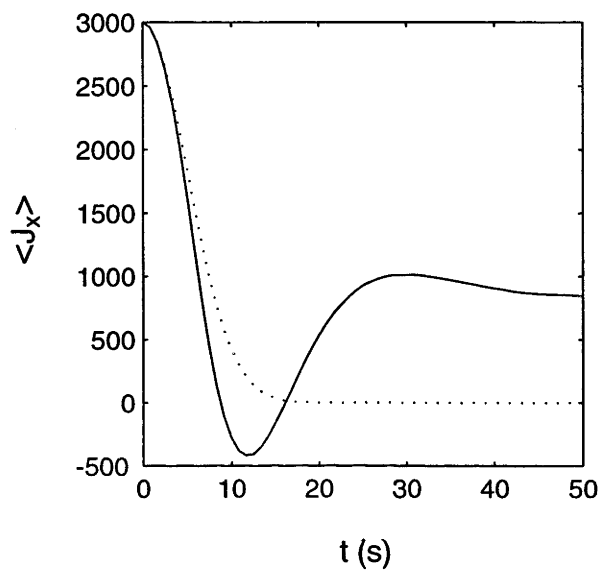

Figure 5.3: Expectation value of J_x for an initial state with $\phi = 0$ and weak Josephson coupling. Parameters are: $N = 3000$ (6000 atoms total), $W - W_{AB} = 2.6 \times 10^{-3}\hbar\,\mathrm{m}^{-1}$, giving $\lambda_C = 3.9\hbar\,\mathrm{s}^{-1}$. The parameter $W - W_{AB}$ was chosen to be consistent with experimental values for ^{87}Rb, except that we have chosen to scale the trap frequencies such that the collapse time for the relative phase, which could be considered to give a timescale for the phase dynamics, is equivalent to that of a total of 5×10^5 atoms in the trap as used in recent experiments. The solid line shows the case of $\lambda = 2 \times 10^{-3}\hbar\,\mathrm{s}^{-1}$ and the dotted line shows the zero Josephson coupling case ($\lambda = 0$). It can be seen that, in the former case, the relative phase initially follows the standard (approximately Gaussian) collapse, but instead of staying at zero until some long time as would be the case for no Josephson coupling, it is immediately partially revived.

5.7 Macroscopic superposition states

In the following section we shall show that in certain parameter regimes the system considered here will dynamically evolve into states which are a superposition of two macroscopically (or mesoscopically) distinguishable states - so called 'Schrödinger's cat states'. As in the cases discussed by Cirac *et al.* [2] and Ruostekoski *et al.* [126], these states consist of superpositions of two states which differ in average relative particle number. Cirac *et al.* [2] have shown that for $W_{AB} > W$ and certain strengths of the Josephson coupling parameter, such states can arise as the ground state of the Hamiltonian. Steel and Collett [127] demonstrate this result from a slightly different viewpoint. Ruostekoski *et al.* [126] have considered the dynamic production of Schrödinger's cat states in a pair of free condensates by a mechanism involving the stimulated scattering of light between the two components, where the atom-atom collisions are ignored. Here, we show that similar states can arise from the unitary evolution under the Hamiltonian (5.11) due to the interplay between the Josephson coupling and the atom-atom collisions. The production of these states does not require the condition that $W_{AB} > W$ as in [2]. Properties of the states, such as the 'size' of the Schrödinger's cat or the degree of number squeezing, can be controlled by varying the strength of the Josephson coupling parameter. Once the system has evolved to such a state, the Josephson coupling can be switched off, effectively 'freezing' the evolution of the number distribution.

Up until now we have looked at expectation values of relevant quantities. In what follows, we shall instead concentrate on the dynamics of the state vector evolving under the Hamiltonian (5.11) and for an initial state (5.17), with $\phi = 0$.

As has been discussed, a $\pi/2$ pulse will produce an initial state with relative phase of $\phi = \pi/2$ between the two components, but the relative phase can be varied by either applying a strong light field to one or both species or by changing the phase of the Josephson coupling relative to the initial $\pi/2$ pulse. In what follows, we will concentrate on the case $\phi = 0$. In this case, the distribution of relative particle number must remain symmetric around $m = 0$, since both the state vector and the Hamiltonian will be invariant under the interchange $A \leftrightarrow B$. For $W_{AA} - W_{AB} = 0$, the initial state is an eigenstate of the Hamiltonian, and thus the number distribution remains constant in time. For $W_{AA} - W_{AB} \neq 0$, the dynamics will be affected by the diffusive collisional terms in the Hamiltonian. Fig. (5.4) shows the evolution of the state vector for $\lambda < \lambda_C$. We see that the interplay of collisional effects and Josephson coupling leads to the creation of a state which is doubly peaked about $m = 0$, similar to the case of [2,126]. One peak describes a situation in which more of the atoms are to be found in species A, and the other peak describes the converse.

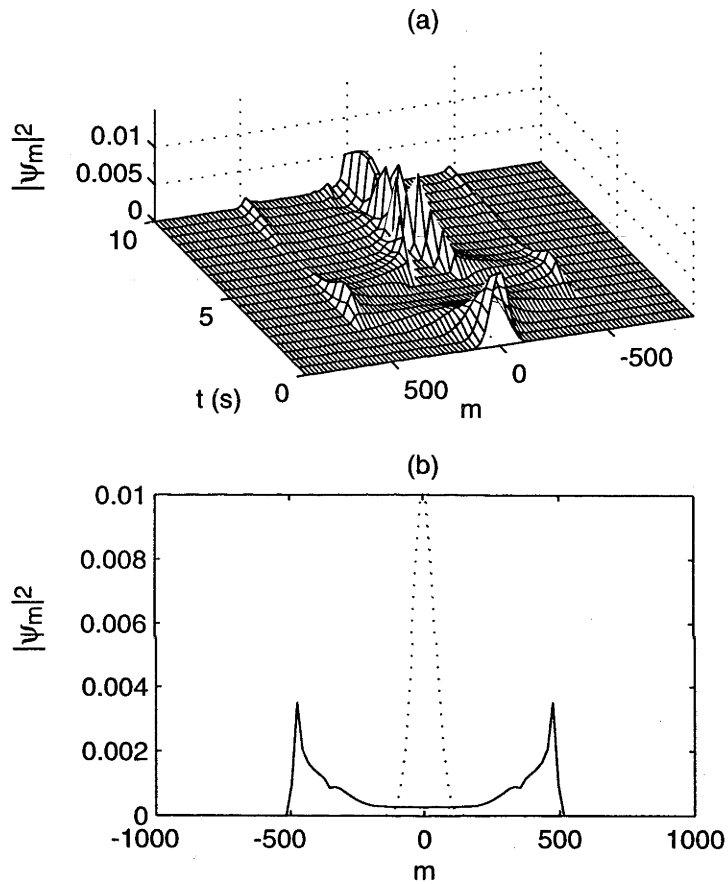

Figure 5.4: (a) Evolution of the relative number distribution for $\lambda = 0.1\hbar\,\mathrm{s}^{-1} < \lambda_C$ and the other parameters as in Fig. (5.3). At $t \approx 4s$ it can be seen that the number distribution has become doubly peaked; this state represents a macroscopic quantum superposition state. In order to give a better idea of the gross features of the probability distribution, the state vector has been 'smoothed' to eliminate fine structure. (b) shows the smoothed probability distribution at $t = 0$ s (dotted line) and $t = 4$ s (solid line).

We find that by varying the strength of the Josephson coupling parameter λ, the 'size' of the cat can be varied. For $\lambda = \lambda_C$ the distribution has peaks at $m = \pm N$, so that the size of the cat is maximal in this case: the state is close to a superposition of 2N atoms in species A and 2N atoms in species B.

This evolution into Schrödinger cat states can be partially understood by considering the effect of the phase spreading on the Josephson dynamics while ignoring the effect of the Josephson coupling on the phase dynamics. This approximation will be valid only for some short time. At $t = 0$, the condensate starts in a state with well defined relative phase and equal particle numbers in each species. The phase then diffuses due to the energy spread which is present in the initial state of the condensate and which is caused by a spread in relative particle number and the atom-atom collisions. The Josephson coupling then acts on these different phases present in the state vector, causing the negative phase half of the wavefunction to move in the direction of increasing m and positive phase half to move in the direction of decreasing m, eventually causing the wavefunction to 'split' into two wavepackets evolving in opposite directions. These wavepackets are eventually stopped in their motion by the self trapping mechanism mentioned earlier, and become highly peaked.

5.7.1 Evolution of the Q-function

It is instructive to consider the formation of cat states from the point of view of the evolution of the Q-function, see Eq. (5.16). In particular, we will compare and contrast this evolution for the cases where Josephson coupling is present and the case where it is absent [130].

Fig. (5.5 (a)) shows the Q-function at four different times for the parameters of Fig. (5.4). At $t = 0$ the Q-function is that of the initial Bloch state $|\pi/2, 0\rangle$. At $t = 1.8$ s, the state has become elongated, leading to a spread in both the phase difference and the relative particle number. By 3.6 s, the Q-function has spread right around the Bloch sphere in a figure eight arrangement. This distribution leads to a double peaked distribution of relative particle number. The Q-function for the plot shown in Fig. (5.4(b)) (t = 4 s) is similar to this plot. The phase difference is not well defined, due to the spreading around the Bloch sphere, although there is some localisation around the ends of the Q-function, seen as peaks on the contour plot. At 4.2 s, these localised peaks become more pronounced and move back toward $\theta = 0$, leading to a cat state in which the relative phase between the two species is better defined, but the difference in relative particle number is less i.e. the cat is smaller.

In Fig. (5.5 (b)) the evolution is shown for the case where Josephson coupling is absent. In such a case, the distribution of the relative particle number must remain constant, and therefore the Q-function must occupy a narrow belt

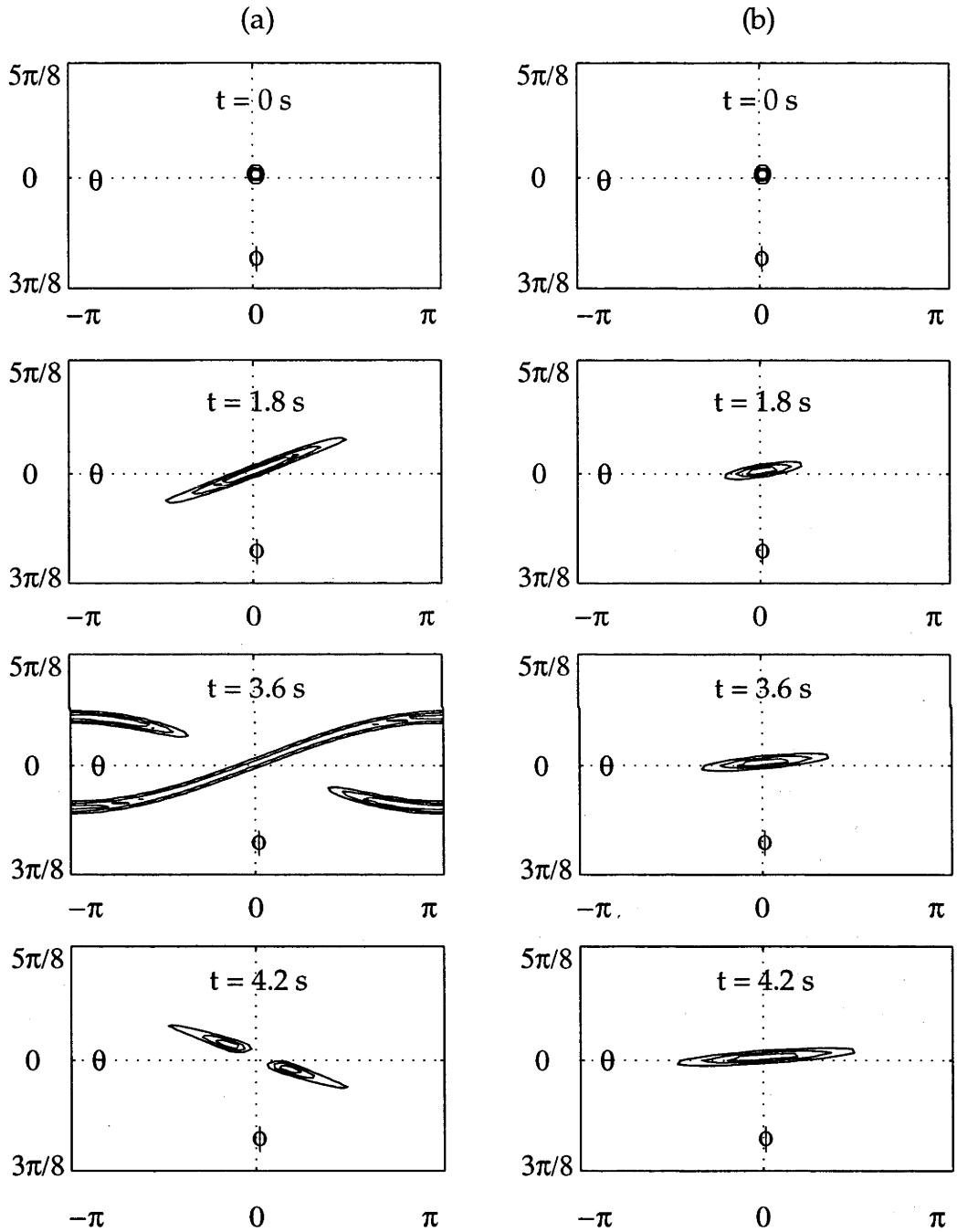

Figure 5.5: (a) The evolution of the Q-function for the parameters of Fig. (5.4). (b) Parameters are the same as in (a) except that Josephson coupling is absent.

around the equator of the Bloch sphere. It is seen to spread out within this belt, leading to a collapse of the phase difference (see Fig. (5.3), dotted line). For later times $t \ll T_R$, the Q-function spreads all the way around the equator of the Bloch sphere. Although ripples form due to a partial rephasing of the various frequency components which are present in the evolution, a cat state does not form in the same way as it does in (a). However, much later, at $t = T_R/4$, a macroscopic superposition between two Bloch states forms, as discussed in Section (5.6.2).

5.8 Validity and feasibility

5.8.1 The two-mode approximation

In making the calculations above, we have relied on the two mode approximation, which is also used in the first part of Cirac *et. al.* [2]. This latter paper is able to go beyond this approximation because it deals only with the time independent rather than time dependent Schrödinger equation. The two-mode approximation will only be quantitatively valid for a limited set of parameters. It would be interesting to see whether the behaviour of the system would change dramatically outside such parameter regimes; this was found not to be so for the case of Cirac *et al.* [2]. Certainly it seems plausible that the scheme might work outside these regimes.

In order for the two-mode approximation to provide a reasonably accurate picture, we must assume that the parameters $E_{A,B}$, $W_{AA,BB,AB}$ and λ are reasonably constant for the cases investigated. These parameters all depend on the self consistently defined condensate modes of the system, which in turn depend on the particle numbers N_A and N_B. Thus the two mode approximation will be most accurate when the state vector has a highly localized particle number distribution. This introduces a possible problem for our approach: we want to investigate the production of Schrödinger cat states consisting of *superpositions* of states with different relative particle number, and thus, to some degree at least, we wish to move away from regimes in which the particle number distribution is highly localized.

However, we can always find regimes in which the dependence of the density profile on the particle number distribution is weak. Some examples are: (i) low density of particles: in this case, the density profiles for the two species approach the single particle eigenfunctions for the ground state of the trap and thus do not vary greatly with particle number. (ii) The regime in which $W_{AA} = W_{BB}$ and W_{AB} is only slightly less than $W_{AA/BB}$. In this case, the dependence of the density profiles on the relative particle number between the

two species is weak and can be made to approach zero[5]. However, we find that in such regimes, the characteristic evolution time is slow and the production of Schrödinger cat states could take a long time, thus exacerbating problems due to decoherence. (iii) If the density of atoms is high enough such that the healing lengths of the two-species condensate are small compared to the size of the trap, then 'hard' traps such as square well traps also show little dependence of the density profiles on particle numbers, providing we are working in the regime in which the two species form a homogeneous mixture e.g. $W_{AA} = W_{BB}$ and $W_{AB} < W_{AA/BB}$.

Furthermore, even in regimes in which the two-mode approximation is not accurate, Schrödinger cat states might be produced under that same conditions as are predicted by the two-mode approximation; this was found to be the case in the calculations of Cirac *et al.* [2].

5.8.2 Decoherence

Such states would be hard to produce in practice. Probably the most serious experimental problem would be decoherence; in the extreme example of a maximal Schrödinger cat state with a superposition between $m = -N$ and $m = N$, the 'detection', or loss, of one atom would be enough to destroy the superposition, since such a detection would tell us which species was populated and hence allow us to distinguish between the two macroscopic states. For less extreme cases, this condition would relax somewhat, but certainly a macroscopic (mesoscopic) loss from the system would always be enough to destroy a macroscopic (mesoscopic) superposition state.

The main reason for the well known rapid decoherence of Schrödinger cat states is that since the states involved in the superposition are macroscopically or mesoscopically different from one another, the decoherence will affect each of these states in greatly different ways and thus the off diagonal elements in the density matrix will rapidly vanish. This is most easily seen in the quantum trajectories picture of decoherence, where each trajectory in the ensemble can evolve into something greatly different from the others.

In the spirit of this idea, and in order to get a crude idea of the kinds of loss rates which might be feasible for a cat of a given size, we have looked at a simplified model in which a series of detections of the species of atoms is simulated. We restrict ourselves to a particular kind of initial state which can be represented as the superposition $|\phi_0\rangle = |N-n, N+n\rangle + |N+n, N-n\rangle$,

[5]The basic reason for this is the fact that the mean field energy of the system can be shown to depend much more on the total number of atoms than the number in each species, and the former is a conserved quantity

where the state $|N_A, N_B\rangle$ contains N_A atoms of species A and N_B atoms of species B, and n is a parameter which controls the degree of 'catness'.

Since each detection removes exactly one atom from the sample, the state will always remain as a superposition between two number states. Similar to Javanainen and Yoo [88], we use a model of detection analogous to the theory of photon detection [137–139]. However, unlike the models of Javanainen and Yoo [88] and other authors [84, 89–92], we consider a detection of atom species rather than position, meaning that the model simplifies due to the fact that there are only two possible results of each detection.

If m_A atoms of species A and m_B atoms of species B have already been detected, then at a given stage in the detection sequence, the state will be

$$|\phi_m\rangle = c_1 |N - n - m_A, N + n - m_B\rangle + c_2 |N + n - m_A, N - n - m_B\rangle \ , \quad (5.26)$$

where $m = m_A + m_B$, and thus the chance of detecting another atom of species A will be

$$P(A) = c_1^2 \frac{N - n - m_A}{2N - m} + c_2^2 \frac{N + n - m_A}{2N - m} \ . \quad (5.27)$$

If an atom of A is in fact detected, then the probability of detecting another atom of A will be enhanced, since the new state will be

$$\begin{aligned} |\phi_{m+1}\rangle &= \mathcal{N}(\hat{a} |\phi_m\rangle) \\ &= \mathcal{N}(c_1 \sqrt{N - m_A - n} \, |N - m_A - n - 1, N - m_B + n\rangle \\ &+ c_2 \sqrt{N - m_A + n} \, |N + m_A - n - 1, N - m_B - n\rangle) \ , \end{aligned} \quad (5.28)$$

where $\mathcal{N}$ indicates that the state should be correctly normalised. We see that the component proportional to c_2 which favours the detection of species A atoms has been enhanced. Thus the sequence of detections constitutes a positive feedback process which drives the state vector towards one of the two components ('cat alive' and 'cat dead') of the original cat state.

In order to get some idea of the rate of decay of cat states under this feedback process, we must come up with a criterion which provides a quantitative measurement of 'catness'. For the particular two-component states discussed above, the standard deviation of the atom number difference $N_A - N_B$ seems to be as good a measure as any; for a completely non-cat state $|N_A, N_B\rangle$ this quantity is zero, and for the cat state $|\phi_0\rangle = (|N - n, N + n\rangle + |N + n, N - n\rangle)/\sqrt{2}$ it is $2n$. We define the half life λ as the number of detections needed to reduce this measure of 'catness' to half of its original value.

Since the state of the system under the process of detections will consist of at most two components, it is easy to simulate a series of detections for condensate containing an arbitrary number of atoms. Averaging over an ensemble

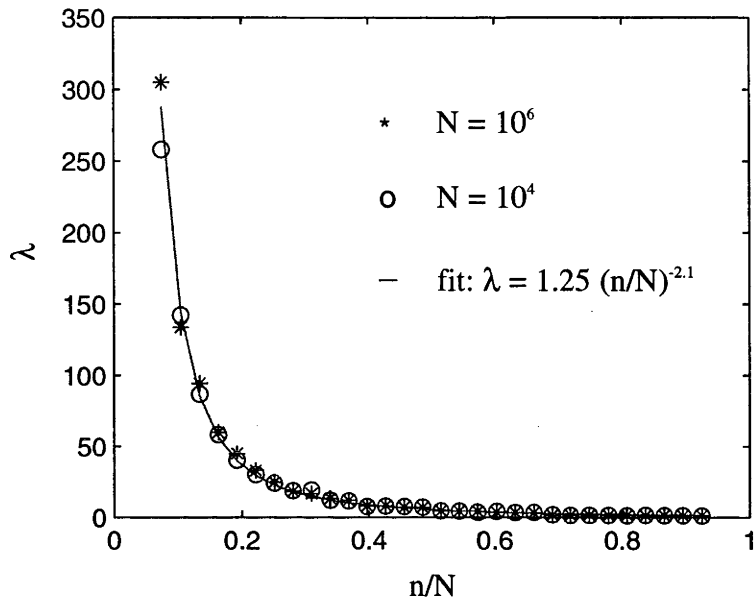

Figure 5.6: The half life of the cat state vs. (n/N) for the two cases $N = 10^4$ and $N = 10^6$. The solid line of fit obeys $\lambda = 1.25(n/N)^{-2.1}$.

of detection sequences gives an idea of the average half life of the cat state for a given value of n. Fig. (5.6) shows a plot of the cat half life λ versus n/N, for the two cases $N = 10^4$ and $N = 10^6$. We see that there is very little difference between these two cases. The line of fit obeys the equation $\lambda = 1.25(n/N)^{-2.1}$, and clearly fits the data very well over a wide range.

Assume that we demand that the cat survive over a timescale T, and that the system loses atoms at a constant loss rate r, then the total number of atoms lost over the time T will be rNT, assuming that this loss does not deplete the number of atoms N too much. When this value has reached the half life number of detections,λ, then the cat can be assumed to have been destroyed. Hence equating rNT with λ and using the equation for the line of fit shown in Fig. (5.6), we obtain an equation for the maximum allowable value of n:

$$n_{\max} = 1.112(rT)^{-0.476}N^{0.523}, \tag{5.29}$$

or equivalently

$$n_{\max}/N = 1.112(rNT)^{-0.476}. \tag{5.30}$$

This means that if we simply want to construct a cat state with the largest possible value of n i.e. the largest macroscopic difference between the two states, then having a large value of N will actually help us, however, if we

want to maximise n/N then it will hinder us. However we have assumed a linear loss rate. If, for example, the main source of loss is three body collisions then the loss will be proportional to N^3 and hence a large value of N will always hinder us. In this case we will have

$$n_{\max} = 1.112(rT)^{-0.476}N^{-0.428}. \tag{5.31}$$

This estimate has been based on the identification of decoherence with a process involving measurement of particle species. Real decoherence will occur through a variety of processes such as collisions with the background gas, interactions with the environment through a 'shaking' trapping potential etc. However, the arguments above suggest that decoherence events which distinguish the particular particle species are probably most destructive to the nature of Schrödinger cat states. A full investigation of the effects of decoherence would involve simulating the evolution of the density matrix of the system, perhaps through an appropriate master equation. Any loss terms in such an equation would destroy the particle number conserving nature of the system, and hence we would need to work in a much larger state space. This would make direct simulation impossible for any large number of atoms.

5.8.3 Temperature restrictions

The paper of Cirac *et al.* [2] also lists as a condition for the production of such states cooling close close to the collective ground state, which is far more restrictive than simply demanding Bose-Einstein condensation i.e. off-diagonal long range order. In terms of the single particle states, the condition they give is that less than one atom can be out of the single particle ground state. This condition is equivalent to demanding that the many body wavefunction has a significant population in the collective ground state (for exactly one particle not in the single particle ground state, the fraction of the many body population in the *collective* ground state is $1/e$ which is of the order of 50% —see Section 5.3.4). The rest of the many body wavefunction will be thermally distributed amongst the other eigenstates of the many body Hamiltonian, which will have very different number and/or relative phase distributions from the Schrödinger cat state. In summary, the scheme of Cirac *et al.* [2] relies on cooling to a *particular* eigenstate of the many body Hamiltonian.

The present scheme is somewhat different, since it relies on unitary evolution rather than cooling in order to arrive at a cat state. In the present case, the effect of having non-zero temperature would be to produce an incoherent ensemble of initial states, each containing a slightly different total number and/or relative number of atoms. Thus in order to be able to observe a

Schrödinger cat state, we would want the final state for each member of the initial ensemble to have a similar number distribution and relative phase. We would thus demand that the final state not be too sensitive to changes in the initial state. In the worst case scenario, in which varying the particle number by one atom would be enough to completely destroy the characteristics of the Schrödinger cat state, then we would recover the condition of Cirac *et al.*, since we would then *need* a significant population in a particular many body state in order to observe the effects of a Schrödinger cat state.

By testing a range of initial conditions, we have found that the most critical factor here appears to be that the peak of the atom distribution must be accurately centered about $m = 0$ compared to the spread in the relative number distribution. Since this latter quantity is of the order $\sqrt{N}$, we require that the variation in the average relative particle number be significantly less than $\sqrt{N}$. If this condition is not satisfied, then the cat will be lop-sided i.e. 'more alive than dead' or vice-versa. Recall the condition of Cirac *et al.*. [2] that no more than one particle be out of the single particle ground state. In the present case, varying particle number by one will cause a variation in the relative particle number of one, which is much less than the spread in relative particle number ($\sqrt{N}$). Thus we believe that the present scheme might exhibit Schrödinger cats at higher temperatures than that of Cirac *et al.* [2].

Chapter 6

Conclusions

In recent years, the field of atom optics has undergone a rapid expansion in both experiment and theory. In particular, the 1995 achievement of dilute gas Bose-Einstein condensation has opened up a whole new field of study. This thesis has examined some aspects of theoretical atom optics including both traditional atom optics and Bose-Einstein condensation.

In the first chapter of this thesis, we have looked at a particular atom optical element: the evanescent wave diffraction grating. This device is a good candidate for an atomic beamsplitter with a large angular separation between the beams. In the case of low angle of incidence beam-splitting, the name diffraction grating is somewhat of a misnomer, since unlike the diffraction of light from a grating, we have found that to achieve efficient beam splitting, one must utilise the multi-level structure of the atomic transition. We have numerically modeled the beam-splitting process for two experimentally relevant parameter regimes and found that efficient diffraction is possible for a variety of parameters. An important parameter is the polarisation of the evanescent wave, since this allows some degree of independent control over the coupling between the light field and the hyperfine sublevels involved in the transition. Our results are consistent with experimental evidence, but as yet there is no detailed evidence with which we can compare our numerical results. In the near future, we hope to use our code to model an experiment currently underway at the Australian National University. This experiment uses a transition in Cs which has a complicated level structure. Our model has showed that, in order to obtain efficient beamsplitting under such circumstances, the laser should be detuned *between* the top two hyperfine levels of the excited state. Atomic evanescent-wave beamsplitters could have future applications in the field of atom interferometry, a field which we hope to look at in the near future.

The rest of this thesis has looked at Bose-Einstein condensates, and in particular the properties of two-species condensates.

In Chapter 4, we have looked at the behaviour of the density profile and the excitation spectrum of a two-species Bose-Einstein condensate. In particular,

we find that in certain parameter regimes, the usual cylindrically symmetric density profile can undergo a process of spatial symmetry breaking, in which the symmetric solution to the Gross-Pitaevskii equation becomes unstable and a new stable, symmetry broken, solution appears. This behaviour is dramatically reflected in the behaviour of the excitation spectrum; as the regime of instability is approached in parameter space, the lowest energy, antisymmetric, linear excitation frequency approaches zero. Following the transition to a symmetry broken state, this frequency again rises.

We have also examined the possibility of creating macroscopic superposition states, or Schrödinger cat states, using two-species BECs. Our scheme can be likened to a non-linear quantum optics experiment, except that the nonlinearities are provided by collisions between atoms rather than non-linear crystals or feedback electronics. Within the context of a two-mode approximation, we show that it is possible to use a series of laser fields working in conjunction with the normal atom-atom collisions to produce states which consist of a coherent superposition of two classically observable states, one containing an excess number of atoms in one species and one containing an excess in the other species. As with other Schrödinger cat schemes, the experimental realisation of such states would be a formidable challenge. Perhaps the most serious limitation would come from decoherence. We have made a first attempt at analysing the effects of such decoherence by simulating particular detection sequences, and have found a fitted expression for the maximum number of atom detections permissible for a cat of a given size. We have also looked at the effects of finite temperature on the system and have presented a plausible argument that our scheme might be better in this regard than another recent proposal [2].

The future looks very exciting for the field of atom optics. As good sources of atoms, either Bose-condensed or incoherent, become run of the mill, there will be a more diverse and sophisticated series of experiments being performed, possibly with new commercial and fundamental applications.

minsofar min cite@temp

Bibliography

[1] M. Anderson, J. Ensher, M. Matthews, C. Wieman, and E. Cornell, Science **269**, 198 (1995).

[2] J. Cirac, M. Lewensten, K. Molmer, and P. Zoller, Phys. Rev. A **57**, 1208 (1998).

[3] R. Penrose, Gravity and Quantum Mechanics, in *General Relativity and gravitation 1992*, edited by R. Gleiser, C. Kozameh, and O. Moreschi, Institute of Physics Publications, Bristol, 1993.

[4] C. Savage, Aust. Journal of Phys. **49**, 745 (1996).

[5] A. Landragin et al., Europhys. Lett. **39**, 485 (1997).

[6] L. Cognet et al., Phys. Rev. Lett. **81**, 5044 (1998).

[7] B. Cuthbertson, private communication.

[8] J. Miller, R. Cline, and D. Heinzen, Phys. Rev. A **47**, R4567 (1992).

[9] J. Dalibard and C. Cohen-Tannoudji, J. Opt. Soc. Am. B **2**, 1707 (1985).

[10] C. Cohen-Tannoudji, Atomic motion in laser light, in *Fundamental systems in quantum optics: Les Houches session LIII*, North-Holland, Amsterdam, 1992.

[11] S. Bose, Z. Phys **26**, 178 (1924).

[12] A. Einstein, Sitzber. Kg. Preuss. Akad. Wiss. , 3 (1925).

[13] K. Davis et al., Phys. Rev. Lett. **75**, 3969 (1995).

[14] M.-O. Mewes et al., Phys. Rev. Lett. **77**, 416 (1996).

[15] C. Bradley, C. Sackett, J. Tollett, and R. Hulet, Phys. Rev. Lett. **75**, 1687 (1995).

[16] D. G. Fried et al., Phys. Rev. Lett. **81**, 3811 (1998).

[17] D. Stamper-Kurn et al., Phys. Rev. Lett. **77**, 2595 (1998).

[18] Y. Gott, M. Ioffe, and V. Telkovsky, in *Nuclear Fusion 1962 Suppl., Pt. 3*, International Atomic Energy Agency, Vienna, 1962.

[19] D. Pritchard, Phys. Rev. Lett. **51**, 1336 (1983).

[20] D. Jin, J. Ensher, M. Matthews, C. Wieman, and E. Cornell, Phys. Rev. Lett. **77**, 420 (1996).

[21] D. Jin, M. Matthews, J. Ensher, C. Wieman, and E. Cornell, Phys. Rev. Lett. **78**, 764 (1997).

[22] M.-O. Mewes et al., Phys. Rev. Lett. **77**, 988 (1996).

[23] M. Edwards, P. Ruprecht, K. Burnett, R. Dodd, and C. Clark, Phys. Rev. Lett. **77**, 1671 (1996).

[24] L. You, W. Hoston, and M. Lewenstein, Phys. Rev. A **55**, R1581 (1997).

[25] C. Bradley, C. Sackett, and R. Hulet, Phys. Rev. Lett. **78**, 985 (1997).

[26] M. O. Mewes et al., Phys. Rev. Lett. **78**, 582 (1997).

[27] M. Andrews et al., Science **275**, 637 (1997).

[28] C. Myatt, E. Burt, R. Ghrist, E. Cornell, and C. Wieman, Phys. Rev. Lett. **78**, 586 (1997).

[29] M. Matthews et al., Phys. Rev. Lett **81**, 243 (1998).

[30] D. Hall, M. Matthews, J. Ensher, C. Wieman, and E. Cornell, Phys. Rev. Lett. **81**, 1539 (1998).

[31] D. Hall, M. Matthews, C. Wieman, and E. Cornell, Phys. Rev. Lett. **81**, 1543 (1998).

[32] D. Stamper-Kurn et al., Phys. Rev. Lett **80**, 2027 (1998).

[33] L. V. Hau, S. Harris, Z. Dutton, and C. H. Behroozi, Nature **397**, 594 (1999).

[34] D. Gordon and C. Savage, Optics Comm. **130**, 34 (1996),
(Erratum: **136**, 503(E) (1996))
(Complete corrected version: atom-ph/9404004).

[35] D. Gordon and C. Savage, Phys. Rev. A **58**, 1440 (1998).

[36] D. Gordon and C. Savage, Phys. Rev. A **49**, 4623 (1999).

[37] D. Gordon, Multi-Level Evanescent Wave Atom Optics, Hons. Thesis, The Australian National University, 1995.

[38] C. Henkel, J.-Y. Courtois, and A. Aspect, J. Phys. II (France) **4**, 1955 (1994).

[39] R. Cook and R. Hill, Optics Commun. **43**, 258 (1982).

[40] J. Hajnal and G. Opat, Optics Commun. **71**, 119 (1989).

[41] M. Christ, A. Scholz, M. Schiffer, R. Deutschmann, and W. Ertmer, Opt. Comm. **107**, 211 (1994).

[42] R. Brouri et al., Opt. Commun. **124**, 448 (1996).

[43] C. Henkel et al., Theory of atomic diffraction from evanescent waves, quant-ph/9806051.

[44] S. Feron et al., Optics Commun. **102**, 83 (1993).

[45] S. Feron et al., Phys. Rev. A **49**, 4733 (1994).

[46] J. E. Murphy, L. L. Hollenberg, and A. Smith, Phys. Rev. A **49**, 3100 (1994).

[47] B. W. Stenlake, I. Littler, H.-A. Bachor, K. Baldwin, and P. Fisk, Phys. Rev. A **49**, 16 (1994).

[48] C. M. Savage, D. Gordon, and T. Ralph, Phys. Rev. A **52**, 4741 (1995).

[49] J. Murphy, P. Goodman, and A. Smith, J. Phys.: Condens. Matter **5**, 4665 (1993).

[50] S. M. Tan and D. F. Walls, Phys. Rev. A **50**, 1561 (1994).

[51] R. Deutschmann, W. Ertmer, and H. Wallis, Phys. Rev. A **47**, 2169 (1993).

[52] E. Merzbacher, *Quantum Mechanics*, Wiley, N.Y., 1970.

[53] M. Born and E. Wolf, *'Principles of Optics'*, Pergamon Press, Oxford, 1980.

[54] R. Kosloff, J. Phys. Chem. **92**, 2087 (1988).

[55] R. Deutschmann, private communication (1995).

[56] A. Parkins and D. Walls, Phys. Rep. **303**, 2 (1998), (review).

[57] E. Lifshitz and L. Pitaevskii, *Statistical Physics Part II*, Pergamon, Oxford, 1970.

[58] M. Edwards and K. Burnett, Phys. Rev. A **51**, 1382 (1995).

[59] P. Ruprecht, M. Edwards, K. Burnett, and C. W. Clark, Phys. Rev. A **54**, 2996 (1995).

[60] M. Edwards, R. Dodd, C. Clark, P. Ruprecht, and K. Burnett, Phys. Rev. A **53**, 1950 (1996).

[61] F. Dalfovo and S. Stringari, Phys. Rev. A **53**, 2477 (1996).

[62] M. Edwards, R. Dodd, and C. W. Clark, J. Res. Natl. Inst. Stand. Technol. **101**, 553 (1996).

[63] P. Ruprecht, M. Edwards, K. Burnett, and C. Clark, Phys. Rev. A **54**, 4178 (1996).

[64] K. Singh and D. Rokhsar, Phys. Rev. Lett. **77**, 1667 (1996).

[65] A. Fetter, Phys. Rev. A **53**, 4245 (1996).

[66] B. Esry, Phys. Rev. A **55**, 1147 (1997).

[67] A. Smerzi and S. Fantoni, Phys. Rev. Lett **78**, 3589 (1997).

[68] R. Ballagh, K. Burnett, and T. Scott, Phys. Rev. Lett. **78**, 1607 (1997).

[69] M. Holland, D. Jin, M. Chiofalo, and J. Cooper, Phys. Rev. Lett. **78**, 3801 (1997).

[70] W. Zhang and D. Walls, Phys. Rev. A **57**, 1248 (1998).

[71] M. Lewenstein and L.You, Phys. Rev. Lett. **77**, 3489 (1996).

[72] C. Gardiner, Phys. Rev. A **56**, 1414 (1997).

[73] Y. Castin and R. Dum, Phys. Rev. A **57**, 3008 (1998).

[74] H. Stoof, Phys. Rev. Lett **78**, 768 (1997).

[75] C. Gardiner and P. Zoller, Phys. Rev. A **55**, 2902 (1997).

[76] D. Jaksch, C. Gardiner, and P. Zoller, Phys. Rev. A **56**, 575 (1997).

[77] C. Gardiner and P. Zoller, Phys. Rev. A **58**, 536 (1998).

[78] D. Jaksch, C. Gardiner, K. Gheri, and P. Zoller, Phys. Rev. A **58**, 1450 (1998).

[79] M. Holland, J. Williams, and J. Cooper, Phys. Rev. A **55**, 3670 (1997).

[80] J. Anglin, Phys. Rev. Lett. **79**, 6 (1997).

[81] Y. Kagan and B. Svistunov, Phys. Rev. Lett. **79**, 3331 (1997).

[82] E. Wright, D. Walls, and J. Garrison, Phys. Rev. Lett **77**, 2158 (1996).

[83] E. Wright, T. Wong, M. Collett, S. Tan, and D. Walls, Phys. Rev. A **56**, 591 (1997).

[84] Y. Castin and J. Dalibard, 'The relative phase of two Bose-Einstein condensates', unpublished.

[85] C. Law, H. Pu, N. Bigelow, and J. Eberly, Phys. Rev. A **58**, 531 (1998).

[86] P. Villain et al., J. Mod. Opt. **44**, 1775 (1997).

[87] P. Villain and M. Lewenstein, quant-ph/9808017(1998).

[88] J. Javanainen and S. Yoo, Phys. Rev. Lett. **76**, 161 (1996).

[89] M. Naraschewski, H. Wallis, A. Schenzle, J. Cirac, and P. Zoller.

[90] J. Cirac, C. Gardiner, M. Naraschewski, and P. Zoller, Phys. Rev. A **54**, 3714 (1996).

[91] T. Wong, M. Collett, and D. Walls, Phys. Rev. A **54**, 3718 (1996).

[92] S. Yoo, J. Ruostekoski, and J. Javanainen, J. Mod. Opt. **44**, 1763 (1997).

[93] F. Dalfovo, S. Gorgini, M. Guilleumas, L. Pitaevskii, and S. Stringari, Phys. Rev. A **56**, 3840 (1997).

[94] A. Csordas, R. Graham, and P. Szepfaslusy, Phys. Rev. A **56**, 5179 (1997).

[95] A. Griffin, Phys. Rev. B **53**, 9341 (1997).

[96] T. Ho and V. Shenoy, Phys. Rev. Lett. **77**, 3276 (1996).

[97] H. Pu and N. Bigelow, Phys. Rev. Lett. **80**, 1130 (1998).

[98] H. Pu and N. Bigelow, Phys. Rev. Lett. **80**, 1134 (1998).

[99] P. Öhberg and S. Stenholm, Phys. Rev. A **57**, 1272 (1998).

[100] A. Smerzi, S. Fantoni, S. Giovanazzi, and S. Shennoy, Phys. Rev. A **79**, 4950 (1997).

[101] G. Milburn, J. Corney, E. Wright, and D. Walls, Phys. Rev. A. **55**, 4318 (1997).

[102] I. Zapata, F. Sols, and A. Leggett, Phys. Rev. A **57**, R28 (1998).

[103] B. Esry, C. Greene, J. J.P. Burke, and J. Bohn, Phys. Rev. Lett **78**, 3594 (1997).

[104] B. Esry and C. H. Greene, Phys. Rev. A **57**, 1265 (1998).

[105] P. Julienne, F. Mies, E. Tiesinga, and C. Williams, Phys. Rev. Lett. **78**, 1880 (1997).

[106] J. James P. Burke, J. L. Bohn, B. Esry, and C. H. Greene, Phys. Rev. A **55**, R2511 (1997).

[107] E. Timmermans, cond-mat/9709301.

[108] B. Esry and C. H. Greene, Phys. Rev. A **59**, 1457 (1999).

[109] R. Graham and D. Walls, Phys. Rev. A **57**, 484 (1998).

[110] T. Busch, J. Cirac, V. P. Garcia, and P. Zoller, Phys. Rev. A **56**, 2978 (1997).

[111] S. Stringari, Phys. Rev. Lett. **77**, 2360 (1996).

[112] E. Schrödinger, Naturwissenschaften **23**, 807 (1935).

[113] H. Price, *'Time's Arrow and Archimedes Point'*, Oxford University Press, Oxford, 1996.

[114] A. Leggett and A. Garg, Phys. Rev. Lett. **54**, 857 (1985).

[115] J. von Neumann, in *Matematische Grundlagen der Quantenmechanik*, Springer, Berlin, 1932.

[116] F. Karolhazy, Nuovo Cimento A **42**, 390 (1966).

[117] A. Komar, International Journal of Theoretical Physics **2**, 157 (1969).

[118] A. R. G.C. Ghirardi and T. Weber, Phys. Rev. D **34**, 470 (1986).

[119] R. G. G.C. Ghirardi and A. Rimini, Phys. Rev. A **42**, 1057 (1990).

[120] L. Diosi, Phys. Rev. A **40**, 1165 (1989).

[121] P. Pearle, Phys. Rev. D **13**, 857 (1976).

[122] R. Penrose, *'Shadows of the Mind'*, Vintage, London, 1995.

[123] H. Everett, Reviews of Modern Physics **29**, 452 (1957).

[124] B. DeWitt and R. Graham, *'The Many Worlds Interpretation of Quantum Mechanics'*, Princeton University Press, 1973.

[125] W. Zurek, Phys. Today **44**, 36 (1991).

[126] J. Ruostekoski, M. Collett, R. Graham, and D. F. Walls, Phys. Rev. A **57**, 511 (1998).

[127] M. Steel and M. Collett, Phys. Rev. A **57**, 2920 (1998).

[128] B. Yurke and D. Stoler, Phys. Rev. Lett. **57**, 13 (1986).

[129] J. Slosser and G. Milburn, Phys. Rev. Lett. **75**, 418 (1985).

[130] B. Sanders, Phys. Rev. A **40**, 2417 (1989).

[131] R. D. B. Ouboter, Metabistability in a SQUID and Macroscopic Quantum Tunnelling, in *Proc. Int. Symp. Foundations of Quantum Mechanics 1983*, edited by S. K. *et. al.*, Physical Society of Japan, Tokyo, 1983.

[132] A. Leggett, The Current Status of Quantum Mechanics at a Macroscopic Level, in *Proc. Int. Symp. Foundations of Quantum Mechanics 1986*, edited by M. N. *et. al.*, Physical Society of Japan, Tokyo, 1986.

[133] D. Bol, R. V. Weelderen, and R. de Bruyn Ouboter, Physica **122B**, 1 (1983).

[134] M. Devoret, J. Martinis, and J. Clarke, Phys. Rev. Lett. **55**, 1908 (1985).

[135] M. Brune et al., Phys. Rev. Lett. **77**, 4887 (1996).

[136] F. Arrechi, E. Courtens, R. Gilmore, and H. Thomas, Phys. Rev. A **6**, 2211 (1972).

[137] R. Glauber, Phys. Rev. **130**, 2529 (1963).

[138] R. Glauber, Phys. Rev. **131**, 2766 (1963).

[139] P. Kelley and W. Kleiner, Phys. Rev. **136**, A316 (1964).